To the Graduate Council:

I am submitting herewith a thesis written by In-Seop Lee entitled "Polarization and Corrosion Behavior of 316L Stainless Steel and Alloy AL6X in Acid Chloride Environments." I have examined the final copy of this thesis for form and content and recommend that it be accepted in partial fulfillment of the requirements for the degree of Master of Science, with a major in Metallurgical Engineering.

E. E. Stansbury

E. E. Stansbury, Major Professor

We have read this thesis
and recommend its acceptance:

Accepted for the Council:

Vice Provost
and Dean of the Graduate School

STATEMENT OF PERMISSION TO USE

In presenting this thesis in partial fulfillment of the requirements for a Master's degree at The University of Tennessee, Knoxville, I agree that the Library shall make it available to borrowers under rules of the Library. Brief quotations from this thesis are allowable without special permission, provided that accurate acknowledgment of the source is made.

Permission for extensive quotation from or reproduction of this thesis may be granted by my major professor, or in his absence, by the Head of Interlibrary Services when, in the opinion of either, the proposed use of the material is for scholarly purposes. Any copying or use of the material in this thesis for financial gain shall not be allowed without my written permission.

Signature Lee, In Seop

Date March 1986

POLARIZATION AND CORROSION BEHAVIOR OF 316L STAINLESS STEEL AND ALLOY AL6X IN ACID CHLORIDE ENVIRONMENTS

A Thesis

Presented for the

Master of Science

Degree

The University of Tennessee, Knoxville

In-Seop Lee

March 1986

DEDICATION

This thesis is dedicated to my parents and wife, particularly my new daughter.

ACKNOWLEDGEMENTS

The author would like to express his deep gratitude to his major professor, Dr. E. E. Stansbury, for his patience, guidance throughout the entire course of this research. Appreciation is also expressed to Dr. C. D. Lundin, Dr. C. R. Brooks and Dr. R. A. Buchanan for their advice and guidance during this work.

The author is grateful to the departmental electronic shop led by Mr. T. A. Long, Sr. and his efficient group, Mr. S. A. Steiner, Mr. R. L. Johnson, Mr. G. Jones and Mr. M. R. Neal, for their work maintaining the corrosion lab equipment and heat treatment facilities.

Special thanks are due to Mr. B. L. McGill for his help in scanning electron microscopy and to Mr. A. W. J. Carter and Mrs. A. Cagle for procuring and distributing many of the materials essential to this research.

The tireless support of Mrs. P. Davis, Mrs. S. Hail, Mrs. B. Frazier, Mrs. S. Turner and Mrs. P. Klindt is acknowledged.

Last but not the least, the author would like to thank his fellow graduate students for their help and support.

ABSTRACT

The pitting susceptibility of 316L stainless steel and alloy AL6X (nominally 20% chromium, 25% nickel, and 6% molybdenum) was evaluated electrochemically and chemically in chloride environments with varing acid pH, ferric ion and chloride ion concentration at room temperature, 135^{o}F, and 170^{o}F. A method was developed for preparing samples to ensure that crevice corrosion does not occur at the metal/epoxy interface prior to general pitting corrosion. The method involved prepassivating samples in 50% HNO_3 + 50% H_2O at 122^{o}F for 30 minutes, painting over the interface between the metal and the epoxy with 1201 Red Enamel and finally removing the prepassivated passive film from the exposed surface by careful hand polishing with 1 micron diamond paste.

This sample preparation allowed confirmation that the pitting potential is decreased with increasing chloride ion concentration and temperature. However higher pitting potentials were observed than previously reported suggesting that crevice corrosion potentials may be erroneously reported as pitting potentials. The critical current density in the anodic polarization curve was not affected significantly with increasing chloride ion concentration. An increase in the anodic maximum current density was observed on decreasing the cathodic potential from which the scan was initiated in determining the polarization curve. This effect was related to oxidation of hydrogen generated in the cathodic potential range and confirmed by related measurements on a platinum electrode.

An effect of heat treatment on the pitting resistance of AL6X was confirmed. Solution annealing in the range of 2050°F-2450°F did not affect the pitting resistance but when solution annealed at 1950°F, sigma phase formation along the grain boundary was associated with pit initiation.

A series of experiments was conducted to further investigate the relationship between electrochemical and chemical methods of determining critical pitting potentials. In the chemical method, the potential was increased by increasing the concentration of ferric ion as ferric chloride while holding the chloride ion concentration constant with sodium chloride. Since the maximum potential that could be produced by ferric ion addition without exceeding the selected chloride ion concentration was 0.76 V (SHE) which was below the electrochemical pitting potential of 0.82 V (SHE), further comparison was made at 135°F based on the decreasing pitting potential with increasing temperature. When 316L stainless steel was immersed in 15g/l $FeCl_3 6H_2O$ containing the same chloride ion concentration as 5% NaCl with pH=2 at 135°F, the corrosion potential increased up to 0.47 V (SHE) due to the initial passivation after 2 minutes. This potential is just above the pitting potential of 0.45 V (SHE) determined by electrochemical method in 5% NaCl, pH=2 at 135°F. A decrease in corrosion potential indicated the initiation of pitting corrosion which was confirmed by visual observation.

TABLE OF CONTENTS

LIST OF TABLES

LIST OF FIGURES

FIGURE PAGE

FIGURE PAGE

FIGURE PAGE

FIGURE PAGE

FIGURE PAGE

CHAPTER 1

INTRODUCTION

Austenitic stainless steels possess good corrosion resistance and for this reason they are widely utilized for severe corrosion environments. However, under certain conditions they undergo localized corrosion such as pitting corrosion (1). Pitting corrosion is one of the most destructive and insidious forms of corrosion, and difficult to assess and predict satisfactorily. Pitting corrosion is observed most often in the presence of chloride ions. This is due not only to their greater aggressiveness, but also to the wider distribution of chlorides in nature, that is, to the greater chance of their being present in aggressive media, including many technically employed solutions. The attack is limited to extremely small areas of the metal surface while the remaining surface is relatively unaffected. Pits start at small points on the surface and enlarge with time. However, the enlargement of the surface area of a pit is small in comparison with its increase in depth and volume. Many investigations have been performed to understand the pitting corrosion phenomena. Major effort has been directed toward the characterization of the pitting corrosion by the determination of a variable usually called the pitting potential (2). The pitting potential (E_p) is the potential above which passive alloys are liable to pitting corrosion in halide solutions but below which they resist pitting corrosion. Various experimental procedures, the most important being potentiostatic, potentiokinetic, galvanostatic and chemical, are proposed to measure the pitting

potential (3). It has been argued that the above methods do not show good correlation under identical conditions (4-6).

The objective of this research is to determine if correlations can be established between chemical and electrochemical measurements showing the corrosion response of type 316L stainless steel and alloy AL6X to environments that may be encountered locally in heat exchangers exposed to natural waters. Test environments are used to simulate the local increase in chloride ion and decrease in pH that may occur. AL6X is a recently developed austenitic, 20% chromium, 25% nickel, and 6% molybdenum containing alloy for service in pitting environments.

Important variables are

a) pH range(controlled by H_2SO_4, NaOH)

b) concentration of chloride ion(controlled by NaCl)

c) temperature

d) potential

e) heat treatment

f) oxidizing species controlling potential as a cathodic reactant(Fe^{+3})

Variation in pH and chloride ion concentration requires investigation since the environments in pits can develop low value of pH and large chloride ion concentration due to the migration of chloride ion to maintain neutrality and the hydrolysis of the dissolved metal ions by water to the hydroxide or oxide and free acid.

CHAPTER 2

LITERATURE REVIEW

There are three main classes of stainless steels designated in accord with their metallurgical structure. Each class is made up of several alloys of somewhat different composition having related physical, magnetic and corrosion properties. The American Iron and Steel Institude (AISI) designates the wrought standard grades of stainless steel by three digit numbers. The austenitic grades are designated by numbers in the 200 series and 300 series. The 300 series austenitic stainless steels are widely utilized for their good corrosion resistance. The 300 series represents compositional modifications of 18%Cr-8%Ni stainless steel. The reasons for the compositional modification are fourfold (7):

a) addition of molybdenum to improve pitting and crevice corrosion resistance (type 316 and 317)

b) lowering carbon content or stabilizing with either titanium or columbium plus tantalum to reduce intergranular corrosion in welded materials (type 321, 347, 348, 304L and 316L)

c) addition of nickel and chromium to improve high temperature oxidation resistance and strength (type 309, 310, 314, 330 and AL6X)

d) addition of nickel to improve stress corrosion resistance (type 305 and 384)

Their good corrosion resistance relates to their passivity in which the surface is covered by a thin protective oxide film (less

than 100 A thick) (8-14). Okamoto (10) assumed a model in which the passive film is a hydrated oxide film having a gel-like structure, as indicated in the schematic sketch of (a) in Figure 1. The proton included in the film structure is pulled out by anodic polarization. The metal ion produced by anodic dissolution through the undeveloped part in the film forms an intermediate denoted as MOH. The MOH is captured by the surrounding H_2O molecules and precipitates as a solid film in the undeveloped part, as shown in Figure 1(b). Freshly formed films thus contain a large amount of bound water, but with time the film changes to the less hydrated structure. At any stage of ageing, the film may contain various forms of bridges between metal ions: there exist three different bridges, H_2O-M-H_2O, -HO-M-HO- and -O-M-O-, depending on the degree of loss of protons. With loss of protons, the bridging between metal ions develops and finally the film completely changes to a perfect oxide (-O-M-O-). Thus, the undeveloped part (H_2O-M-H_2O) of the structure is most reactive to corrosion. McBee and Kruger (12) have found that the passive film tends to become amorphous as the Cr content of the alloy is increased. In the lower Cr-content alloy, the passive film is able to sustain an epitaxial relationship with the substrates but the higher alloy containing 25%Cr does not show any oxide pattern. Thus, the more stable passivity or better corrosion resistance encountered when Cr is added to iron may be due to the formation at its surface of a mixed oxide of iron and chromium tending toward the amorphous.

A convenient way to understand the passivity of stainless steels is by condsidering the potential/current density diagram, generally

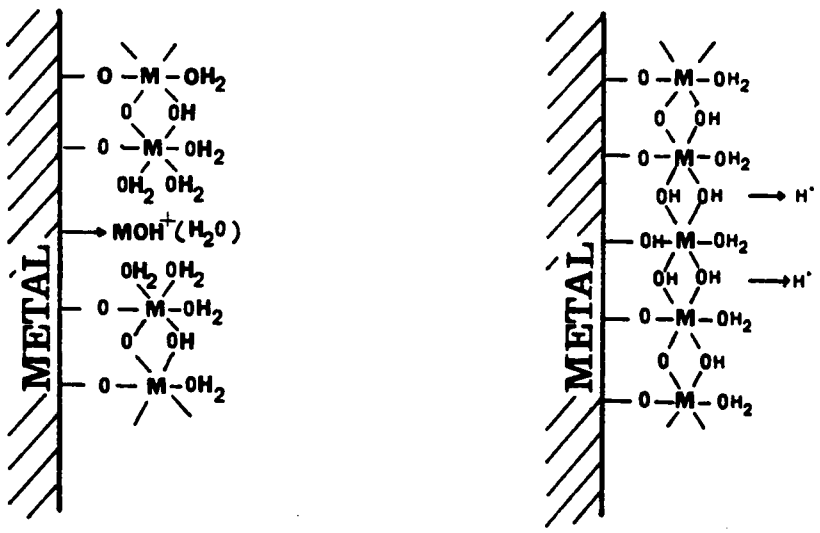

(a) (b)

Figure 1. Metal ions dissolved through the undeveloped part in the film(a) are captured to form the film(b) due to the bridging of OH bond to metal ions

Source: Go Okamoto, "Passive Film of 18-8 S.S. Structure and Its Function," Corr. Sci., Vol. 13, p. 471-489,(1973).

known as a polarization curve. Figure 2 shows the potentiodynamic anodic polarization curve for AISI 304 stainless steel in 1N sulfuric acid solution (15). The behavior of this alloy can be conveniently divided into three regions; active, passive, transpassive. In the active region, the behavior is identical to that of a normal metal. Slight increases in applied potential cause a corresponding rapid increase in the corrosion rate. If the applied potential is increased sufficiently, the corrosion rate shows a sudden decrease corresponding to the beginning of the passive region. Further increases in applied potential produce little if any change in the corrosion rate of the material. Finally, at very high applied potential, the corrosion rate again increases with increasing applied potential. This region is termed the transpassive region. The potential at which this current increase takes place is critically dependent on the alloy composition and pH when due to formation of soluble ions such as $HCrO_4^-$. An increase in current density can also represent the onset of the evolution of gaseous oxygen by the electrolysis of water (16). In chloride ion containing solutions the current density may increase at lower potentials and is associated with the beginning of pitting corrosion. This breakdown potential is called the pitting potential (17-19). A number of theories have been proposed that attempt to explain the initiation of pits in a perfect surface (ie. surfaces not containing physical defects such as inclusion, compositional heterogeneity, etc.). These consider pit initiation to be a result of certain interaction between discrete species in the environment (eg. chloride ion) and the passive surface. To date, no entirely

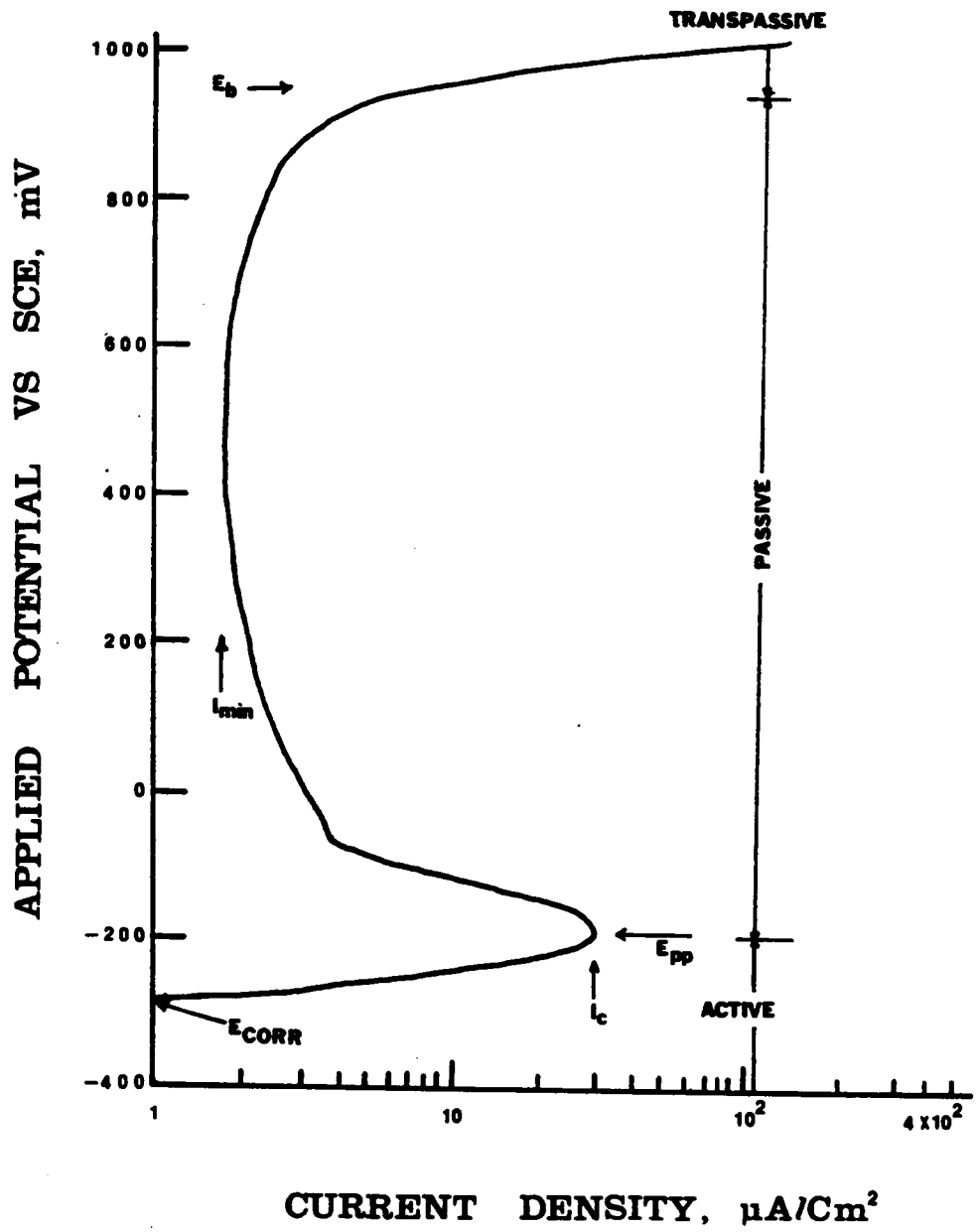

Figure 2. Potentiodynamic anodic polarization curve for 304 stainless steel in 1N H_2SO_4.

Source: W. Y. C. Chen and J. R. Stephens, "Anodic Polarization Behavior of Austenitic Stainless Steel Alloys with Lower Cr Content," Corrosion, Vol. 35, p. 443-451,(1979).

satisfactory theory has been developed and the theories that are available are not entirely independent of each other. The following theories have been proposed.

Penetration Theory

This model was proposed by Hoar (20) and is based on the fact that the initiation of pits is due to the adsorption of the aggressive anions on the surface of the oxide film followed by the penetration of ions throught the film. Evans (21) thought that the specific pitting tendency of halide ions was due to their small diameter which could lead to easy penetration of the passivating oxide film. Therefore, Cl^- is, as usually found, more aggressive than Br^- or I^-. The aggressive anion, adsorbed on the oxide film surface, begins to enter and penetrate the film (without exchange) under the influence of the electrostatic field across the film/solution interface when the field reaches the pitting potential. The initial entry of anions is at a regions of the film corresponding to a grain boundary, grain-margin, disarrayed or impurity zone in the metal; films over these regions are less perfect and more easily entered than that on more ordered regions (16,22). The oxide film begins to be contaminated with significant amounts of the anion. This "contaminated oxide" film is a much better ion conductor than the original passivating oxide, so that the cations migrate through the film into the solution very much more readily than in the absence of halide ions. Under the anodic field, the rate is increasd at which cations pass through the film to replace the dissolved cation. Thus, once localizd breakdown starts, it accelerates explosively.

Adsorption Displacement Theory

According to this theory, Cl^- adsorbs on the metal surface in competition with dissolved O_2 or OH^-. Once in contact with the metal surface, Cl^- favors hydration of metal ions and increases the ease with which metal ions enter into solution, opposite to the effect of adsorbed oxygen, which decreases the rate of metal dissolution. The specific value of Ep (pitting potential) represents the minimum electrode potential value at which the aggressive anions become capable of reversibly replacing the passivating oxygen from the metal surface. Kolotyrkin (23-24) presumes that the dissolution of solid metals always takes place nonuniformly. Consequently, there is always an uneven distribution of current on the surface even during the dissolution of passivated metal. Under these circumstances the critical concentration of the aggressive anions is achieved first near those areas of the surace which dissolve at the highest rate. When a certain potential (pitting potential) is reached, conditions are created for displacement of one component by another, and consequently for a change in mechanism of the process. If there is a component having a greater affinity for the metal and forming more stable complex than the halide ions, such as NO_3^- and SO_4^{-2}, the adsorption of these anions on the surface of the metal will lead not to acceleration, but to deceleration of the dissolution process (25). Therefore, the dilution of aggressive anion concentration caused by other anions could account for a higher pitting potential in their presence.

Pit Propagation

After a pit initiates, the pit begins to propagate. There is a relatively wide acceptance of the pit propagation mechanism. The pitting corrosion usually requires an extended initiation period before visible pits appear. Once started, however, a pit penetrates the metal at an ever-increasing rate. Initially, the oxidation and the reduction reactions

$$M \rightarrow M^{+} + e^{-}$$

$$O_2 + 2H_2O + 4e^{-} \rightarrow 4OH^{-}$$

occur uniformly over the entire surface although at low rates corresponding to the current density to maintain the passive film. During a short interval of initial pit formation the oxygen within the pit is depleted because of the restricted condition, so oxygen reduction ceases in this area. This, by itself, does not cause any change in corrosion behavior. Since the area within a pit is usually very small compared with the external area, the overall area available for oxygen reduction remains almost unchanged. However, the rate of corrosion within the pits corresponding to unpassivated surfaces is high, but on the unpitted surfaces the rate remains the same as the passive current. This condition is equivalent to galvanic coupling between the large passive surface supporting oxygen reduction and the very small anodic areas of the pits. Since the total corrosion current over the surface increases, the rate of oxygen reduction must increase on the passive surface. The high rate of local metal dissolution in the pit tends to produce an excess of positive charge in the pit (M^{+}) which is necessarily balanced by the inward migration of chloride ions

as shown in Figure 3. Thus, in the pit there is an increased concentration of the metal chloride. This enrichment of chloride ions has been confirmed by means of electron microprobe analysis of residues in pits (26). Hydrolysis of metal salts results in a high concentration of hydrogen ions according to the following rection:

$$MCl + H_2O \rightarrow MOH + H^+ + Cl^-$$

As a result, the composition of the solution inside the pit is characterized by a higher concentration of the chloride ion and a noticeably lower pH compared with the bulk solution. Both hydrogen and chloride ions stimulate the dissolution of most metals and alloys, and the entire process accelerates with time. An important feature of pitting corrosion is the localization of the reaction; while the anodic reaction is concentrated completely on comparatively small active pitted sections of the surface, the cathodic reaction (reduction of the oxidizing agent) takes place almost entirely over the remaining very large passive surface. This is confirmed by the results of experiments with artificial pits. Particularly in the work of Greene and Fontana (27), using the metal of an artificial pit geometrically similar to corrosion pits, they showed that the anodic current density in a pit can surpass that of the passive surface by a factor of almost 10^5.

There have been a few attempts to explain the pitting corrosion process by using mathematical models. Galvele (28) has presented a theory based on simple transport equations and equilibrium expressions between ionic species in which the following variables are considered: corrosion product metal ion concentration and hence alloy composition,

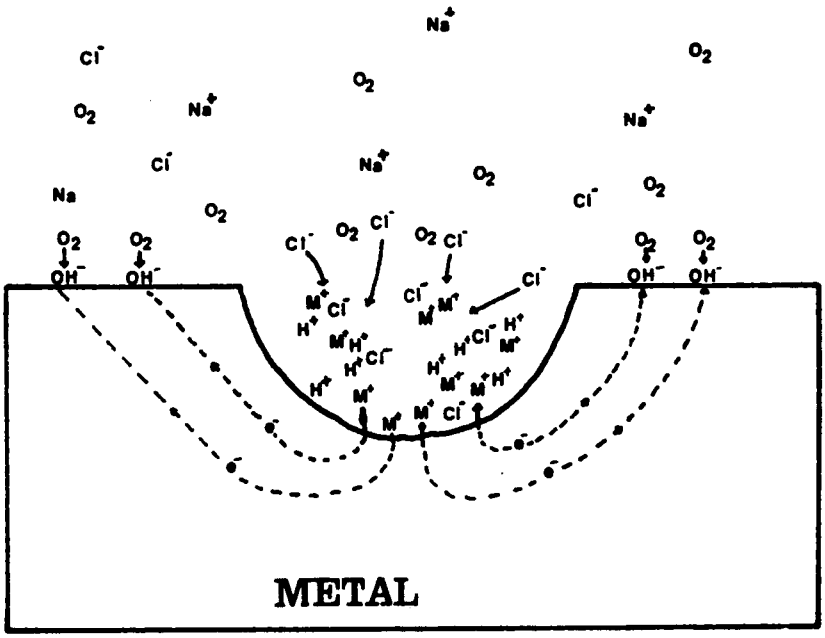

Figure 3. Autocatalytic processes occurring in a corroding pit.

Source: Fontana and Greene, "Corrosion Engineering" p. 52,(1978).

aggressive anion concentration, nonaggressive anion concentration, external pH and presence of weak acid salts. He assumes that the pit is cylindrical in which the dissolution reaction does not take place at the walls of the pit but occurs only at the bottom. The transport equations are simplified to diffusion migration only by ignoring the electrical migration terms on the basis that pit initiation takes place with small changes in the bulk electrolyte composition. Solutions of the sets of equations are presented as plots of ionic concentration of the several species as function of the product Xi where X is the pit depth and i is the current density. Galvele argues that pit initiation occurs when a critical acidification (decrease in pH) occurs preventing passivation or, equivalently sustaining active dissolution at the base of a defect in the passive film (or a pre-existing crevice). The critical acidification is calculated from the chemical equilibria involved with passive film formation and is defined as the pH below which the film is chemically unstable. The criteria are similar to those presented by Pourbaix (29) and represented by him on potential/pH diagrams. Galvele concludes from a review of the literature that pits propagate at a current density of at least 1.0 A/cm^2. It follows that the requirement for initiation of pitting corrosion at a defect of depth, X, is the application of a potential that results in a current density of about 1.0 A/cm^2. The diagrams show that the pH decreases with increasing Xi value (pit propagation) but the concentration of chloride ion does not increase significantly in the pit until the Xi value reaches a certain higher value. Galvele argues that the primary condition for pit initiation is

is not affected by the concentration of chloride ion. He explains why the pitting potential is lowered with increasing the concentration of chloride ion as follow. The reference electrode placed above the bulk metal surface measures the potential which is the sum of the potential of the bottom of the pit and the IR voltage drop of the electrolyte column within the pit. The IR voltage drop decreases with increasing the concentration of chloride ion, therefore, the lower pitting potential is measured at the higher concentration of chloride ion. He insists that the pitting potential is the minimum potential at which localized acidity could be maintained inside a pit. As soon as the system reaches the Xi minimum value for pit growth the pit will start to propagate. If the potential is lowered, the current density (i) will drop but the pit depth (X) is increased due to the pit propagation. Therefore, the pit will continue to grow while the value Xi is higher than the minimum value for pit growth. This means that a pit will grow at potentials lower than the pitting potential. The theory then provides an explanation for the observation that crevice corrosion occurs at much lower potential than the pitting potential in the sense that the crevice is a pre-existing deep pit.

Metallurgical Factors

Alloying elements which have a beneficial effect on pitting corrosion shift the pitting potential (E_p) to more positive values, while those elements having a detrimential effect shift E_p to more negative values. Research has shown that both of the major alloying elements of stainless steels, chromium and nickel, increase resistance to pitting corrosion. Horvath and Uhlig (30) found that in Cr-Fe

alloys the pitting potential increases with increasing Cr content as shown in Figure 4. Also they found that for 15Cr-Fe the pitting potential is shifted slightly in the positive direction as the Ni concentration is increased (Figure 5). In Chen et al.'s experiments (15), incrementally reducing the Cr content in 304 stainless steel from the normal 18% level to approximately 8% increases the critical current density. Okada et al. (31), using Auger Electron Spectroscopy, report that Cr is enriched in the surface layer of the passive film in proportion to matrix Cr contents, which increases the stability of the passive film. The beneficial effect of Mo on pitting corrosion has been assessed (32-36). In the presence of Mo, not only does the pitting potential become more positive, but also the critical current densities and primary passivation potentials decrease considerally. Bond and Lizloves (37) explained that the beneficial effect of Mo was due to the passive film thickening. According to Lizlove and Bond (38), small additions of Ti have a beneficial effect on pitting corrosion because Ti binds carbon and nitrogen, preventing the formation of chromium and molybdenum carbides and nitrides, and consequently prevents the formatiom of zones depleted in chromium and molybdenum. But for higher Ti contents, new phases may develop which are assumed to be susceptible to pitting corrosion; therefore, higher concentration of Ti (to about 1.8%Ti) reduce the pitting potential in comparison with alloys containing less Ti. A recent paper by Bandy and Rooyen (39) has shown that nitrogen additions increase the pitting corrosion resistance of an entire group of Fe-Cr-Ni duplex alloys due to an increase in the fraction of more noble austenitic phase. Other

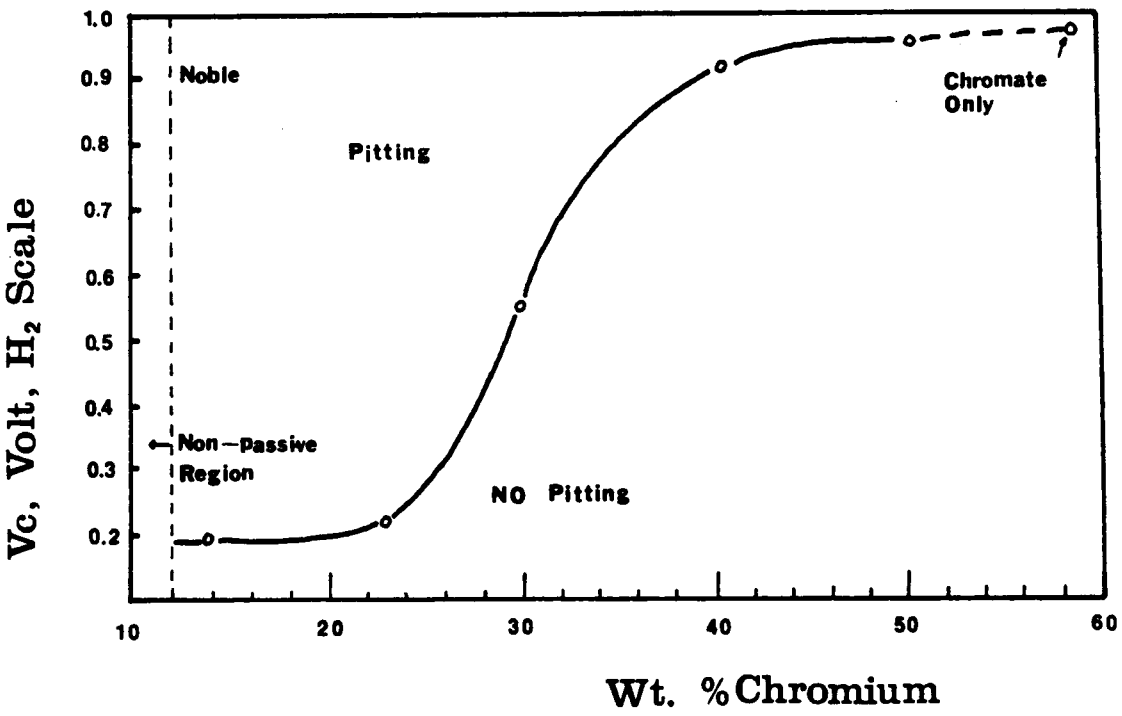

Figure 4. Critical pitting potentials for Cr-Fe alloys in 0.1N NaCl.

Source: J. Horvath and H. H. Uhlig, "Critical Potentials for Pitting Corrosion of Ni, Cr-Ni and Related Stainless Steels," J. Electrochem. Soc. Vol. 115, p. 791-795,(1968).

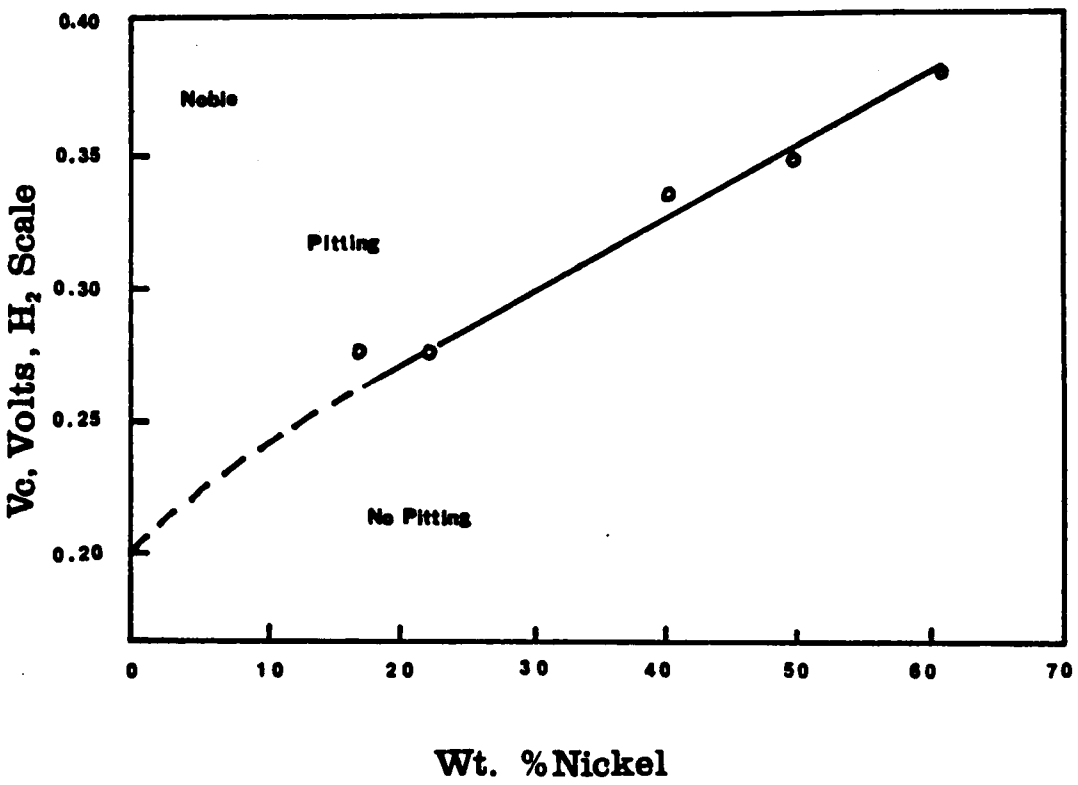

Figure 5. Critical pitting potentials for 15%Cr-Fe alloys with increasing Ni content, in 0.1N NaCl, 25°C.

Source: J. Horvath and H. H. Uhlig, "Critical Potentials for Pitting Corrosion of Ni, Cr-Ni and Related Stainless Steels," J. Electrochem. Soc., Vol. 115, p. 791-795,(1968).

elements that have been shown to improve the pitting corrosion resistance including Re, Si, W and V (18,36,40-42). Tomasho, Cheronova and Marcova (18,42) stated that considerable increase in pitting corrosion resistance was exhibited when 18Cr-8Ni stainless steel had been alloyed with 2.5%V, 2.5%Si, 2.5%Mo and 0.2%Re and that pitting corrosion did not occur on the Fe-18Cr-14Ni stainless steel alloyed with 5% of V, Si, Mo or Re in 0.5N $FeCl_3$. Rhenium produces a considerable effect on the resistance of steels to pitting corrosion at much lower concentrations of the element in the alloy in comparison to Mo, V and Si (18). The positive effect of Mo, Si and V was attributed to the increased stability of the passive film.

The resistance of a metal to pitting corrosion is higher the better the homogeneity of the surface (24). Thus, the nucleation of pits may be delayed both through polishing and long prepassivation. The most susceptible sites for pitting corrosion are the grain boundary which can be especially inhomogeneous with regard to the chemical composition (16,43). Any chemistry changes that lead to the presence of soluble inclusions, particularly sulfides and oxides, may decrease the pitting corrosion resistance. Szklarska-Smialoska (44) found that the most susceptible sites for pit nucleation were the inclusions of manganese sulfides during corrosion of stainless steel and mild steel in chloride solutions. She explains the role of sulfide inclusions in the pit nucleation process in chloride ion containing media as follows: Because the manganese sulfide, which usually occurs in steels, is chemically more active than other nonmetallic inclusions, it can be dissolved by acid media, and this process may

play a role in the formation of pits. Also, Eklund (45) has shown that preferential dissolution of sulfides resulting in small grooves serves as crevice initiation sites. Referring to Manning et al. (46) pit initiation in single-phase stainless steels occurs at austenite/sulfide interfaces, while pit initiation in duplex alloys occurs at δ/γ interfaces. The role of inclusion for pit initiation includes (47).

1. micro-crevices between the inclusion and the matrix itself due to inclusion dissolution
2. irregular current density distribution at regions of the inclusion
3. regions of a different composition around inclusion
4. inclusion acting as local cathodes

The value of the pitting potential of a stainless steel in a chloride solution also depends on its heat treatment and its cold work. The passive current density increases with increase in cold work but the primary passive potential and the pitting potential do not exhibit any dependence on degree of cold work (46,48). Manning et al. (46) observed that edge effects (edge sides usually have less pitting corrosion resistance) were eliminated by spherodizing the sulfides in the alloy by heat treating at 1300^{o}C for 8 hours. Tomashov, Chernova and Marcova (18) found the resistance to pitting corrosion of 18Cr-14Ni stainless steels containing 5%Si was greatly decreased after heat treatment at 650^{o}C (1202^{o}F) for 2 hours. In the corrosion behavior of ultrafine grained AISI 304 stainless steel, Masayoshi Hasegawa et al. (49) have shown the effect of grain size by recrystallization. The

pitting corrosion of coarse grained steel initiates at limited sites, but the individual pits are large and deep. In contrast, the pitting corrosion of ultrafine grained steel initiates in many sites, but the individual pits are small and shallow, which results in a decreasing corrosion rate.

Environmental Factors

Many environmental factors influence of the pitting potential and perhaps the most completely documented of these is the concentration of the aggressive anion in the environment. The pitting corrosion in stainless steel has long been associated with the presence of halide ions in the environment. By far, the chloride ion has been identified most often as the aggressor leading to pitting corrosion in stainless steel. As the concentration of chloride ion is increased in an environment the pitting potential is decreased (50). Pitting corrosion depends not only on the concentration of chloride ions, but also on the concentration of nonaggressive ions, and more precisely on the ratio of aggressive to nonaggressive anions. Rosenfeld et al. (25) reported that various anions such as NO_3^-, CrO_4^-, OH^-, ClO_3^- and CO_3^{-2} when added to chloride ion containing solutions shift the pitting potential to more positive values, accounting for an increased resistance to pitting corrosion. Leckie et al. (51) showed potentiostatic polarization curves for 18Cr-8Ni stainless steel in 0.1M HCl solution with different additions of Na_2SO_4 (Figure 6). The critical concentrations of these anions needed to prohibit the pitting corrosion depend upon a number of alloy composition and environmental variables. The minimum anion acitivities necessary to inhibit pitting

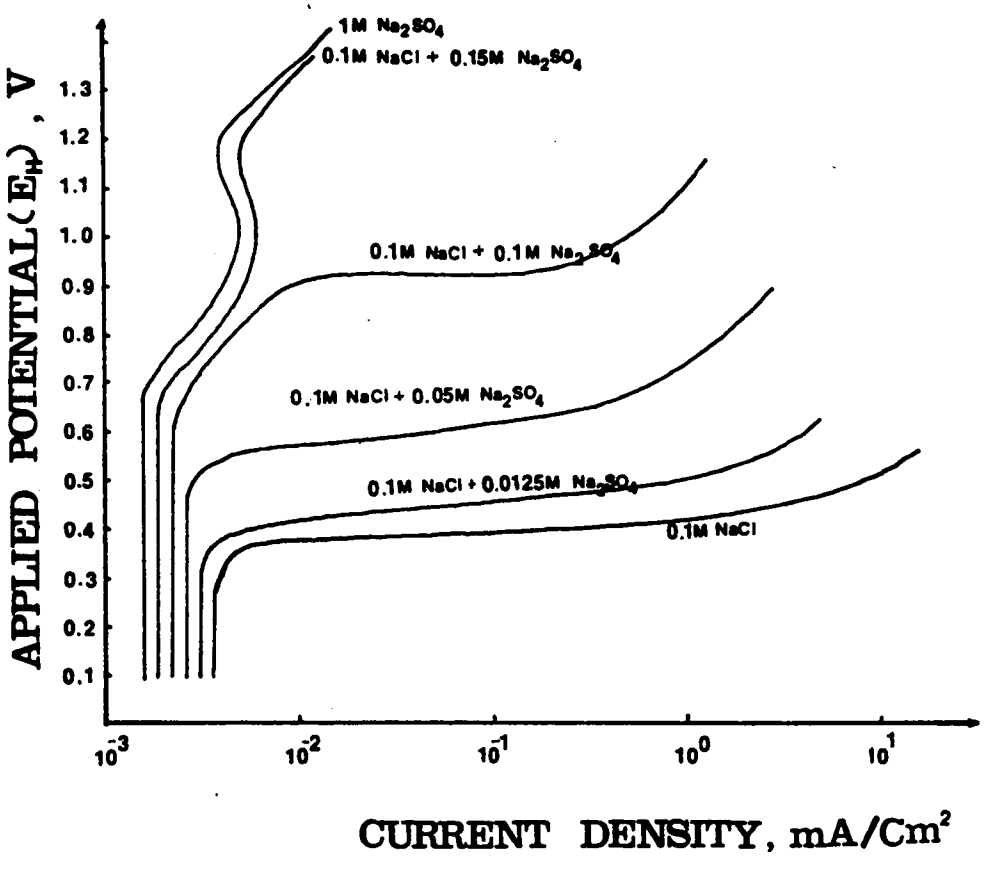

Figure 6. Potentiostatic polarization curves in 0.1N NaCl showing increasingly noble values of the critical potential with additions of Na_2SO_4, 25°C.

Source: H. P. Leckie and H. H. Uhlig, "Environmental Factors Affecting the Critical Potential for Pitting in 18-8 Stainless Steel," J. Electrochem. Soc. Vol. 113, p. 1262-1267,(1966).

corrosion of 18Cr-8Ni stainless steel in solution with different chloride ion acitivities were determined by Uhlig et al. (52). The general equation obtained for 18Cr-8Ni stainless steel under potentiostatic conditions was

$$\log a_{Cl^-} = B \log a_A + C$$

where a_A is the acitivity coefficient of the given inhibiting anion. For 18Cr-8Ni stainless steels the values of B and C that were determined experimentally are given Table 1. Referring to Kolotyrkin (53) when nonaggressive anions are present, these also tend to adsorb on the passive alloy surface substituing for chloride ions that displace oxygen of the passive film thereby destroying the passive film locally.

Some investigators (51,54-55) have found that the pitting potential is not affected appreciably in the acid pH range but moves markedly in the positive direction in alkaline media. Because OH^- with sufficient concentration is available for adsorption, its high affinity for the metal surface makes it an effective inhibitor. Also, the temperature of the environment is an important consideration in pitting corrosion (33,51,55-56). Increase in temperature leads within certain limits to important shifts of the pitting potential toward more negative values. This indicates that the resistance to pitting corrosion of alloys under consideration decreases with increasing temperature. Brigham and Tozer (56) have shown that the results of long term exposure tests correlate with critical pitting temperature values obtained when the temperature of the solution is increased at the rate of 0.6^oC per minute at 500 mV (SCE) for the same alloys in a

Table 1. Constants for 18-8Ni stainless steels.

	B	C
OH^-	1.62	1.84
NO^{2-}	1.88	1.18
SO_4^{2-}	0.85	0.05
ClO_4^{2-}	0.83	0.44
CH_3COO^-	1.13	0.06

Source: H. P. Leckie and H. H. Uhlig, "Environmental Factors Affecting the Critical Potential for Pitting in a 18-8 Stainless Steel," J. Electrochem. Soc., Vol. 113, p. 1262-1267, (1966).

solution of similar chloride activity and pH. These studies have led to the concept of a critical pitting temperature as a measure of the resistance of an alloy to pitting corrosion, the temperature above which pitting corrosion has been observed to occur in oxidizing acid chloride media and below which the stainless steel is immune to the initiation of pits. Another factor which can affect the pitting behavior of stainless steel is dissolved gas in the solution. Wilde and Williams (57) have shown that considerable differences in pitting potential can be observed in the presence of different dissolved gases. Their studies, shown in Table 2, demonstrate that the most positive potentials are observed when a high concentration of oxygen is present in the solution.

Pourbaix (58) has described the concept of a protection potential which stems from the observation that, under conditions of cyclic potentiodynamic anodic polarization, stainless steels exhibiting active pitting in halide media exhibit, on downscan, a potential where pits cease to propagate and repassivate. Pits initiated at potentials positive to a pitting potential for a short period of time will continue to grow when the specimen is held at a potential between a pitting potential and a protection potential. At potentials negative to a protection potential, pits cease to grow and repassivate. There is a evidence, however, that the protection potential is not a unique property of the material since this potential is intimately related to the electrode potential within the pit, which in turn depends on the way the experiment is performed. Wilde (59) demonstrates how the protection potential depends on the extent of pit propagation allowed

Table 2. Effect of dissolved gases on the pitting potentials of type 304 and 430 stainless steels in 1M NaCl solution at 25°C.

Dissolved Gas	Oxygen Content (ppm)	Pitting Potentials (Volts vs. SCE)	
		Type 304	Type 430
Hydrogen	0.076	-0.050	-0.185
Nitrogen	0.460	-0.020	-0.130
Argon	0.057	0.050	-0.100
Oxygen	30.1	0.065	-0.035

Source: B. E. Wilde and E. Williams, "On the Breakdown of Passivity on Stainless Steels in Halide Media," J. Electrochem. Soc., Vol. 116, p. 1539-1540,(1969).

to occur prior to repassivation. As shown in Figure 7, a more negative value of protection potential is required to repassivate the more propagated pits.

AL6X

Alloy AL6X is one of a number of austenitic stainless steels developed in recent years with higher nickel, chromium and particularly molybdenum contents to resist localized corrosion, such as pitting corrosion and crevice corrosion, in chloride containing environments. Table 3 shows a typical analysis of AL6X. The 20% chromium and 6% molybdenum contents of AL6X provide greatly increased resistance to pitting corrosion in chloride containing solutions compared to Type 316 stainless steel and to non-molybdenum Type 304 stainless steel. The high nickel and molybdenum provide good resistance to stress corrosion cracking. The alloy content of the material produces excellent general corrosion resistance in a number of media. The physical properties and mechanical properties of AL6X are shown in Table 4. As the high chromium and molybdenuum content of the alloy renders the material sensitive to precipitation of molybdenum bearing phases, high annealing temperatures coupled with rapid cooling are necessary to provide maximum corrosion resistance. When AL6X is held for long periods in the 800-1500^{o}F range, some carbides are precipitated, and when held in the 1100-2000^{o}F range, a molybdenum containing second phase (sigma phase) precipitates. Therefore, AL6X should be annealed above 2000^{o}F. In several recent publications including AL6X (60-62) in studies of pitting corrosion and/or crevice corrosion, Manning (60) has shown that AL6X has outstanding corrosion resistance.

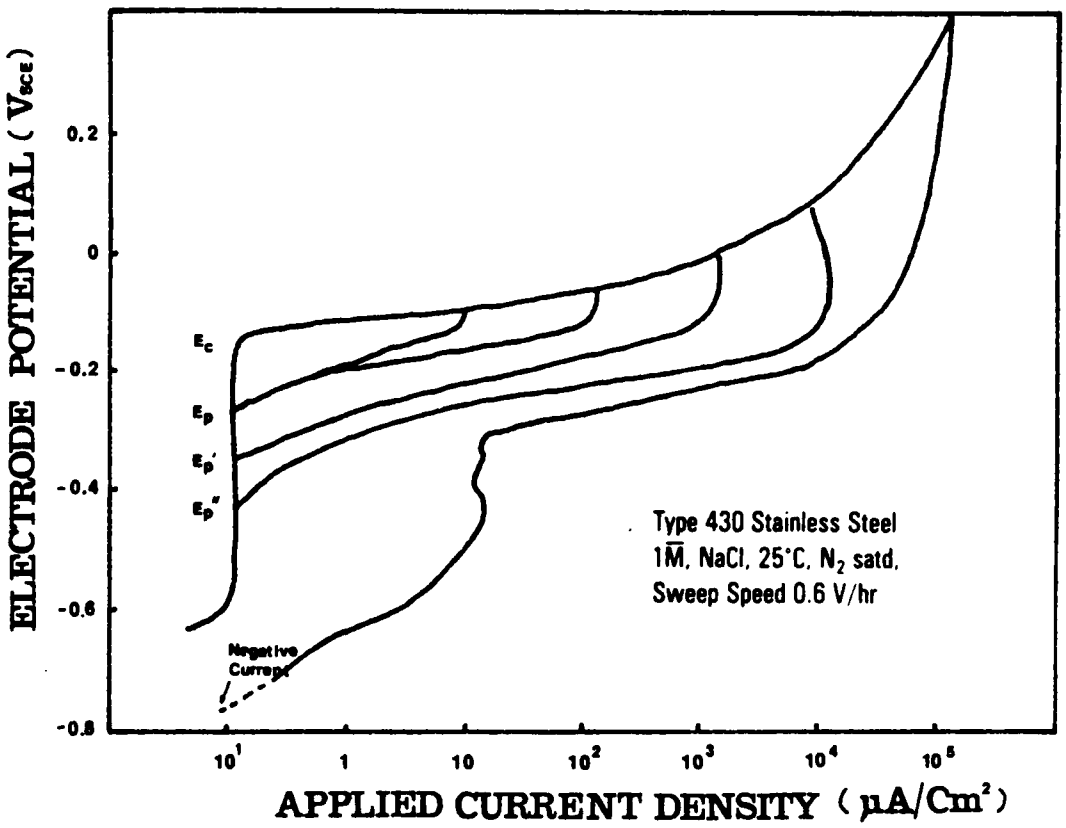

Figure 7. "Cyclic" polarization behavior of Type 430 stainless steel in 1M NaCl demonstrating the marked effect of pit propagaton on E_p.

Source: B. E. Wilde, "On Pitting and Protection Potentials Their use and Possible Misuses for Predicting Localized Corrosion Resistance of Stainless Steel Alloys in Halide Media," Localized Corrosion, p. 342-350,(1974).

Table 3. The typical analysis of AL6X.

Carbon	0.025
Manganese	1.50
Phosphorus	0.025
Sulfur	0.010
Silicon	0.50
Chromium	20.25
Nickel	24.50
Molybdenum	6.25

Table 4. The physical properties and mechanical properties of AL6X.

Melting Point, °F	2500
Density, lbs. per cu in.	0.293
Specific Gravity	8.0
Yield Strength,.2 % Offset, psi	40000
Tensile Strength, psi	90000
Elongation in 2in., percent	45
Reduction in Area, percent	60
Modulus of Elasticity, psi	29×10^6

Measurement of Pitting Corrosion

There are many methods to determine the resistance of stainless steel to pitting corrosion. These methods can be divided into two procedures. First are electrochemical methods, i.e. potentiostatic, potentiokinetic, or galvanostatic methods, so that only the anodic reaction occurs on the electrode being studied. Second are chemical methods in which solutions containing chloride ions and substances with a suitable redox potential higher than the pitting potential are used. Under such conditions cathodic and anodic processes occur on the surface being investigated.

Electrochemical methods are being used more extensively to study the corrosion behavior of stainless steel. The theoretical basis for electrochemical corrosion testing is derived from the mixed potential theory. This theory is briefly discussed by Fontana and Greene (63). In essence this theory separates the oxidation and reduction reactions of corrosion and postulates that the total rates of all the oxidation reactions equal the total rates of all the reduction reactions on a corroding surfaces. Oxidation reactions, referred to as anodic since they involve a loss of electrons, occur at the anodic sites on a corroding metal or at the anode in an electrochemical cell, can be represented by the general reaction

$$M \rightarrow M^{+n} + ne^{-}$$

This is the generalized corrosion reaction that removes the metal atom from the metallic state by oxidizing it to its ion in solution. In this reaction the number of electrons produced equals the valence of the metal ion produced. The mixed potential theory has proposed that

all the electrons generated by the anodic reactions are consumed by corresponding reduction reactions. Reduction reactions are known as cathodic and occur at the cathodic sites of a corroding metal or at the cathode of an electrochemical cell. More than one anodic and more than one cathodic reaction may be operative during corrosion. Consider, for example, the corrosion of a stainless steel in a hydrochloric acid solution contaminated with ferric ions. By means of the anodic reaction all the component elements (i.e., iron, chromium, nickel, etc.) of the alloy go into the solution as their respective ions. The electrons produced by these anodic reactions can be consumed depending on the potential by the cathodic reactions

$$2H^+ + 2e^- \rightarrow H_2$$

$$O_2 + 4H^+ + 4e^- \rightarrow 2H_2O$$

$$Fe^{+3} + e^- \rightarrow Fe^{+2}$$

Removing one of the available cathodic reactions (e.g. ferric ions) will reduce the corrosion rate. Thus, the observation that hydrochloric acid contaminated with ferric ions is more corrosive than pure hydrochloric acid can be easily explained in terms of the mixed potential theory of corrosion. The corrosion potential, E_{corr}, is the potential at which the total rates of all the anodic actions are equal to the total rates of all the cathodic reactions. The current density at E_{corr} is called the corrosion current density, I_{corr}.

Electrochemical methods have been used to measure the pitting potential from the anodic polarization curve in a given alloy/environment combination (24,30,52-53,64-65). As is known, below the pitting potential (E_p) the metal is in the passive state, while

above the pitting potential pitting corrosion occurs, i.e., on the metal surface passive and active sites coexist. The anodic polarization curve is determined by changing the potential in the positive direction from E_{corr} at a known scan rate and recording the current. The potential scan rate is defined as the rate at which the applied potential is linearly increased with time. The potential scan rate strongly influences the determination of pitting potential. Several workers investigated the effect of potential scan rate on pitting potential determination (37,39,56,66-67). Based on these results, it is difficult to justify a general behavior that is valid for the alloy/environment combinations that have been studied. In some cases, decreasing the potential scan rate caused the pitting potential to increase. In other cases, the reverse is observed. Bond et al. (37) have found that the pitting potential increases with decreasing the scan rate for 17.6%Cr-13.5%Ni-2.93%Mo stainless steel in 1.0M sodium chloride solution. Assuming that the passive film thickens with time, they explain that as the film thickness increases with slower speed of scanning, a larger fraction of the potential difference between metal and solution would be expected to occur within the film and thus not be available at the film-solution interface to assist in the entry of chloride ions into the film. Manning (68) proposed that the faster scan rate tends to yield a higher pitting potential because of allowing limited induction time at a given potential.

Another method to determine the pitting potential (E_p) involves measurement of current vs time as shown Figure 8 (61). At a constant potential at which $E<E_p$, the current decreases with time indicating

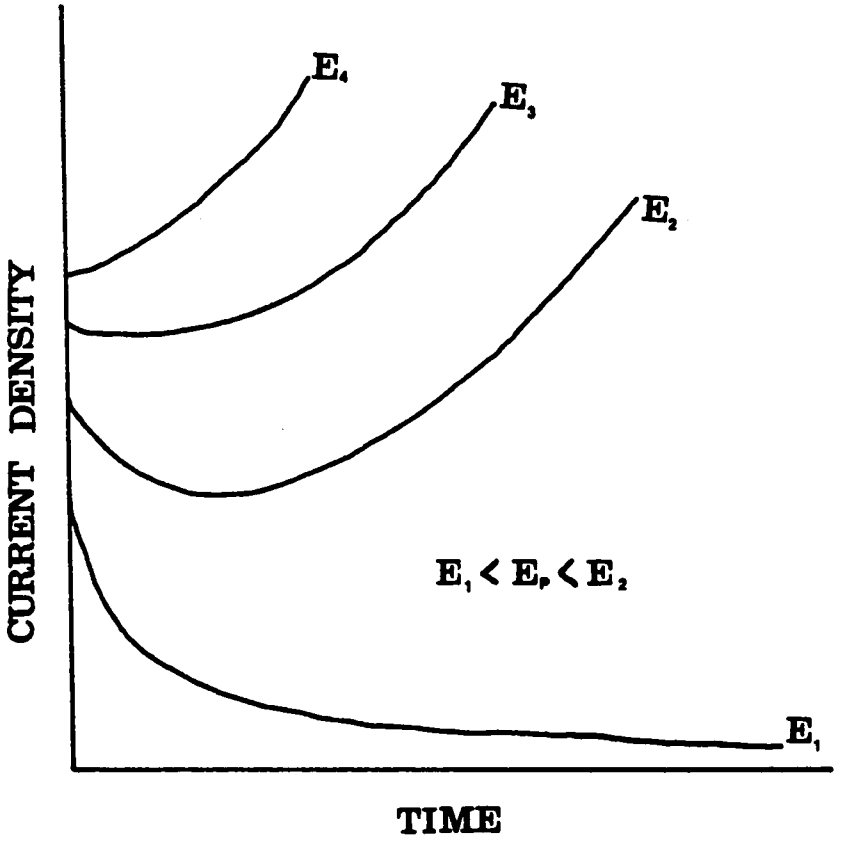

Figure 8. Schematic representation of current density vs. time I-t at constant potential: changes of current density in time.

Source: Z. Szklarska-Smialowska and M. Janik-Czachor, "The Analysis of Electrochemical Methods for the Determination of Characteristic Potentials of Pitting Corroson," Corr. Sci., Vol. 11, p. 901-914,(1971).

the formation and build up of a passive film and a final steady passive state current density characteristic of the metal/environment system is reached. At a potential at which $E>E_p$ the current increases after an induction time is exceeded because the metal is subjected to pitting corrosion. Therefore, the pitting potential is determined as the potential above which the current density increases with time. This method gives a well defined value of pitting potential because the measurement, performed at one definite potential, excludes phenomena which might occur at other potentials (69).

An electrochemical technique, based on identifying the pitting potential as the potential at which a mechanically introduced scratch will repassivate, has been proposed by Pessal and Liu (70). Another technique for measuring pit initiation is that proposed by Morris (32). This technique measures pitting potential by rapid potential scanning (60V/hr) and derives its justification both from the empirical observation that for austenitic alloys it gives rise to less positive values of the pitting potential, and that it minimizes the time dependent chances of developing crevice corrosion on the specimen which could cathodically protect the specimen against pitting corrosion. In the electrochemical technique, the oxidizing power can be varied simply by increasing the potential.

On the other hand in the immersion test, the oxidizing power is controlled by the addition of oxidizing agents such as ferric ions. Conceptually, a series of immersion test solutions could be devised, capable of establishing a pitting threshold, without the use of electrochemical stimulation. A ferric chloride test for pitting

corrosion has been standardized as ASTM practice G48-76 (71). In the immersion test, the pitting resistance is quantified in terms of readily measurable parameters such as number of pits per unit area and weight loss per area.

So far the discussion has centered on determining pitting potential by different techniques. It has been argued that the above methods do not show rates or type of attack that correlate with freely corroding systems. Manning (60) has pointed out that the electrochemical pitting potential, defined as the lowest potential at which a pit propagates, i.e., potential at which a monotonic increase in current occurs, is determined under artificial propagation conditions. The potentiostat controls the potential at fixed anodic values after initiation to determine whether the pit will repassivate or grow (monotonic current increase). This growth does not represent conditions that occur on freely corroding materials because the corrosion potential changes after pit initiation. France and Greene (5) have presented a theoretical explanation for the difference in pitting potentials determined by chemical and electrochemical methods. They propose that in the chemical method charge balance is maintained at the metal surface without the necessity of negative ion migration from the bulk across the imaginary boundary (X-X') as shown in Figure 9(a) (5). But in the electrochemical method, the metal oxidation reaction

$$M \rightarrow M^{+2} + 2e^{-}$$

yields two electrons which are conducted through the electrical circuitory to the platinum cathode where a reduction reaction occurs.

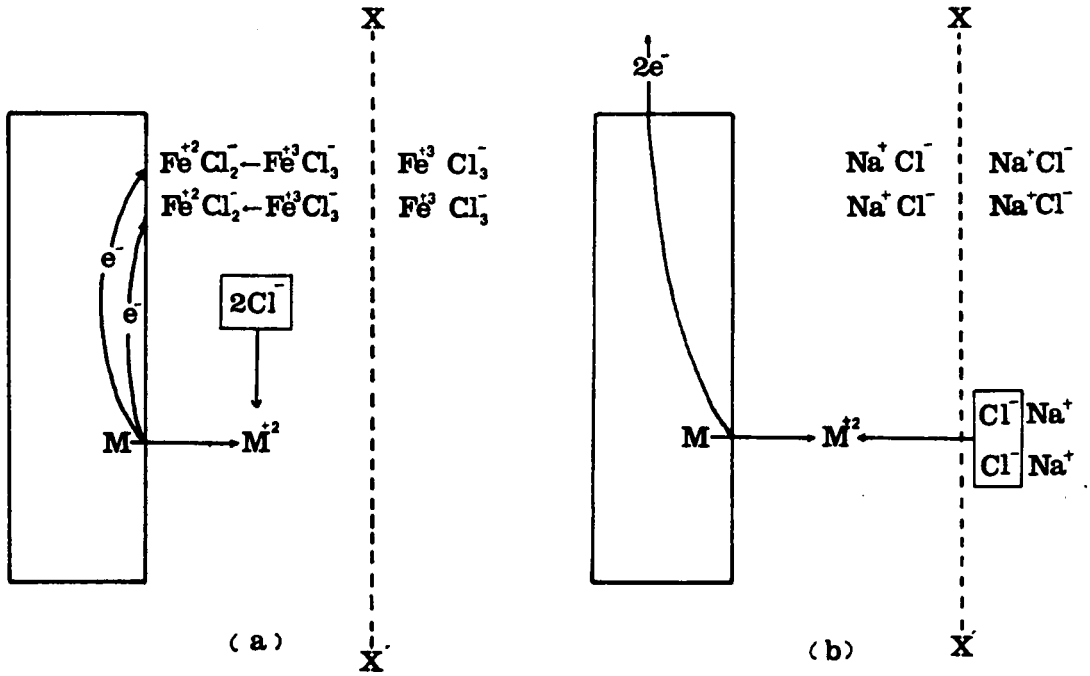

Figure 9. Schematic representation of reactions during controlled potential and conventional corrosion tests in acid chloride solutions.

Source: W. D. France, Jr. and N. D. Greene, "Comparison of Chemical and Electrolytically Induced Pitting Corrosion," Corrosion, Vol. 26, p. 1-4,(1970).

Once the M^{+2} enters the imaginary boundary layer solution, charge balance is maintained only if negative ions migrate into this region as depicted in the Figure 9(b). Thus, chloride ions tend to accumulate at the electrode surface because they migrate more rapidly than sulfates. The migrated chloride ions increase the dissolution rates of most metals and tends to produce more negative pitting potential than in the chemical mathod. Brigham (6) published an argument against France and Greene's theoretical explanation for the lack of correlation between chemical and electrochemical exposure tests. He presented that the pitting potential for Type 430 stainless steel determined by France and Greene in hydrogen saturated 1M NaCl solution using the potentiostatic technique of 0.05V potential step per 5 minute was lower than the pitting potential if determined in oxygen saturated 1M NaCl. He proposed that their result was misinterpreted by ignoring the fact that the pitting potential varied not only with experimental variables but also with the nature of the gases dissolved in the corrodent as observed by Wilde and William (57). Therefore, he claimed that the chemical and electrochemical techniques would give the same pitting potential when identical conditions were used. Wilde and Williams (72) have presented excellent agreement between two measurements for Type 430 stainless steel in 1M NaCl as shown in Table 5. In the chemical test, a sample is exposed to a hydrogen saturated solution of 1M NaCl containing $K_4Fe(CN)_6$ and $K_3Fe(CN)_6$ to give a chemically induced corrosion potential of -0.100V (SCE). The electrochemical test on the same material is conducted potentiostatically at -0.1V (SCE) in hydrogen saturated 1M NaCl.

Table 5. Weight-loss data on AISI type 430 stainless steel after electrochemical and chemical corrosion tests.

	Type of Test	
	1M NaCl Electrochemical	1M NaCl in H_2O + $[Fe(CN)_6]^{4-}$ + $[Fe(CN)_6]^{3-}$
Solution Temperature	25°±1°C	25°±1°C
Exposure Time	24 hr	24 hr
Specimen Potential	-0.100V_{sce}	-0.100V_{sce}
Corrosion Rate (mpy)	96.4	128
Initial pH	6.3	6.7
Final pH	8.3	6.9
Type of Corrosion	Pitting	Pitting

Source: B. E. Wilde and E. Williams, "On the correspondence between Electrochemical and Chemical Accelerated Pitting Corrosion Tests," J. Electrochem. Soc., Vol. 117, p. 775-779,(1970).

CHAPTER 3

EXPERIMENTAL METHOD

Material

All of the materials used in this investigation were supplied in plate forms (12"x12"x0.065") by Allegheny Ludlum. The chemical analyses are shown in Table 6.

Polarization Test

Specimens, 0.8"x 0.8"x 0.065", of the alloys were subjected to anodic polarization in deaerated 2.5% NaCl solution prepared from reagent grade sodium chloride and distilled water adjusted to different pH(2,4,6) with H_2SO_4. Tests were conducted at room temperature, and at 135^{o}F and 170^{o}F. A brass screw was soldered to each specimen for electrical connection to the potentiostat. The specimen was then mounted in Maraglas epoxy with the screw extending from the back of the mount. After baking at 170^{o}F for 8 hours, the sample was polished using standard metallographic methods through 1 micron, degreased with soap and rinsed with distilled water. In order to prevent crevice corrosion at the specimen/Maraglas interface, the sample was prepassivated in 50% HNO_3 + 50% H_2O at 50^{o}C for 30 minutes. The sample was then carefully removed from the prepassivation solution and the interface at the mount surface was covered with General Electric 1201 Red Enamel (Figure 10) using a small artist brush. The enamel was thinned with solvent and care used that the surface to be painted was dry and clean to prevent crevice corrosion at the enamel/specimen interface. After painting, the specimen was baked for

Table 6. Chemical composition of materials tested.

MATERIAL	CONDITION	%C	%Mn	%P	%S	%Si	%Cr	%Ni	%Mo	%N	%Cu
AL-6X	Cold Rolled Bright Annealed	.020	1.47	.030	.002	.50	20.45	24.65	6.30	.042	–
316L	Cold Rolled Annealed	.022	1.79	.026	.002	.39	17.57	11.12	2.14	–	0.28

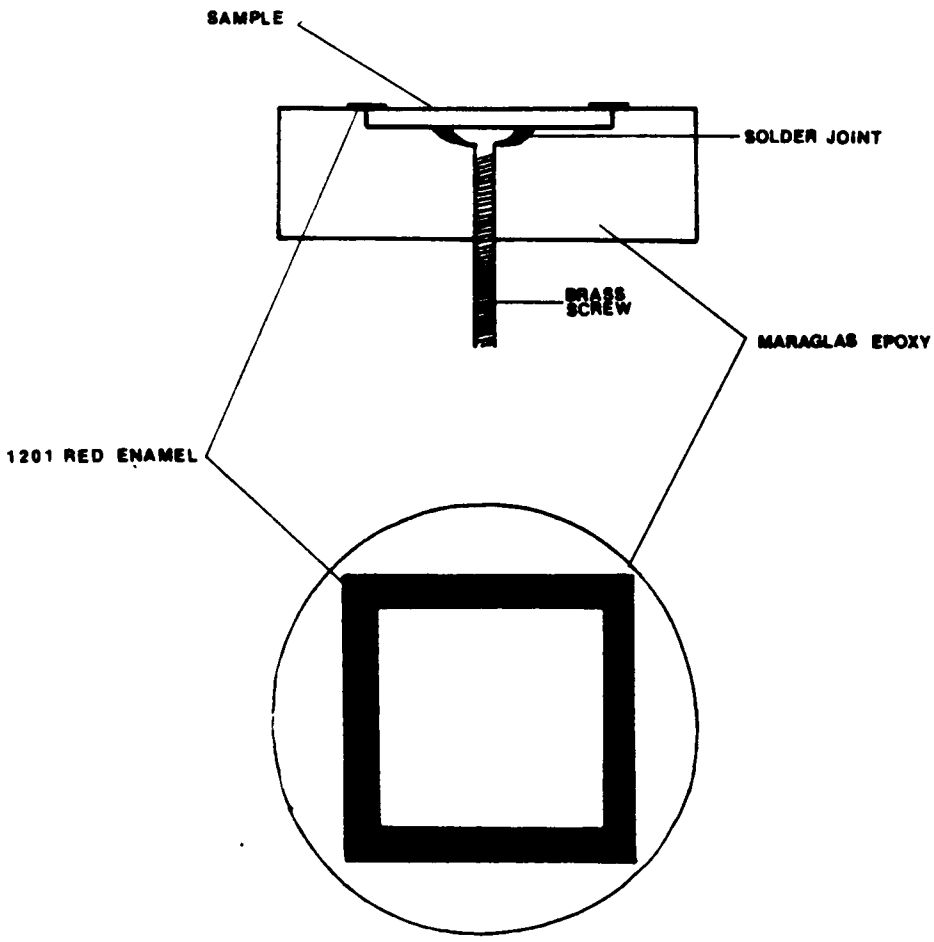

Figure 10. Schematic presentation of sample.

a period of 2 hours at 125°C.

The polarization cell is indicated in Figure 11. A 2-liter Pyrex container was closed by a PVC plate containing several drilled and tapped holes for various electrodes (specimen electrode, platinum auxiliary electrode, Ag-AgCl reference electrode) and to allow auxiliary devices such as a thermometer and sparging tubes to be introduced. Brass screws near the edge of the top were used to compress an O-ring between the top and the flange of the 2-liter vessel, thus sealing off the test cell from the atmosphere. The reference half-cell was a saturated silver-silver chloride electrode contained in a capillary tipped glass tube with the tip positioned about 1-2 mm from the surface of the specimen. The reference electrode was checked with respect to a standard saturated calomel electrode before use in the polarization cell.

The procedure involved the following as required:

(1) introduction of the test solution into the 2-liter polarization cell

(2) setting the temperature of the solution using an Athena controller and heating tape surrounding the cell

(3) deoxygenating the solution with prepurified nitrogen starting 30 minutes before immersion of the specimen and continuous purging during the test

(4) removing the passive film formed during prepassivation using 1 micron cloth and cleaning the specimen by degreasing with soap, rinsed in distilled water, and dried just prior to transferring to the cell

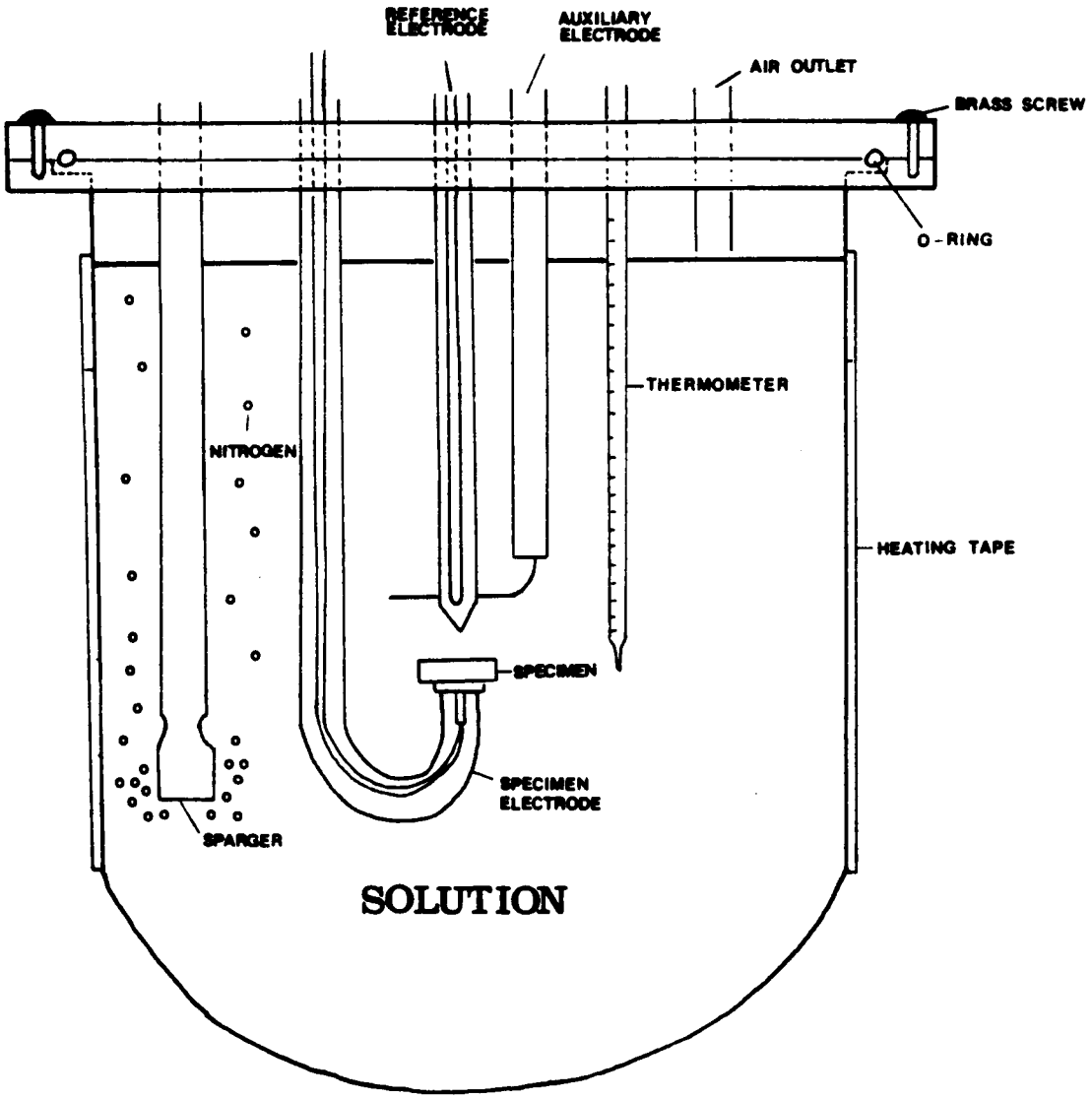

Figure 11. Schematic presentation of polarization cell.

(5) determining the anodic polarization curve by increasing the potential difference between the sample electrode and the Ag-AgCl reference electrode at a scan rate of 2.5 V/hr toward the positive end of the potential scale

The potentiostat incorporated a logarithmic current converter and an X-Y recorder which allowed a direct plot of the polarization curve on a semi-logarithmic paper as potential versus log current per unit area. All potential scans were started from approximately 0.2 V below the open circuit potential.

Ferric Chloride Test

Specimens were cut from the plates into 0.75"x1.5"x0.065" slices, ground flat, and polished to 120 grit. Reagent grade $FeCl_3$-$6H_2O$ was dissolved in distilled water to prepare 1% and 10% ferric chloride solutions. The samples were placed in glass racks (Figure 12) and then immersed in flasks containing 800 ml of test solution after it had reached the desired temperature while placed in a water bath. Tests were done at room temperature, and at 135^{o}F and 170^{o}F; the higher temperatures were maintained at the set point+2^{o}C. Before testing, each sample was degreased by acetone, and dried by methanol. The test period was 30 days for both 1% and 10% $FeCl_3$ at room temperature. At 135^{o}F and 170^{o}F the exposure period was 7 days for both solutions although in some cases, less than 7 days was used.

Comparison of Electrochemical Test with Chemical Test

To determine if correlations can be established between chemical and electrochemical measurements, 316L stainless steel was tested at

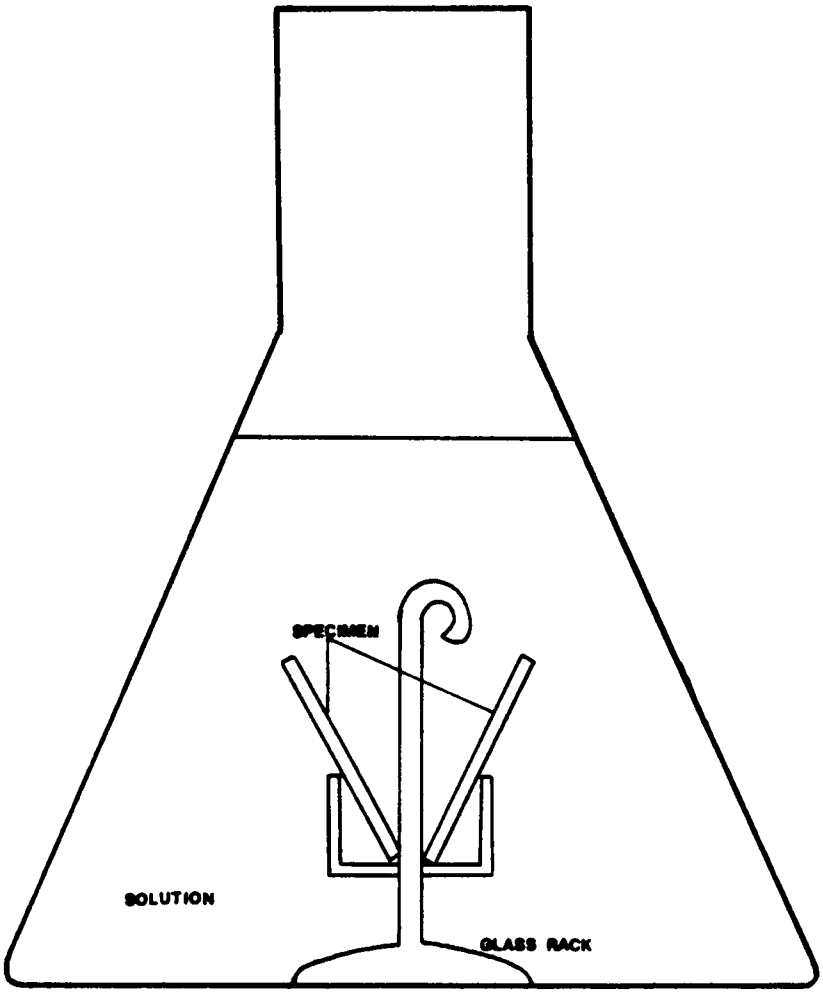

Figure 12. Schematic of immersion test cell.

room temperature in a solution of 10% NaCl adjusted to pH=2 with H_2SO_4. Constant potential and potentiodynamic measurements were conducted using the potentiostat. Corrosion potentials developed by variable concentrations of Fe^{+3} ion were measured with a reference electrode and electrometer. The pitting potential was determined electrochemically by (1) observing the potential at which a rapid increase in current occurred during a continuiously increasing potential using a scan rate of 2.5 V/hr and (2) increasing the potential in 20 mV step every 2 hours until the current increased with time. To dertermine the pitting potential by chemical method, ferric chloride was used as an oxidizing agent. One gram of $FeCl_3$-$6H_2O$ was dissolved in two liters of distilled water and 104.6g NaCl added to the solution to give the same amount of chloride ions as 5% NaCl which has 31940ppm Cl^-. The acidity was adjusted to pH=2 with H_2SO_4. The sample was immersed in the solution and the potential was recorded throughout the test. A decrease in the potential was taken as an indication the onset of the pitting corrosion. If the potential had not decreased within 24 hours, a new solution was used containing a higher concentration of $FeCl_3 6H_2O$ adjusted with NaCl to the chloride ion as a 5% NaCl solution.

CHAPTER 4

RESULTS AND DISCUSSION

Polarization Test

An anodic polarization curve for 316L stainless steel in 1N H_2SO_4 is shown in Figure 13. Alloys that obtain their corrosion resistance from passive film formation exhibit a typical S shaped curve as was shown in Figure 2, page 7. The shape of the anodic polarization curve is affected by the composition, thickness, and physical properties of the film formed on the material on passing from the active dissolution range to the range of passivity. The passive film on stainless steel at ambient temperature is principally Cr_2O_3 (13). The passive film having an epitaxial relationship with the substrates at low Cr content tends toward the amorphous as Cr contents increase (12). Since the mobility of ions is less in glasses than in crystalline structures containing defects and grain boundaries, the corrosion resistance increases with higher Cr contents. In terms of the potentiodynamic anodic polarization curve, good corrosion resistance is characterized by low value of the critical current density (i_{crit}), the passive current density (i_{pass}), and the primary passivation potential (E_{pp}). Good corrosion resistance is also characterized by a high value of the pitting potential (E_p). The pitting potential is the potential where a sudden increase in current occurs indicating a breakdown of a passive film and formation of pits on the surface of the test specimen in the presence of aggressive anions such as chloride ions. In Figure 13, the current increase of 316L stainless steel near 1.2 V (SHE) represents

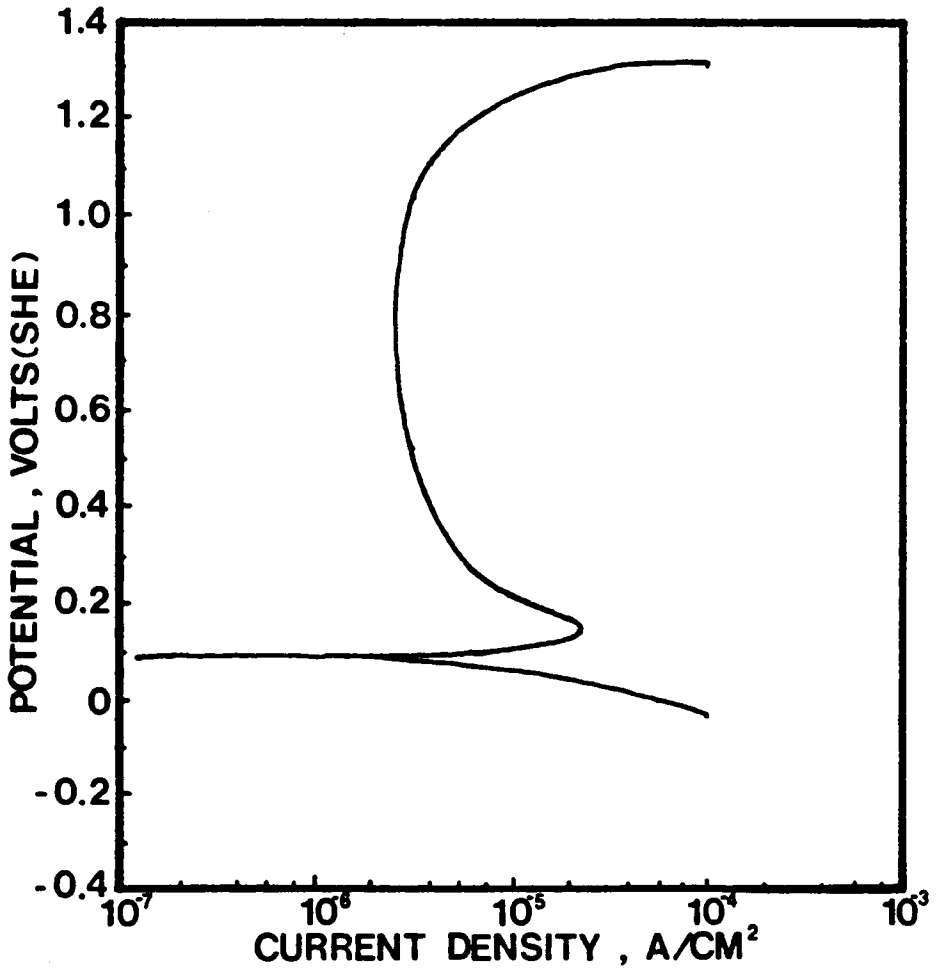

Figure 13. Potentiodynamic polarization curve for 316L stainless steel in 1N H_2SO_4 at room temperature.

the onset of transpassivity where the passive film is anodically oxidized to $HCrO_4^-$ ion so that general dissolution occurs. The increase in current is also due to evolution of oxygen by the electrolysis of water (16).

Anodic polarization data was obtained by a potentiodynamic scanning method using a 2.5 V/hr scan rate. The potential scan rate is defined as the rate at which the applied potential is linearly increased with time. Scanning rate has been found to have a considerable influence on the pitting potential (37,67-68,73). Inconsistency in the observations, however, leads to difficulty in establishing a general behavior of scan rate effect on pitting potential. Leckie (73) found that increasing scan rate resulted in a shift in the pitting potential in the positive direction. This behavior is explained by incubation time considerations (67). Since pit initiation occurs after an incubation time at a certain potential, the higher pitting potential is observed with higher scan rate due to allowing limited induction time at a given potential. Bond and Lizlovs (37) observed the oposite result of Leckie's. They explained that the slower scan rate allows time for film thickening to occur which causes a larger fraction of the metal-solution potential difference to be within the film and, thereby, not at the film/solution interface to assist the entry of chloride ions into film. Manning (68) concludes that the effect of the potential scan rate on the pitting potential varies with the material examined. If a material can form a stable passive film within a short time, it shows a higher pitting potential with a higher scan rate because of limited induction time for pit

initiation; otherwise, it shows a lower pitting potential due to less time for film development during the anodic sweep. However, Pessall and Liu (62) ascribed the differences in experimental results not to the potential scanning rate, but to the mode of preparation of the electrode surface. According to their findings, the pitting potentials for mechanically polished surfaces should be essentially independent of the potential scanning rate, as opposed to electropolished or etched surfaces where such dependence could be found.

In the present study, the pitting potential of 316L stainless steel was observed to decrease by increasing the scan rate as shown in Figure 14. This is interpreted as indicating that the passive film was thicker the slower the scan rate. Consistent with this interpretation is also a lower passive current with a lower scan rate (Figure 15). It is concluded that the slower scan rate gives a more useful value for the pitting potential since it allows enough time for pit initiation at a given potential. However, when a slower scan rate is employed, materials usually fail by crevice corrosion during the test as has been observed by other investigators (32,37,74). As a consequence it is very difficult to prevent crevice corrosion during pitting tests. Because of this difficulty, considerable time was spent during the present research to more clearly define the conditions under which crevice corrosion occurs such as to prevent observations of the pitting potential and the nature of pitting. In fact, with alloy/environment combinations which are extremely susceptible to crevice corrosion, the question arises as to whether or not the pitting charactersitics can be investigated because of the

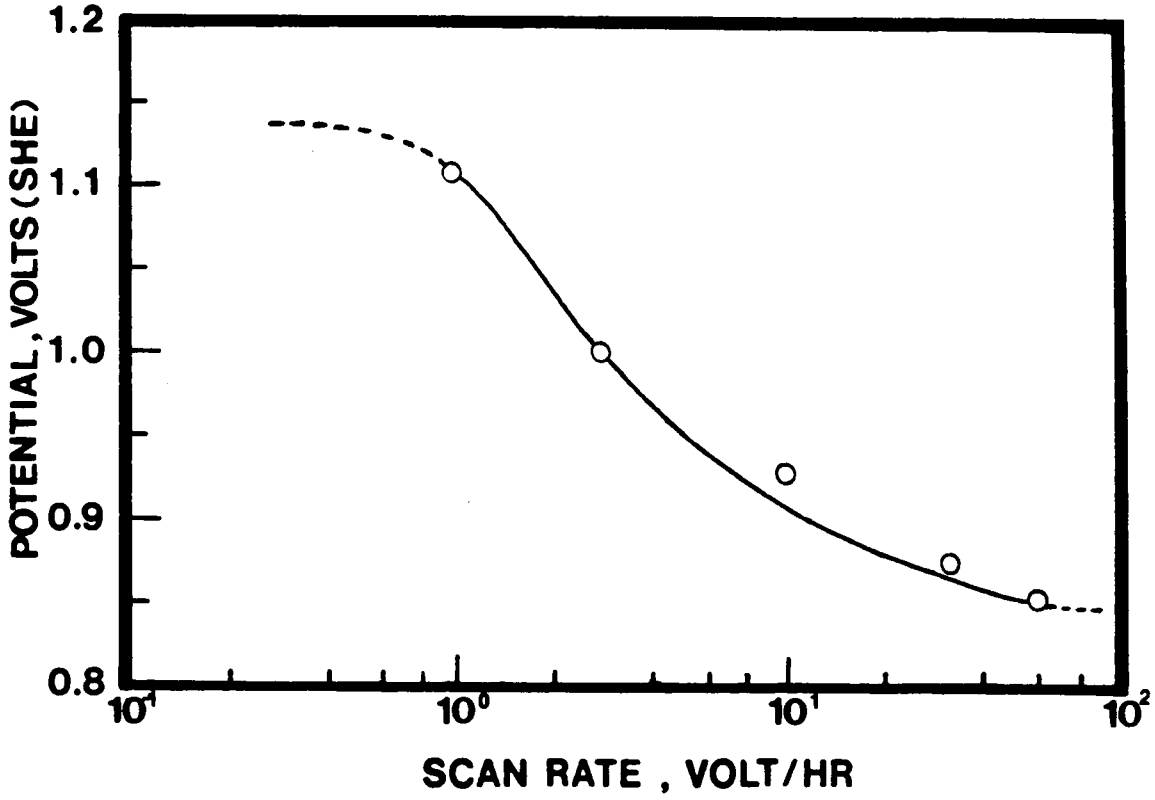

Figure 14. Effect of potential scan rate on the pitting potential of 316L stainless steel in 2.5% NaCl adjusted to pH=2 at room temperature.

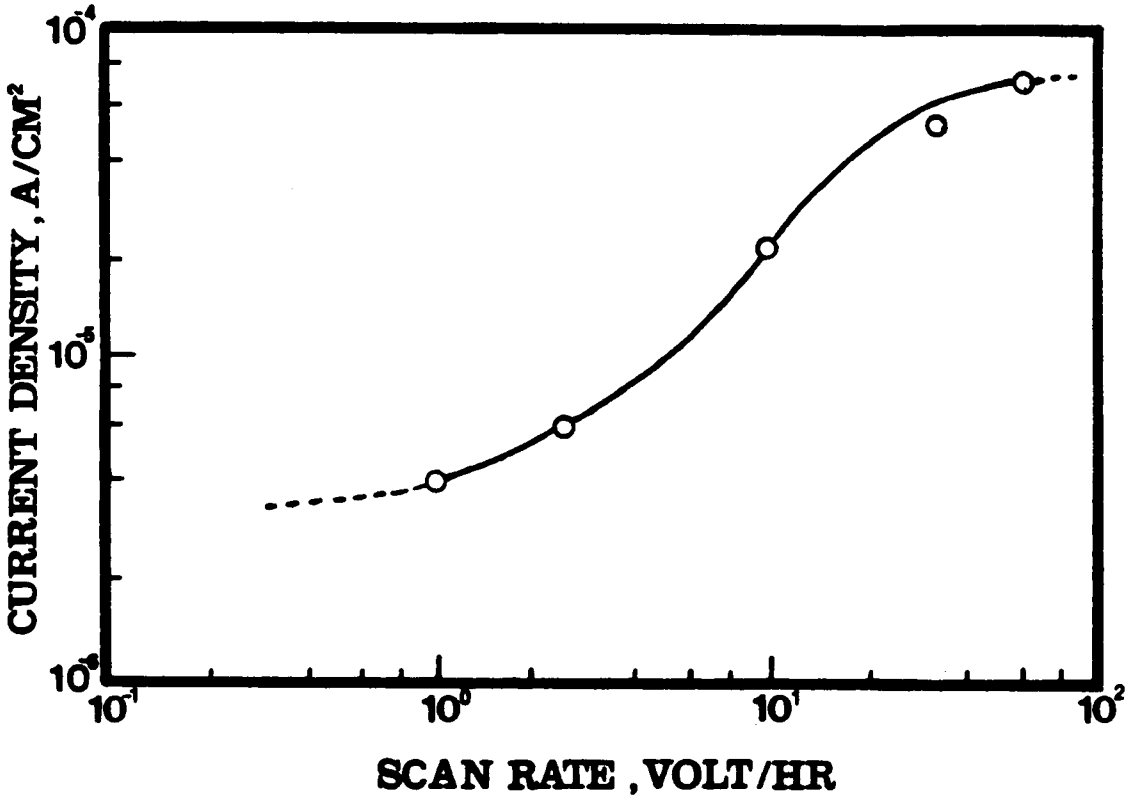

Figure 15. Effect of potential scan rate on the passive current density of 316L stainless steel in 2.5% NaCl adjusted to pH=2 at room temperature.

interferring crevice corrosion.

Maraglas 655, an epoxy casting material made by ASME Chemical and Insulation Co, was employed to mount most of the specimens in this research. This epoxy is easy to use, readily coats the specimen because of its low viscosity and, on curing, yields void free castings. Although the epoxy exhibits good resistance to most chemicals and has good adhesion to wide variety of materials, problems were encountered in this research due to very narrow crevices at the epoxy/metal interface which serve as sites for crevice corrosion. Figure 16 shows the type of polarization curve for 316L stainless steel which results when crevice corrosion occurs at the interface before pitting corrosion occurs on the specimen surface. Comparison will be made between this curve and the polarization curve without occurrence of crevice corrosion. Figure 17 is an example of failure by crevice corrosion at the interface between the metal and epoxy before pitting corrosion occurred. Other epoxies such as the Stycast 2850FT and Eccobond 1760 were used for mounting instead of Maraglas but they were less satisfactory.

The problem just described led to investigation of specimen mounting methods which would avoid occurrence of crevice corrosion and thus permit correct estimates of the pitting potential. Manning et al. (46) used a specimen supporting configuration consisting of a platinum wire platform on which the specimen, by its own weight, created a three point contact as shown in Figure 18. They observed no crevice corrosion at the platinum/specimen contact points. In their experiment, they prepared two kinds of sheet specimens, one

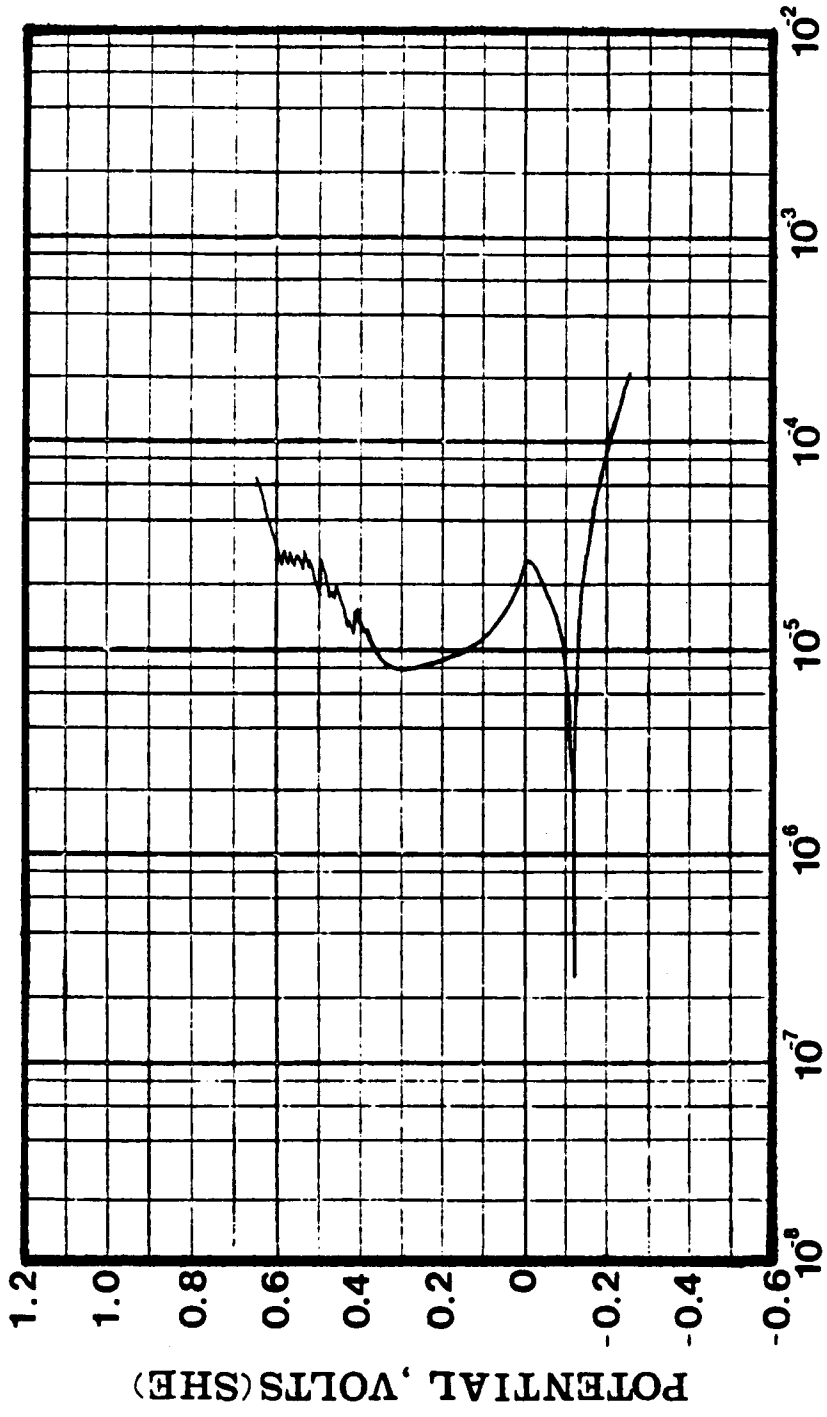

Figure 16. Polarization curve for 316L stainless steel indicating the onset of crevice corrosion in 2.5% NaCl solution adjusted to pH=2 at room temperature.

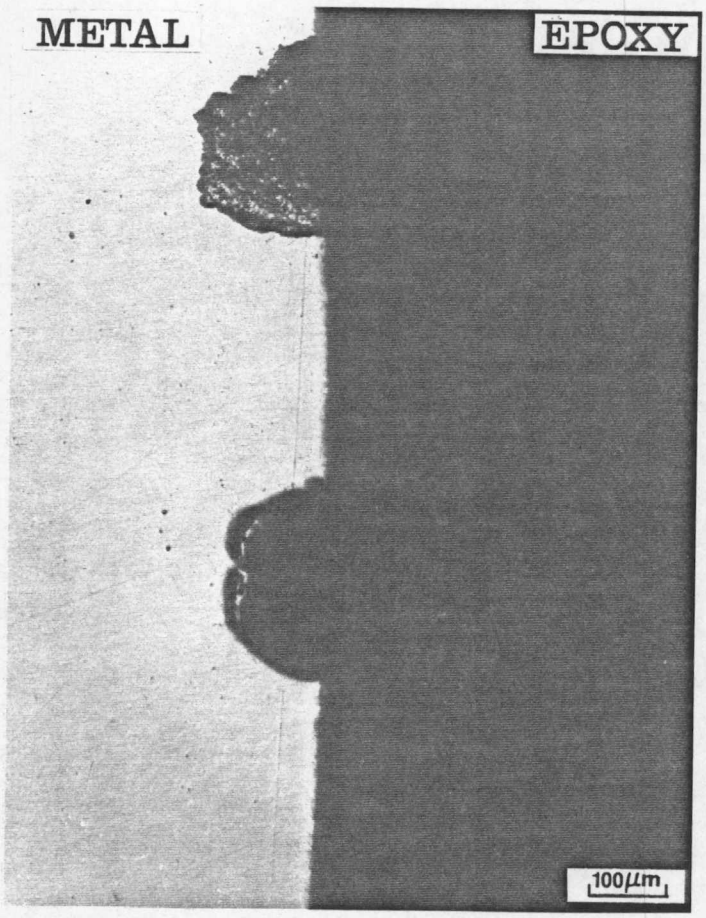

Figure 17. Sample failed by crevice corrosion at the interface between the metal and the epoxy.

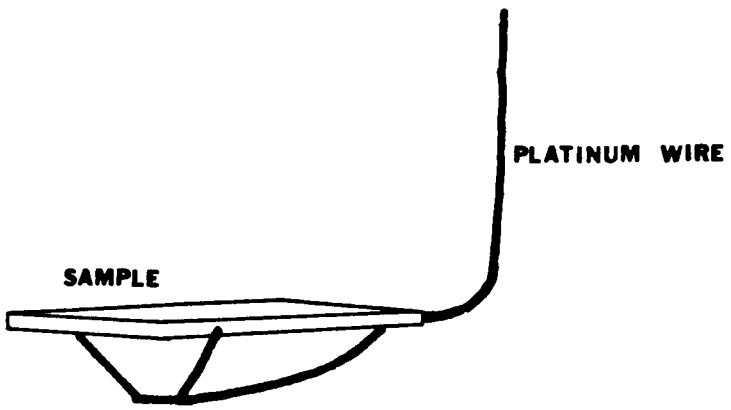

Figure 18. Specimen holder used in pitting corrosion test.

Source: P. E. Manning et al., "The Effect of Test Method and Surface Condition on Pitting Potential of Single and Duplex Phase 304L Stainless Steel," Corrosion, Vol. 35, p. 151-157,(1979).

prepassivated in 50% HNO_3 + 50% H_2O at 50°C for 30 minutes and one without the prepassivation treatment. The prepassivated sample was carefully removed from the prepassivating solution and lightly abraded on both rolling surfaces using 600 grit paper with care being applied to retain the passive film along the edges. These two procedures were investigated because of the frequent observation that pitting corrosion is much more severe at edges for most alloys since edges expose larger numbers of inclusions which serve as sites for pitting corrosion initiation. When edge pitting corrosion occurs and no pits are formed away from the edges, it is impossible to know whether the pitting potential applies only to the edges and therefore is not a measure of the pitting behavior of the major surface in the given environment. Therefore, special care is required in interpreting electrochemical measurements on unmounted specimens.

The three wire support method of Manning(46) just described was tried but the configuration created problems of inserting the sample into the polarization cell and was generally unsatisfactory. An alternative method was tried in which a platinum wire was spot welded to the specimen as shown in Figure 19. AL6X was polarized at 170°F in a solution of 2.5% NaCl adjusted to pH=2 with this assembly. Pitting corrosion occurred at the welded region due to the weld heating cycle and to crevices created by the welded wire. Also, as shown in Figure 20, AL6X failed by pitting corrosion on the edge of the material but not on the major surface. Therefore, even if pitting corrosion had not occurred on the welded region, the pitting potential would be a measure of the pitting tendency of the edges, and while

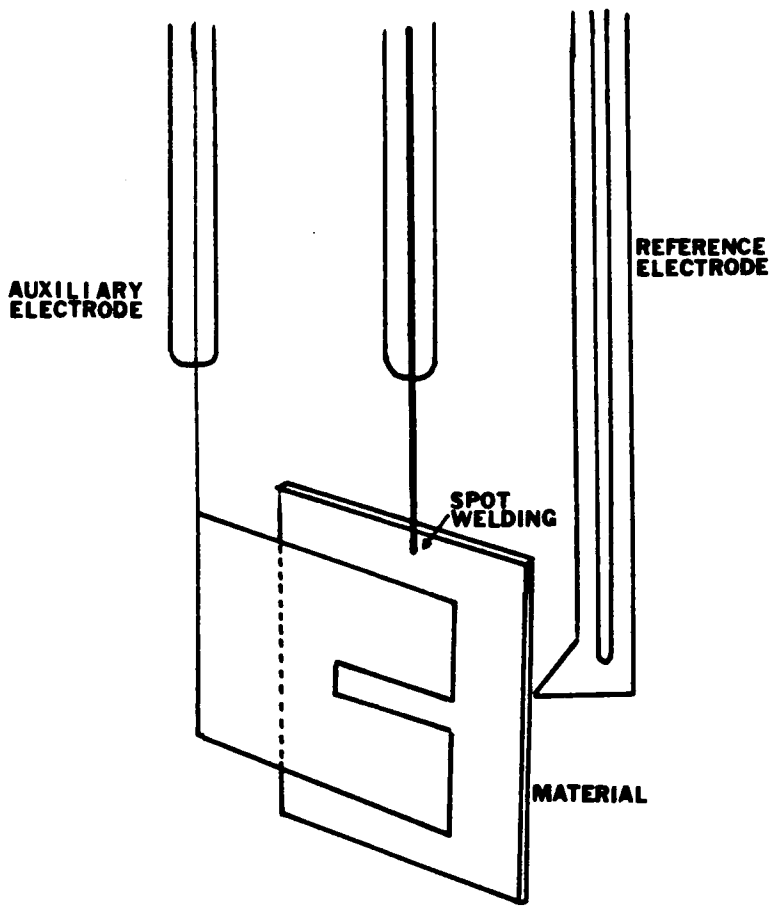

Figure 19. Specimen holder for unmounted samples.

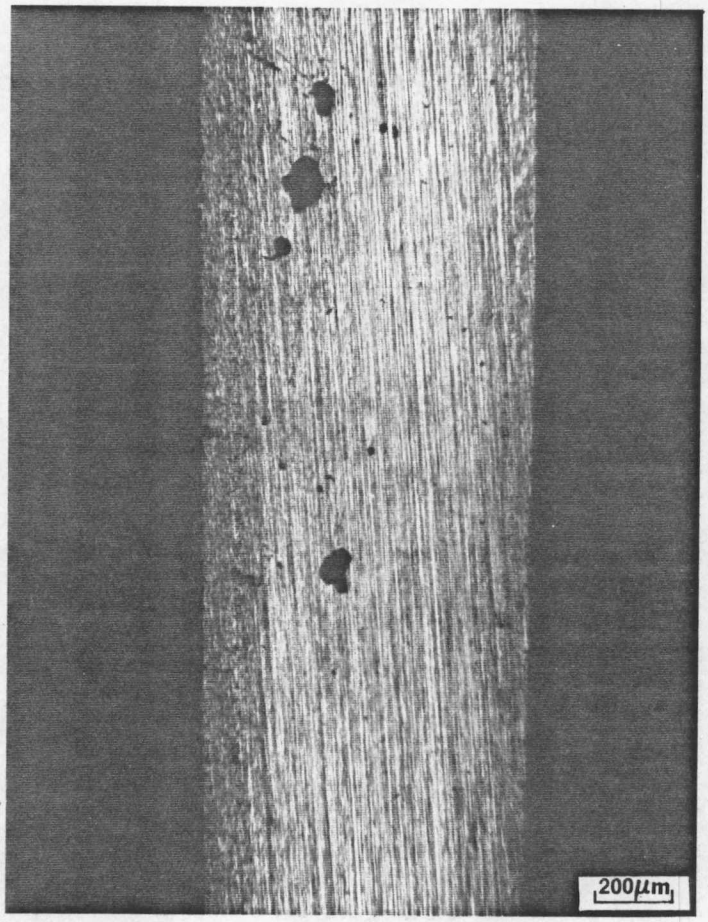

Figure 20. Pits on the edge of an unmounted sample of AL6X in 2.5% NaCl solution adjusted to pH=2 at 170°F.

this is of practical significance, it masks the pitting tendency of the flat surface. Another technique involved uses of electroplaters tape placed over the surface of the maraglas and specimen with a one square centimeter opening to the metal surface. Crevice corrosion did not occur if the test was done in a short time and at room temperature. For longer times and at elevated temperatures, however, the electroplaters tape become detached sufficiently to produce a gap which served as a crevice.

The best results were obtained when the sample was prepassivated in 50% HNO_3 + 50% H_2O at 50°C for 30 minutes before painting across the metal/epoxy interface with General Electric 1201 Red Enamel. Crevice corrosion always occurred at the enamel/metal interface of non-prepassivated samples when the surface was finished with 600 grit paper and frequently occurred on surfaces polished with 1 micron diamond. Figure 21 shows a sample, finished with 600 grit paper, with crevice corrosion at the specimen/paint interface after removing the paint by acetone. A sample ground with 600 grit paper has small peaks and valleys as shown in Figure 22 (46). These irregularities produce crevices where the paint fails to flow into the depressions in the surface. On the assumption that part of the problem was the absence of any passive film under the paint prior to polarization, samples prepared with the 600 grit finish and 1 micron diamond polish were prepassivated in the 50% HNO_3 + 50% H_2O at 50°C prior to coating across the interface with enamel. After coating, the samples were briefly but carefully polished with one micron diamond to remove the passive film from the surface but allow it to remain under the paint.

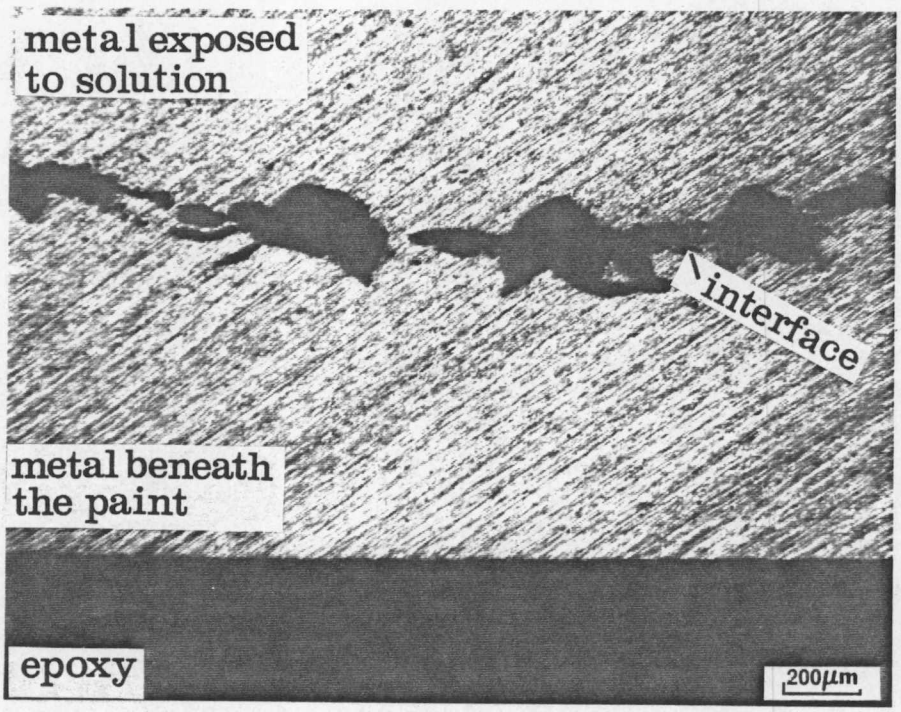

Figure 21. Photograph showing crevice corrosion occurred at the interface between the metal and the paint.

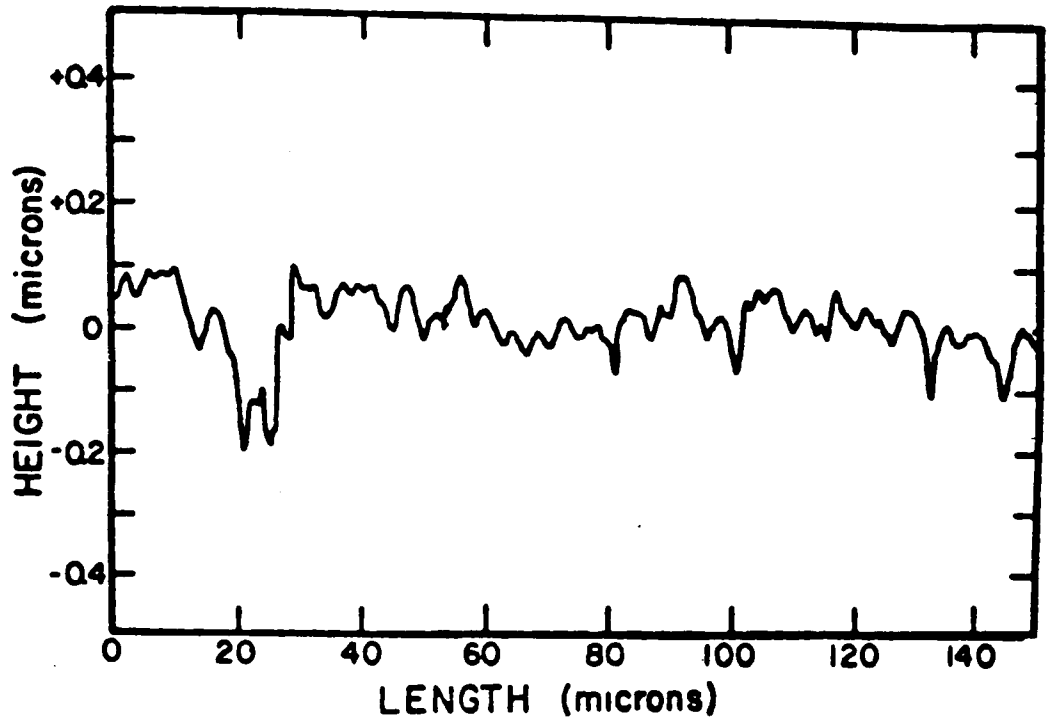

Figure 22. Profilometer traces of specimens mechanically polished to 600 grit paper.

Source: P. E. Manning et al., "The Effect of Test Method and Surface Condition on Pitting Potential of Single and Duplex Phase 304L Stainless Steel," Corrosion, Vol. 35, p. 151-157, (1979).

Significantly, this procedure generally eliminated crevice corrosion on samples prepared by either method.

The above observations led to a re-examination of the mechanism of crevice corrosion, particularly how it is initiated. During an up-scan starting at the corrosion potential in the active region, metal dissolution occurs with a relatively high corrosion rate on the entire surface until the passive film forms. The metal ions dissolved from the bulk surface spread out to the bulk solution. But inside the crevice, the accumulation of metal ions occurs due to the restricted fluid condition, resulting in an increase in the acidity by the reaction,

$$Me^{+n} + H_2O \rightarrow Me(OH)^{+(n-1)} + H^+$$

Crevice corrosion occurs when the acidity reaches the minimum value for the breakdown of the passive film. However, if the sample is prepassivated before painting, the metal dissolution rate is very low and the above reaction is restricted. Therefore, the conditions favorable for crevice corrosion are greater for non-prepassivated samples.

Since crevice corrosion occurs at much lower potentials than the pitting corrosion in a given alloy/environment combination and most materials are very susceptible to crevice corrosion, a conclusion of this research is that many reports of pitting potentials in the literature are actually potentials for crevice corrosion at the interface between the specimen and the mounting material. For example, Bandy and Rooyen (39) reported that pitting corrosion occurred on AL6X at 0.2 V (SCE) in deaerated 1N NaCl + 0.5N HCl at 50^{o}C as shown in

Figure 23. To confirm that the sample preparation developed in the present study results in a higher pitting potential than reported by Bandy and Rooyen, a sample of AL6X was mounted, prepassivated in 50% HNO_3 + 50% H_2O at 50^{o}C for 30 minutes and painted. With this specimen preparation, pitting corrosion was not observed up to 1.2 V (SHE) as shown in Figure 24. Thus, it appears that these authors are reporting the crevice corrosion potential instead of the pitting potential.

As known, pitting corrosion is observed most often in the presence of chloride ions. The aggressive action of chloride ions stimulating the formation of pits is displayed only at potentials more positive than a certain critical value. The critical value is called the pitting potential (E_p) which is usually determined by electrochemical measurements. The polarization curve of 316L stainless steel obtained in a solution of 2.5% NaCl adjusted to pH=2 at room temperature is shown in Figure 25. The curve ABCDE on Figure 25 shows the dependence of the metal's dissolution rate on the potential. When a certain potential is reached (marked D), pits form on the surface and the dissolution rate increases rapidly in accordance with DE. If a crevice is formed or exists on the sample, the current density increases at a much lower potential than the potential, D, due to the occurrence of crevice corrosion as was shown in Figure 16. Figure 26 shows the pit formed on 316L stainless steel after the current increased; it shows the sharply defined hole which is frequently observed to be in the passive film spreading over a much larger underlying pit. Concentric rings of stain occur near the pit but there is a lack of attack on the most of tha metal surface. In Figure 27,

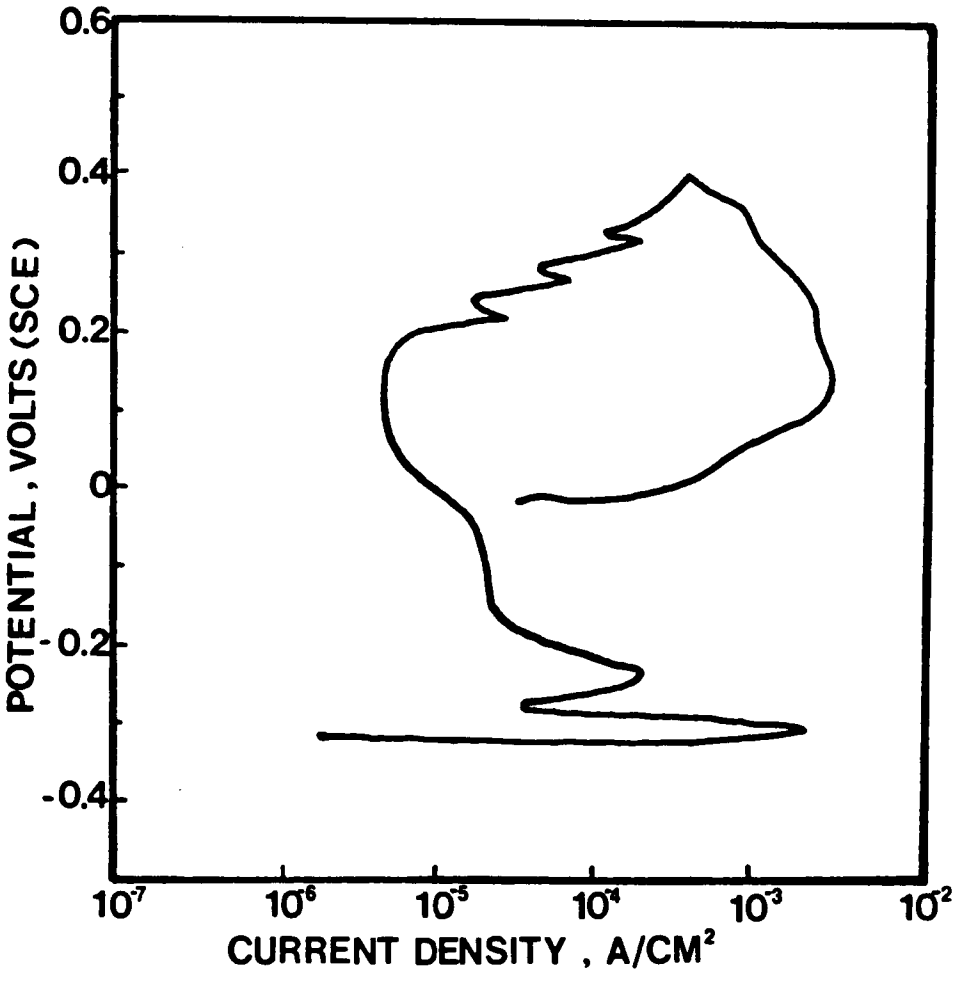

Figure 23. Anodic polarization curve for AL6X in deaerated 1N NaCl+0.5N HCl at 50°C.

Source: R. Bandy and D. Van Rooyen, "Pitting Resistant Alloys in Highly Concentrated Chloride Media," Corrosion, Vol. 39, p. 227-236,(1983).

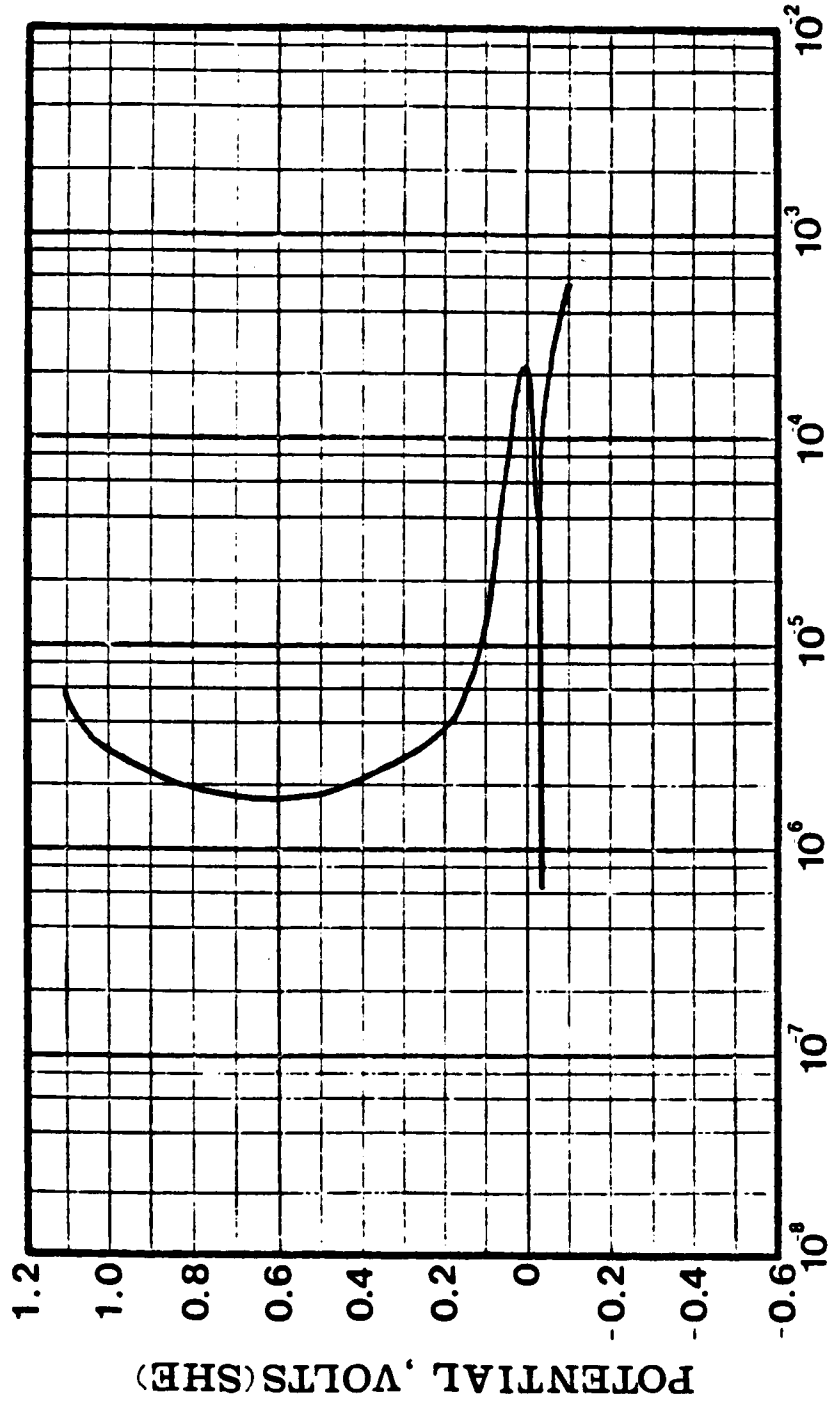

Figure 24. Polarization curve for AL6X showing no pitting corrosion in deaerated 1N NaCl+0.5N HCl at 50°C.

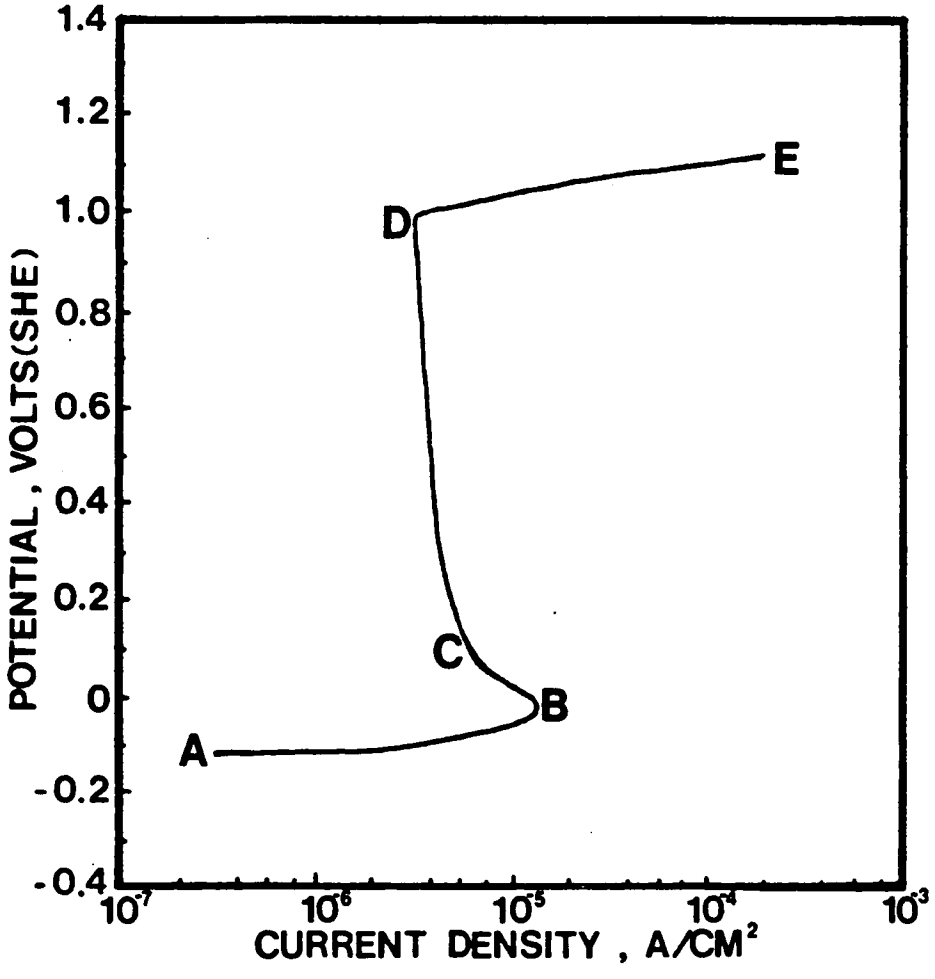

Figure 25. Anodic polarization curve for 316L stainless steel in deaerated 2.5% NaCl solution adjusted to pH=2 at room temperature.

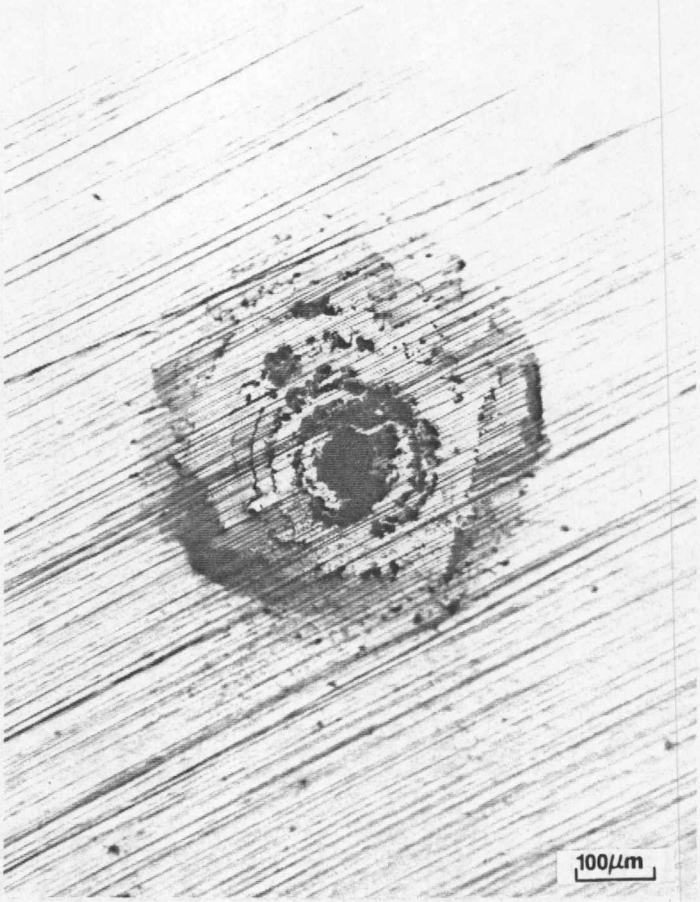

Figure 26. Pit formed in 316L stainless steel after polarization in 2.5% NaCl solution adjusted to pH=2 at room temperature.

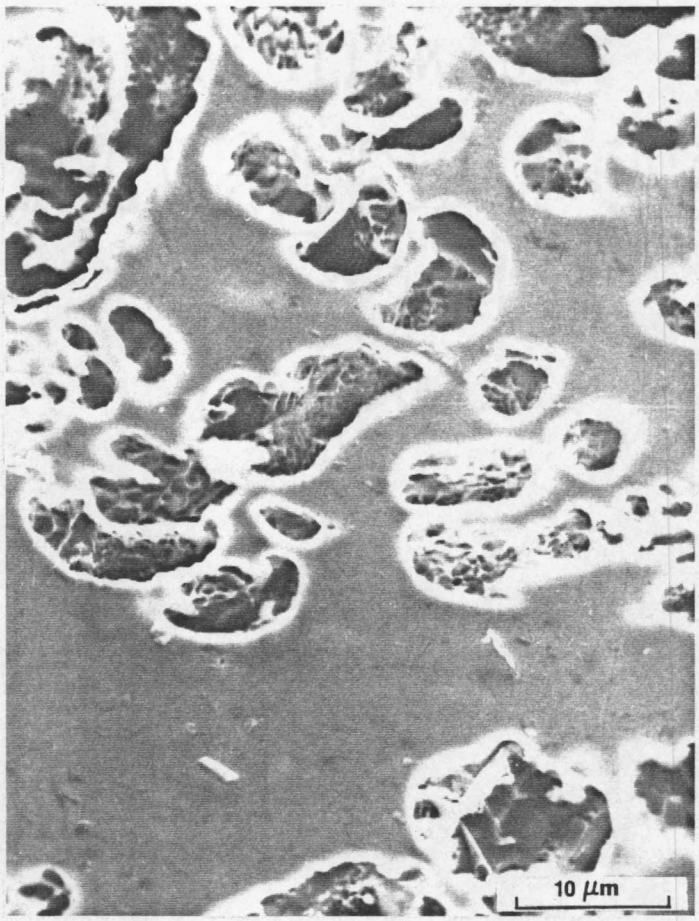

Figure 27. SEM photograph showing inside of the pit.

tiny pits are shown inside the large pit. It appears that some pits can form, reach a critical stage, perhaps associated with rupture of the passive film covering it, and then on contact with the solution, repassivate partially but remain with many smaller pits forming as shown.

The critical potential of pitting formation (pitting potential, E_p) is a very important characteristic both for understanding the nature of the process and for finding effective methods of protection against pitting corrosion. The value of this potential greatly depends both on the nature of the metal or alloy and on the nature and concentration of the aggressive anion. Polarization curves of 316L stainless steel were determined in different chloride ion concentrations. Figures 28 and 29 show that the addition of chloride ion has little effect on the primary passivation potential and the passive current but the pitting potential is lowered with increasing chloride ion concentration as shown in Figure 30. Small differences in microstructure, composition and physical condition of the surface of each sample and slight changes in the diffusion condition of reactive species cause modifications in the rates of the reactions involved at the surface. As a result, differences in the pitting potentials of samples of the same alloy are expected and, indeed, observed. Thus, when the scattering of the pitting potentials is unavoidable, a single value cannot be considered representative of the examined system. In this study, the mean value of the pitting potentials was used.

Figure 31 shows the dependence of the critical current density on the chloride ion concentration. When the sodium chloride concentration

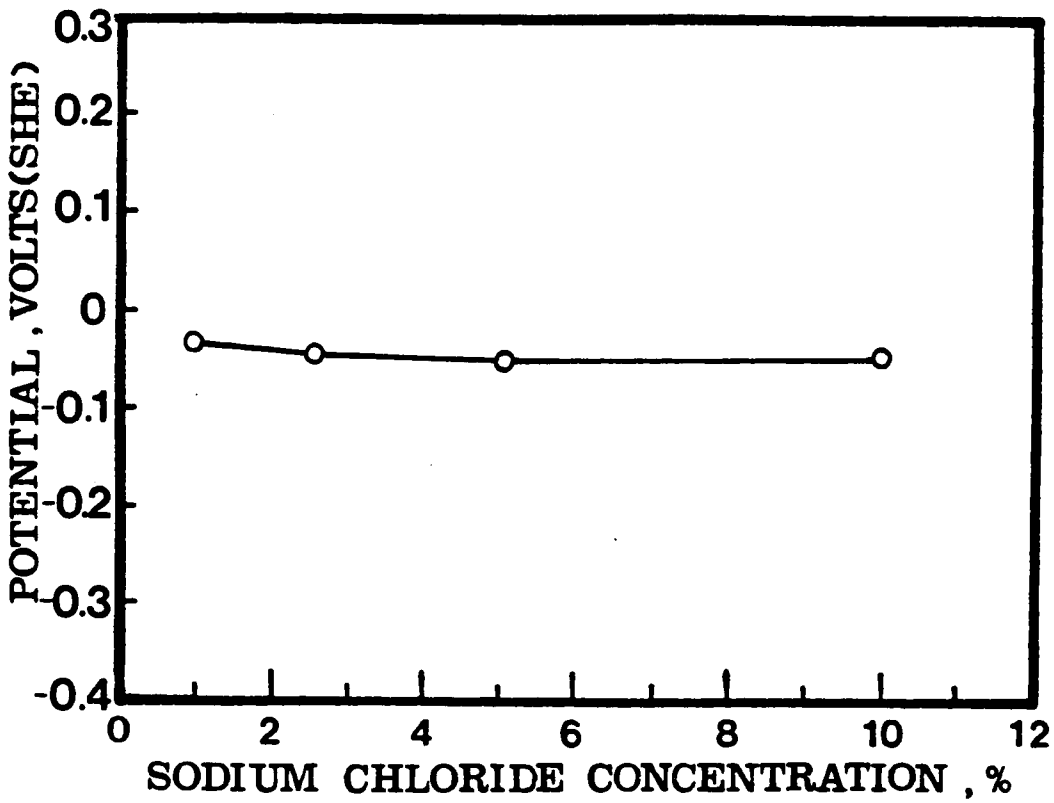

Figure 28. Effect of chloride ion concentration on the primary passivation potential of 316L stainless steel with pH=2 at room temperature.

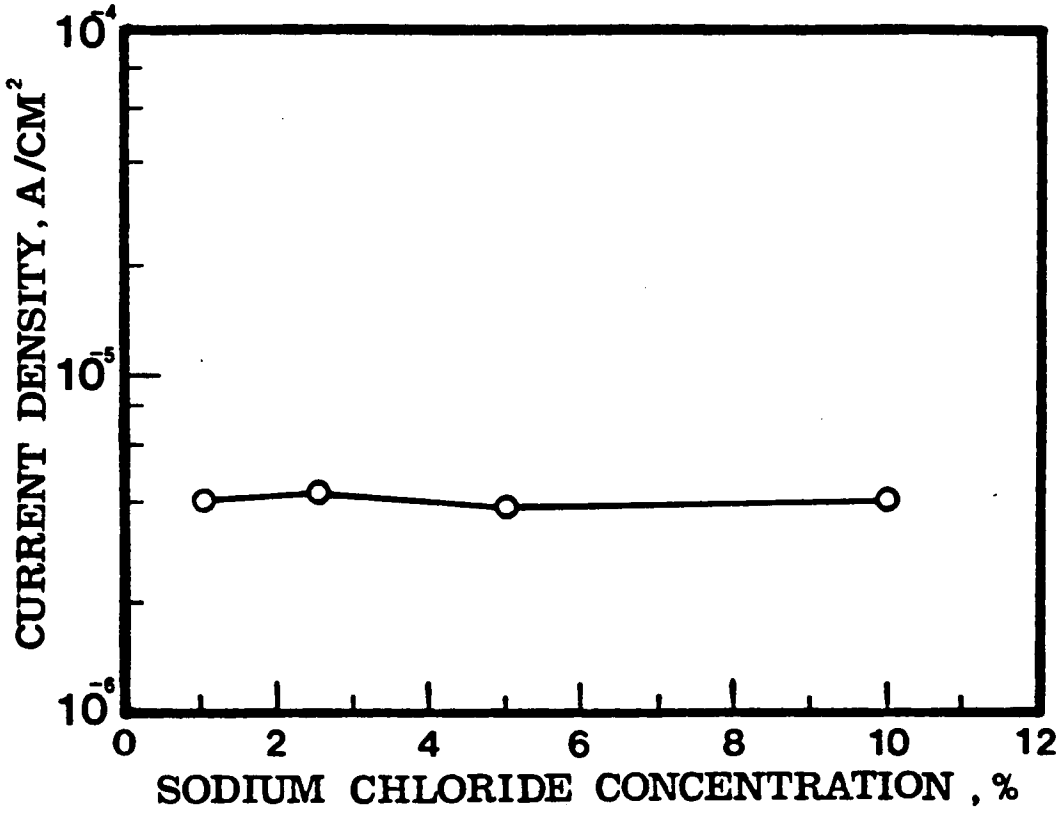

Figure 29. Effect of chloride ion concentration on the passive current density of 316L stainless steel with pH=2 at room temperature.

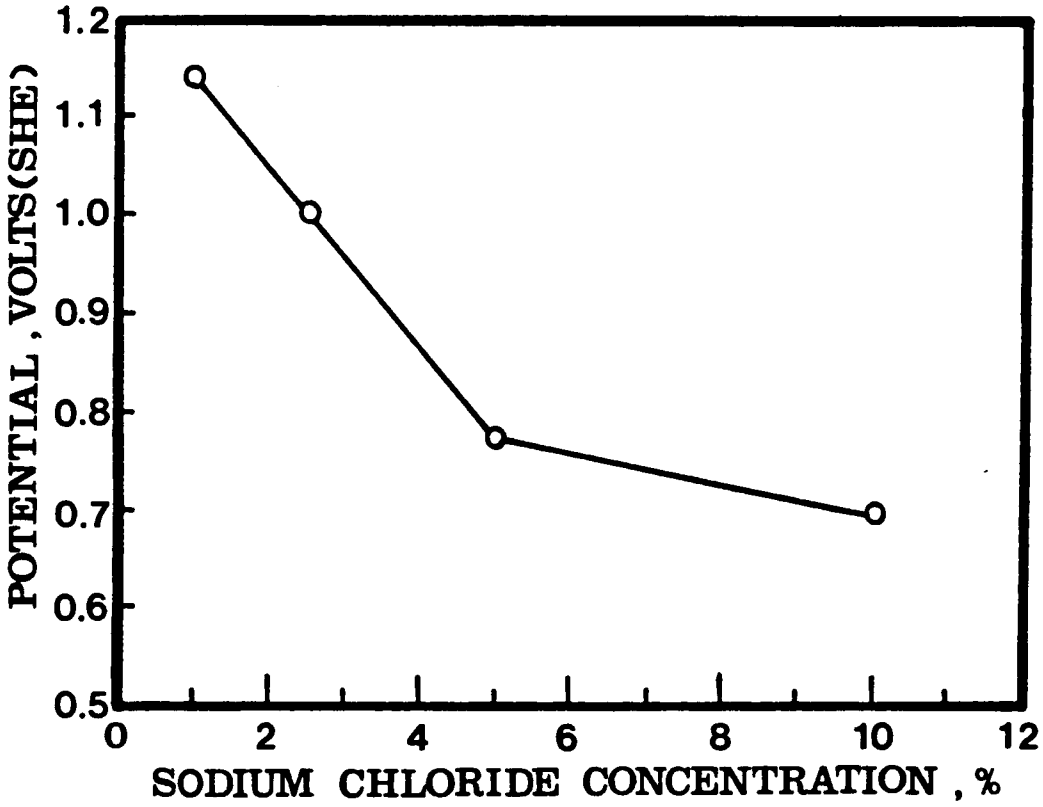

Figure 30. Effect of chloride ion concentration on the pitting potential of 316L stainless steel with pH=2 at room temperature.

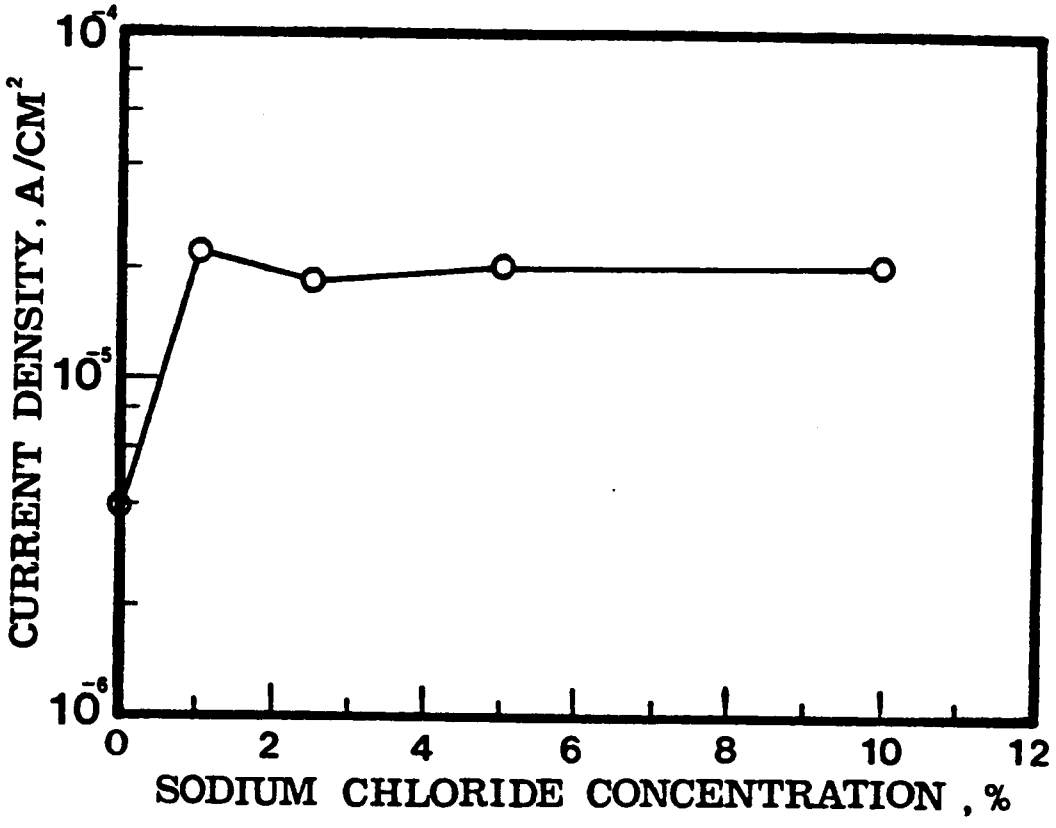

Figure 31. Effect of chloride ion concentration on the critical current density of 316L stainless steel with pH=2 at room temperature.

increased from 0% to 1%, the critical current density increased from 4×10^{-6} A/cm^2 to 2×10^{-5} A/cm^2 but did not change significantly at the higher chloride ion concentrations. There is considerable uncertainty in the literature relating to the effect of chloride ions on the value of the critical current density. It appears, however, that one reason for this uncertainty is associated with the experimental procedure followed in determining the polarization curve. One factor is that a reproducible critical current density is measured only for scan rates less than some limiting value. Another factor, which does not appear to have been recognized, is a possible effect of the potential from which the scan is initiated. For example, the anodic polarization curves for 316L stainless steel in nitrogen sparged 5% NaCl adjusted to pH=2 at room temperature were determined starting at two different potentials with the result shown in Figure 32 as curves A and B. Curve A represents an upscan initiated after the open circuit (corrosion) potential was established at a stable value. Curve B is the result of an upscan initiated at -0.3 V (SHE) following cathodic cleaning at -0.8 V (SHE) for 1 minute. It is evident that the measured critical current density determined after the cathodic pretreatment is higher. Explanations for the larger value in the latter case include effects of surface cleaning by the cathodic pretreatment and/or the presence of hydrogen on the specimen surface.

In order to more clearly define the influence of the several variables apparently influencing the polarization curve in the potential range from cathodic pretreatment through the passivating potential, the above determinations were repeated with some added

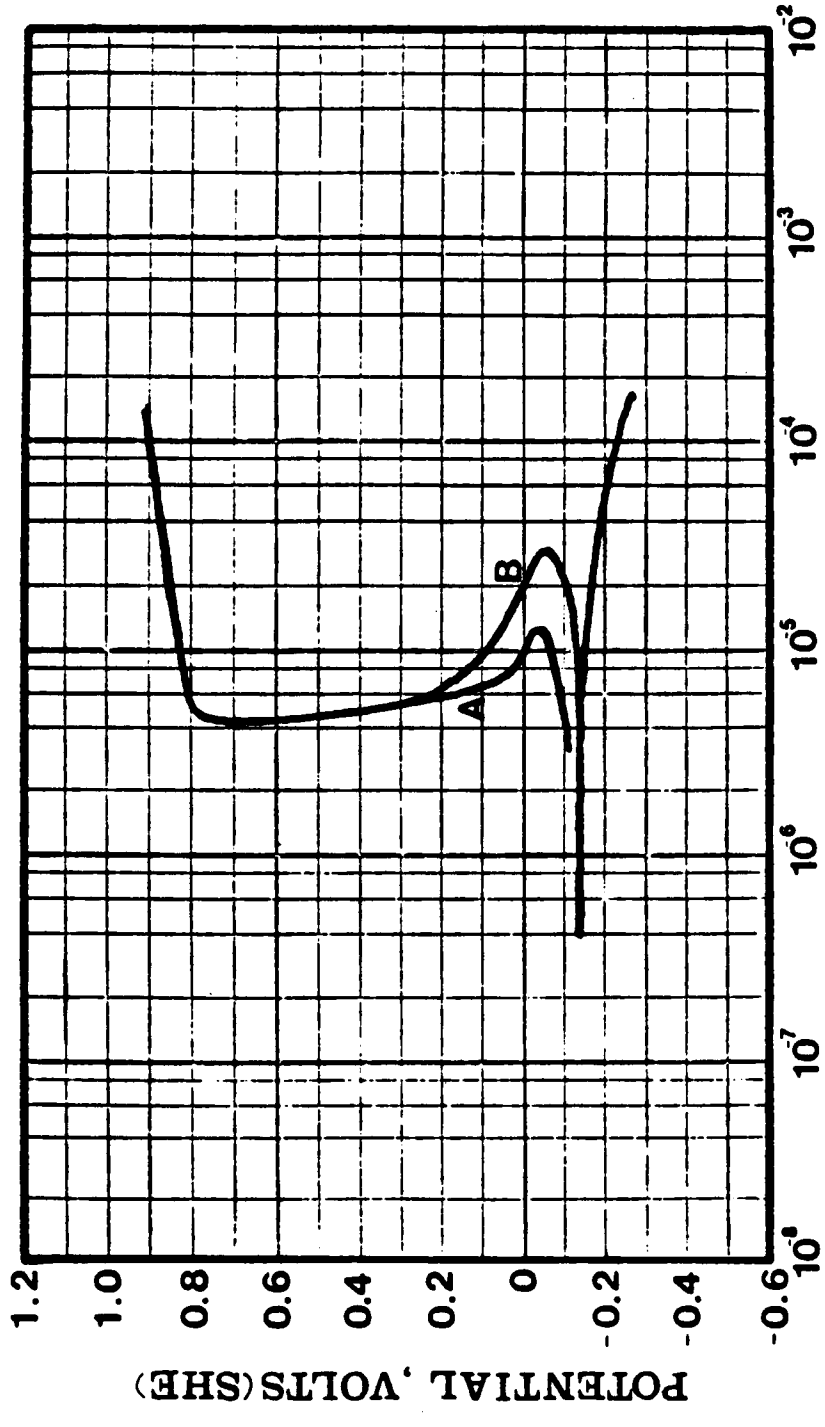

Figure 32. Effect of test method on the critical current density of 316L stainless steel in 5% NaCl solution adjusted to pH=2 at room temperature.
A: upscan from the open circuit potential with N_2 sparging
B: upscan from the cathodic region with N_2 sparging

variations. Since slight variations in a polarization curve had been noted when different samples of the 316L stainless steel were used, in the following experiments the same sample was used but with repolishing through 600 grit paper prior to each determination. The results are shown in Figure 33. Curve C results from an upscan from the corrosion potential with nitrogen sparging, agreement with Curve A of Figure 34 is good. Curve D is an upscan from a cathodic potential of -0.3 V (SHE) while nitrogen sparging; this curve agrees with Curve B of the previous figure. Curve E is an upscan from -0.3 V (SHE) while sparging hydrogen through the cell. There is good agreement with Curve D except in the early passive region where the current density is slighly higher for Curve D and both of these curves show a higher current density at the anodic current density maximum than for the upscan from the corrosion potential with a nitrogen sparge, Curve C. A final curve was determined by re-establishing the steady state corrosion potential while nitrogen sparging and then conducting a down scan to record the cathodic branch of the polarization curve, Curve F.

In addition to the difference in critical current density noted above, it is evident that the steady state corrosion potential of Curves C and F is slightly higher than the dynamic corrosion potential shown by Curve D and E. It is observed however that the cathodic polarization curves are essentially identical below about -0.15 V (SHE).

In order to better understand the hydrogen reaction in the cathodic potential region where hydrogen gas is evolved and the

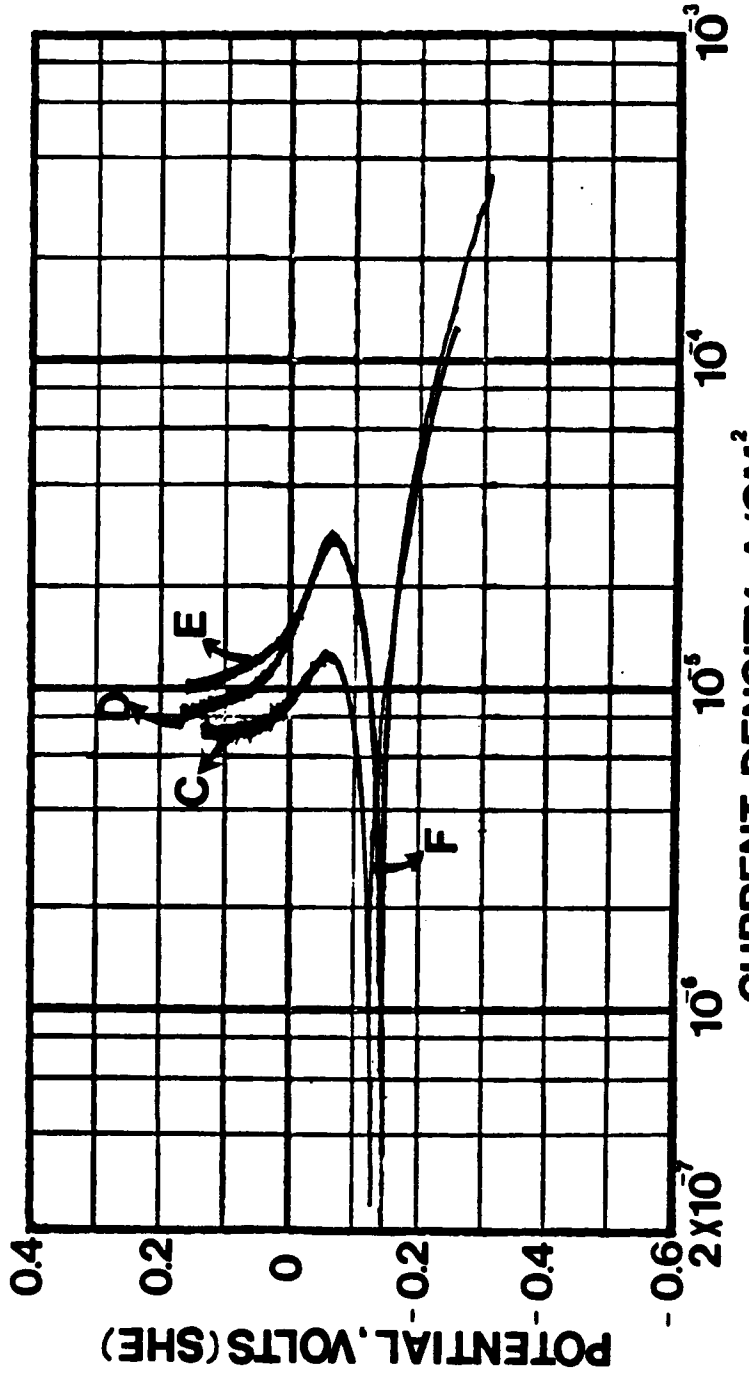

Figure 33. Effect of test method and dissolved gas on the critical current density of 316L stainless steel in 5% NaCl solution adjusted to pH=2 at room temperature.
C: upscan from the open circuit potential with N_2 sparging
D: upscan from the cathodic region with N_2 sparging
E: upscan from the cathodic region with H_2 sparging
F: downscan from the open circuit potential with N_2 sparging

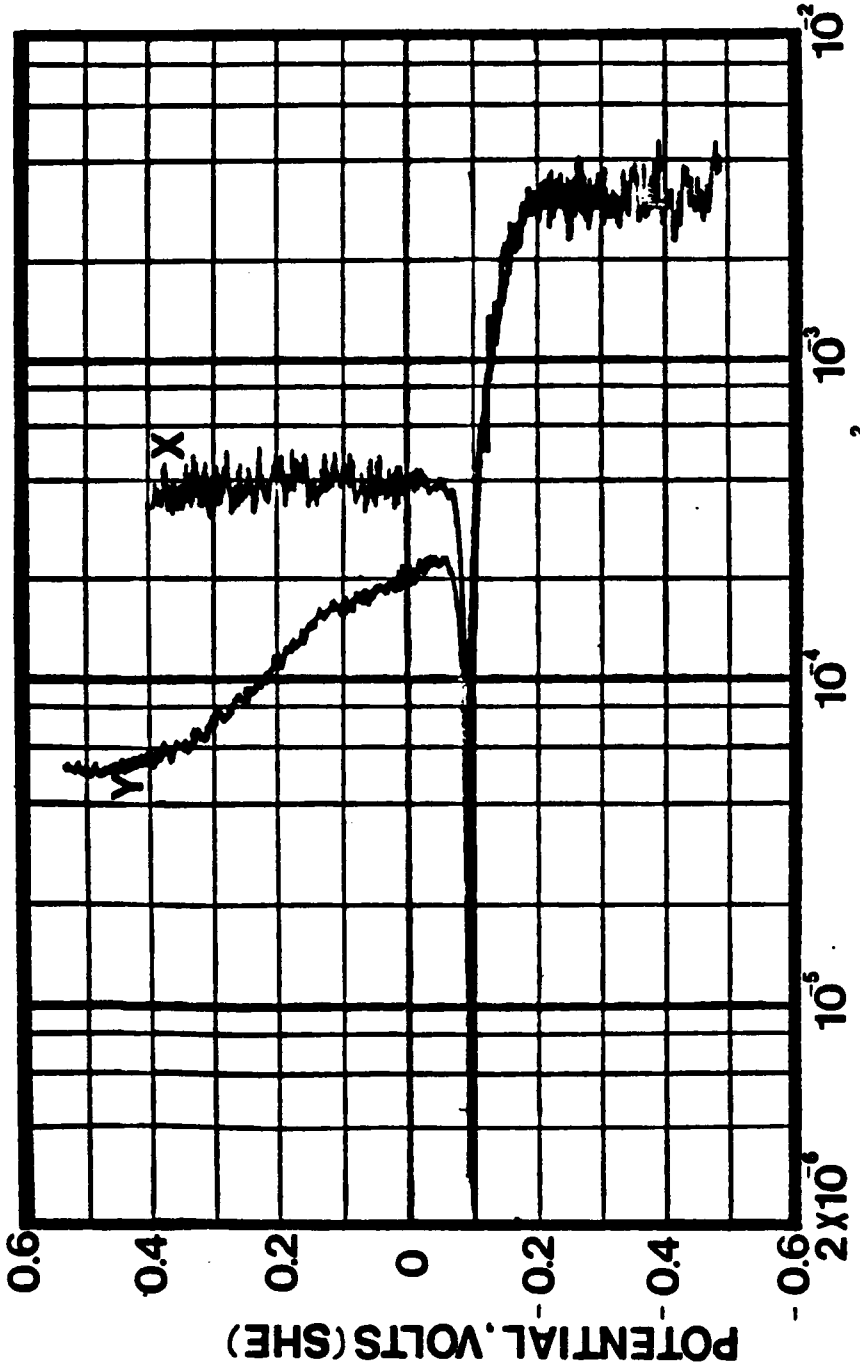

Figure 34. Effect of dissolved gas on the polarization curve of H on platinum in 5% NaCl solution adjusted to pH=2 at room temperature X: with H_2, Y: with N_2.

effects of sparging the gas through the cell during a polarization scan from cathodic to anodic potentials, polarization curves were determined on platinum. The resulting experimental curves are shown in Figure 34 for the same pH and NaCl concentration as used for the stainless steel curves. One curve (X) was determined with hydrogen gas sparged into the polarization cell and the other (Y) with a nitrogen sparge. Both curves were initiated in the diffusion controlled potential range of the cathodic reaction, at -0.5 V (SHE). In both cases, hydrogen gas was evolved from the platinum surface at this potential. On upscan, the transition from net cathodic to net anodic current occurred near -0.1 V (SHE) which is near the equilibrium half-cell potential, -0.118 V (SHE), for the hydrogen reaction at P_{H_2} = 1 atm. With the hydrogen sparge, the anodic curve shows diffusion control with i = 4 x 10^{-4} A/cm^2 with this behavior continuing to +0.4 V (SHE) where the scan was terminated. With the nitrogen sparge, the hydrogen produced by the cathodic pretreament allows essentially the same cathodic to anodic transition (due to essentially equivalent amounts of hydrogen on the surface) but the anodic curve quickly passes through a maximum current density of about 2 x 10^{-4} A/cm^2 with the current density continuing to decrease until termination of the scan at +0.5 V (SHE), the decrease in current density being due to the depletion of the hydrogen generated by the pretreatment.

A correlation of these experimental observations can be made by reference to Figure 35. Curves A and B of Figure 32 are reproduced as Curves A and B. The anodic Curve A can be extrapolated to lower potentials only in the symbolic representation of the dashed curve

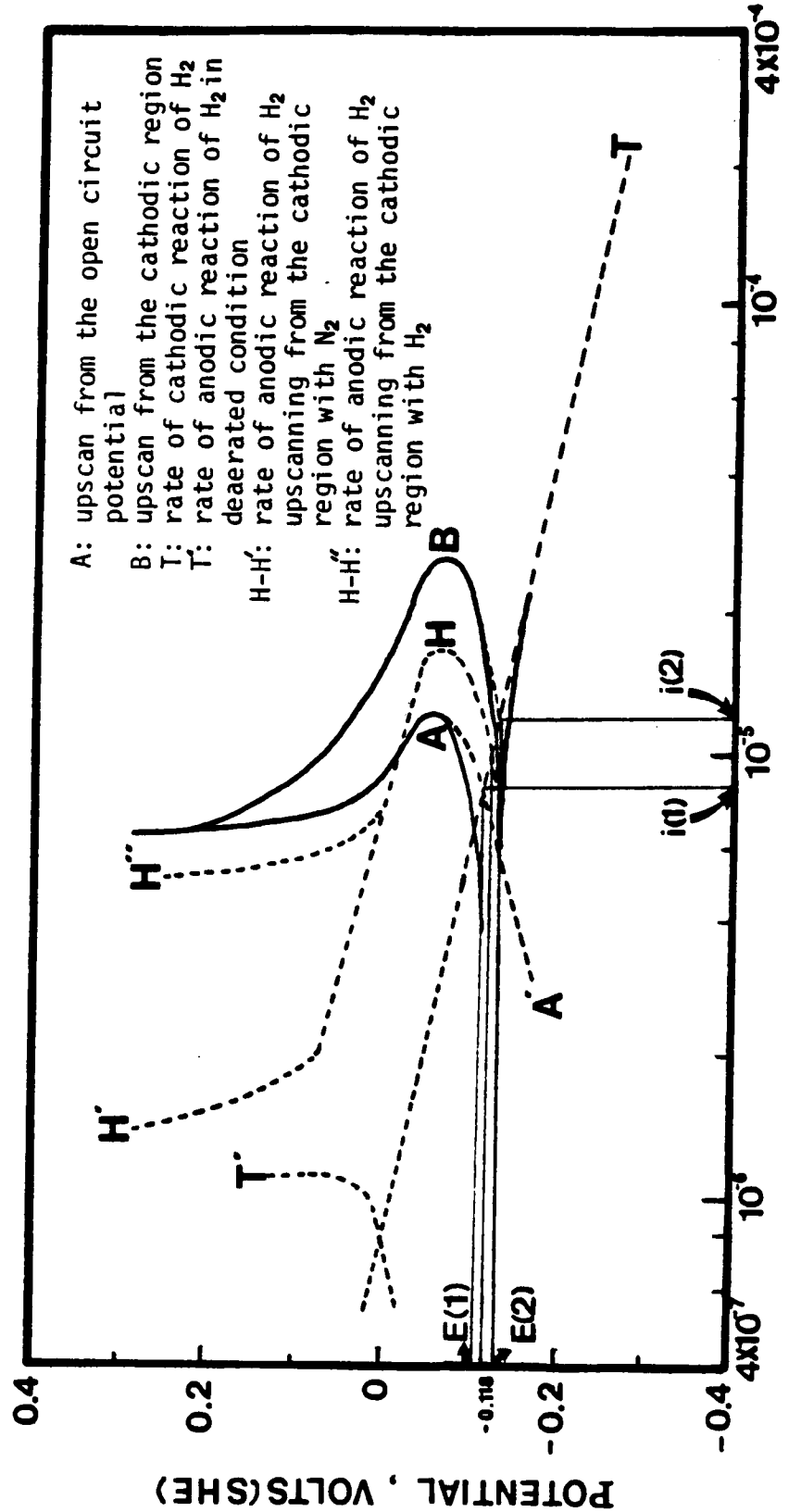

Figure 35. Interpretation of the effect of test method and dissolved gas on the polarization curve of 316L stainless steel in 5% NaCl solution adjusted to pH=2 at room temperature.

extending to A'. This uncertainty results from the difficulty of estimating the slope of the downward extension of Curve A. In addition, both an eqilibrium half-cell potential and an exchange current density for an alloy are difficult to define and hence the parameters are not available to locate a point of initiation of the anodic polarization curve. From the cathodic portion of Curves D and E in Figure 33, the Tafel slope of the hydrogen reaction on the 316L stainless steel can be estimated and this value used to plot the Tafel Line T in Figure 35. Since Curve A was determined by an upscan from the corrosion potential, the hydrogen concentration in the system is very small and would correspond to that evolved from the steady state corrosion of the 316L stainless steel at pH=2. The hydrogen-hydrogen ion equilibrium potential is given by

$$E = -0.059pH - 0.03 \log P_{H_2}$$

The effective partial pressure of the hydrogen is not known, but assuming some small value of 10^{-4} atm, the equilibrium potential is

$$E = -0.059 \times 2 + 0.03 \times 4 = 0.002 \text{ V (SHE)}$$

Extrapolation of Curve T to this potential gives the exchange current density for the hydrogen reaction on the stainless steel initially polished through 600 grit paper and then exposed 2 minutes to establish a steady state corrosion potential. Although this potential is in the active region of the polarization curve, the surface on which the hydrogen reaction is occurring is probably a chromium-rich hydrated film (75). The Curve T' is a consistent representative anodic polarization curve for the hydrogen reaction indicating almost immediate transition into diffusion control because of the low

hydrogen concentration.

However if the 316L stainless steel is polarized from the cathodic region, the corrosion potential obtained on an upscan is different than described above and the current maximum is larger. During polarization where the net current is cathodic, larger amounts of hydrogen are evolved. In spite of agitation of the solution due to nitrogen purging, hydrogen bubbles exist on the surface of the sample. This indicates that the pressure of the hydrogen is near 1 atm; therefore the hydrogen-hydrogen ion equilibrium potential is changed to

$$E = -0.059 \times 2 = -0.118 \text{ V (SHE)}$$

An anodic hydrogen curve, H, is now constructed such that the sum of this curve and the Curve A for the stainless steel equals the experimentally determined Curve B. This leads to an exchange current density for the hydrogen reaction on the cathodically "cleaned" stainless steel of about 10^{-5} A/cm^2, a factor of ten larger than on the non-cathodically cleaned surface.

An apparent inconsistency exists between the maximum current density of Curve B, about 3×10^{-5} A/cm^2, and the much higher limiting current density shown in Figure 34 for the anodic polarization curve for hydrogen on platinum (4×10^{-4} A/cm^2) when hydrogen is sparged into the cell or even the maximum current density of 2.2×10^{-4} A/cm^2 when a nitrogen sparge is used. It is also noted in Figure 33 that the anodic curve obtained on 316L stainless steel with a hydrogen gas sparge shows a maximum and decreases to 10^{-5} A/cm^2 in the conventional passive range. Thus in the presence of the hydrogen

sparge, the limiting anodic current density of 4×10^{-4} A/cm^2 observed on platinum must be reduced to values less than the passive current density for the stainless steel. Since a limiting diffusion current density must be independent of the substrate toward or away from which the diffusion is occurring, some additional factor must be current limiting. It is suggested that this is the ohmic resistance of the passive film which limits acceptance of electrons from the hydrogen oxidation reaction and therefore the current density to values of the order of or less than the passive current density. It also follows that this influence starts to become effective near the potential of the current density maximum of Curve A or B and leads to an anodic curve for the hydrogen of the general form shown by H". The maximum is attributed to the initiation of formation of the passive film and the associated decrease in current density is therefore due to the changing structure of the film. The position of Curve H" indicates that as the structure of the passive film changes, the hydrogen reaction rate rapidly decreases due to the increasing ohmic resistance. In contrast, with the cathodic pretreatment and nitrogen sparge, the hydrogen generated is consumed and the anodic curve takes the general form of the curve extending to H'. However, Okamoto (14) has shown that the kinetics of different cathodic reactions are affected differently when occurring on a passive film. He shows a large decrease for cathodic reduction of oxygen but less effect for the reduction of ferric ion. These observations suggest that the ohmic resistance is not the controlling factor. Another possibility is species dependence of electron transfer at the Pt/solution interfaces

compared to the passive film/solution interface. This would be consistent with the Fe^{+3}/Fe^{+2} reaction being simpler than the hydrogen reaction and the much more complicated oxygen reaction.

In summary of the above discussion, the intersection of Curve T in Figure 35 with A-A' gives the corrosion potential, E(1), and corrosion current density, i(1) for a nitrogen sparge. This is consistent with the corrosion potential indicated by the polarization Curve A in Figure 32, page 76, which results on polarization. On the other hand, the intersection of the cathodic Curve T with the anodic Curve B, the sum of the anodic polarization of the hydrogen and 316L, gives the corrosion potential E(2) and the slighly higher corrosion current density i(2). This construction is consistent with Curve B in Figure 32.

The effect of temperature on the pitting potential of 316L stainless steel in 2.5% NaCl adjusted to pH=2 is seen in Figure 36, where an increase in temperature from room temperature to $135^{o}F$ is shown to cause a rapid decrease in pitting potential but relatively small decrease occurs for a temperature change from $135^{o}F$ to $170^{o}F$. This pattern of behavior was reported previously (51). The pitting potential is not affected by the temperature above a certain value and the material shows a constant corrosion resistance.

Pitting corrosion was not observed on AL6X in 2.5% sodium chloride solution adjusted to pH=2 at room temperature, and at $135^{o}F$ and $170^{o}F$. Also, the AL6X did not exhibit any current increase due to the onset of pitting corrosion in the more aggressive environment, 1N NaCl+0.5N HCl at $122^{o}F$ as was shown in Figure 24, page 66. The main

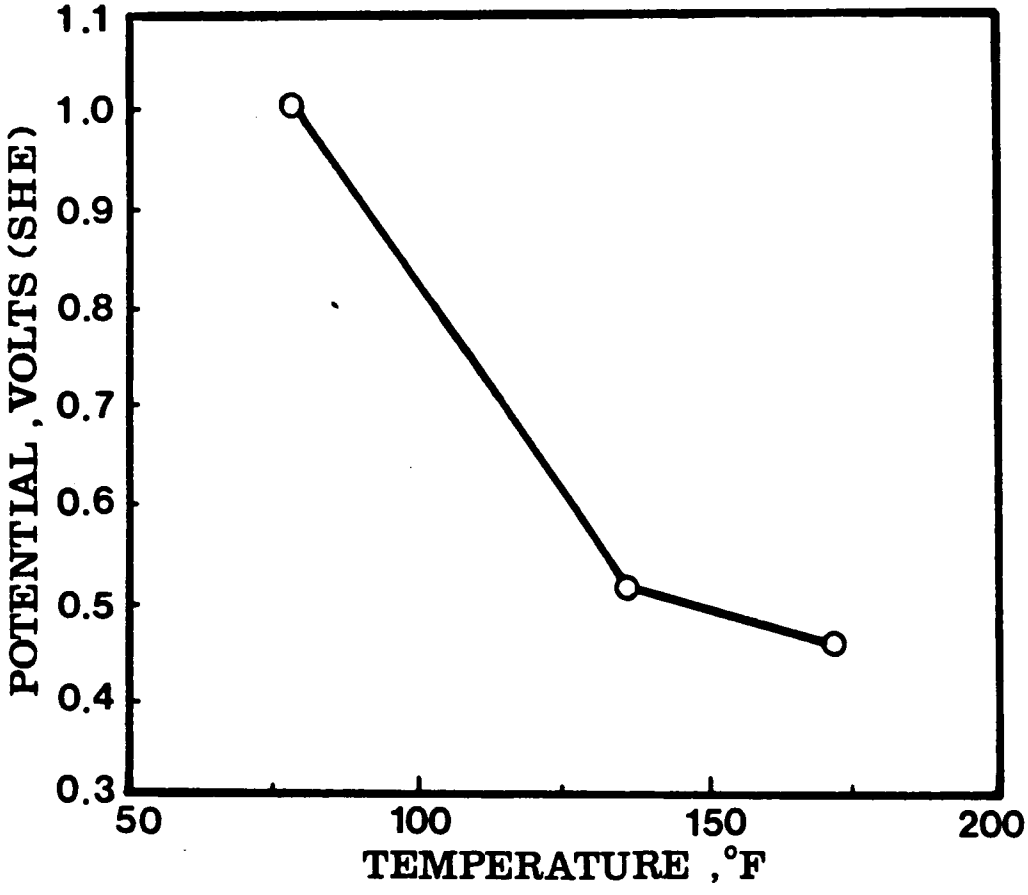

Figure 36. Effect of temperature on the pitting potential of 316L stainless steel in 2.5% NaCl solution with pH=2.

reason that pitting corrosion occurs on 316L stainless steel but not on AL6X in the same environment is the higher chromium, nickel, and molybdenum content of AL6X. It has been reported that Cr, Ni and Mo have a beneficial effects on the pitting corrosion (27,31-36,76). Steigerwald (76) found that higher chromium alloys had much better resistance to pitting corrosion and the critical potential for passivation became slightly more negative as the chromium content increased. In stainless steel, the passive film is mainly composed of Cr_2O_3. The chromium is enriched in the surface layer of the passive film in proportion to the matrix chromium contents, which increases the stability of passive film (31). Figure 37 shows the microstructure of AL6X in the as-received condition (heat treatment at 2350^{o}F for 1 hour and water quenching). It was electroetched in 10% oxalic acid solution with 10 V, 0.25 A/cm^2 for 60 seconds. As shown in Figure 37, the microstructure of AL6X is typical austenite. To study the effect of heat treatment on the pitting corrosion of AL6X, it was solution annealed at several temperatures in the range of 1950^{o}F to 2450^{o}F for 1 hour followed by water quenching. It was found that the pitting corrosion resistance of AL6X was not affected by solution annealing above 2050^{o}F but solution annealing at 1950^{o}F reduced the pitting corrosion resistance. The effect of the lower temperature heat treatment was to produce a microstructure containing sigma phase in the grain boundaries as shown in Figure 38. AL6X solution annealed at 1950^{o}F did not exhibit any current density increase implying no occurrence of pitting corrosion in 2.5% NaCl adjusted to pH=2 at room temperature and 135^{o}F during polarization test. However, at 170^{o}F,

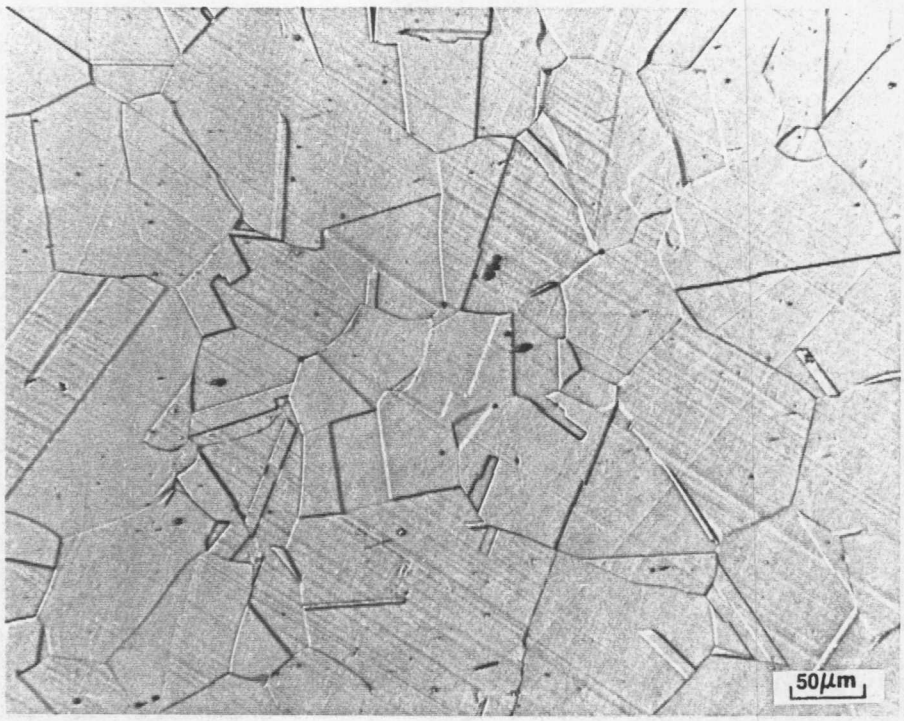

Figure 37. Microstructure of as-received AL6X, electrolytic etch in 10% oxalic acid.

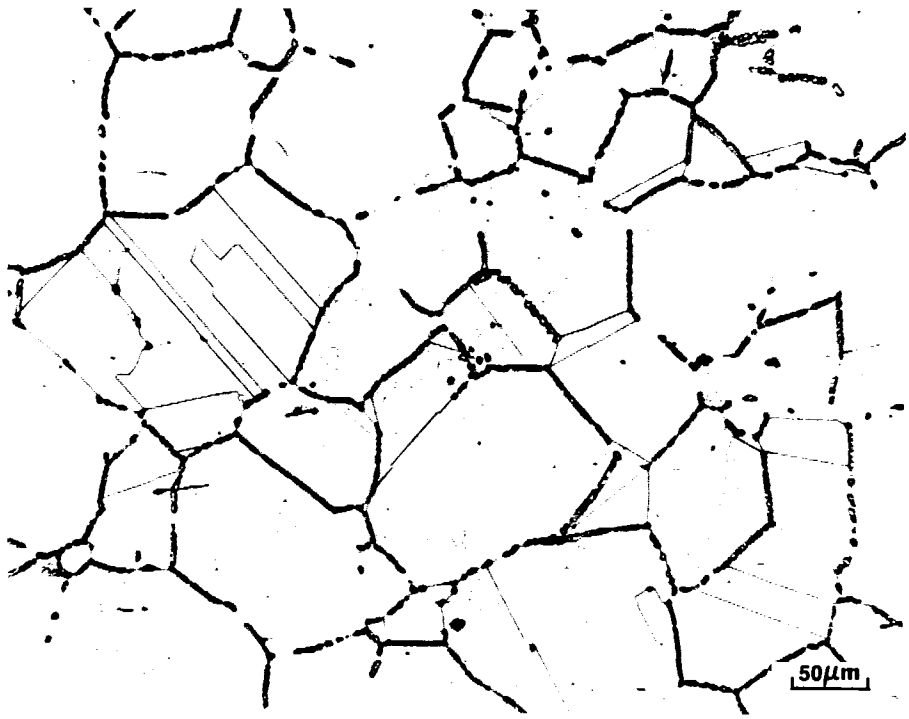

Figure 38. Microstructure of AL6X after heat treatment at 1950°F for 1 hr and water quenched, electrolytic etch in 10% oxalic acid.

pits started to form along the sigma phase at 0.8 V (SHE) as shown in Figure 39. It was confirmed by Energy Dispersive X-ray Analysis (EDXA) that the sigma phase has higher chromium and molybdenum contents than the austenitic matrix (Figure 40). As a consequence, some chromium and/or molybdenum depletion is occurring within the austenite immediately adjacent to the precipitation sigma, and that the pit sites may be associated with such depleted regions.

Immersion Test

The corrosion behavior of 316L stainless steel and AL6X was studied in 1% and 10% ferric chloride solutions at room temperature, and at 135^{o}F and 170^{o}F. The measured pH was 2.6 for the 1% ferric chloride solution and 1.9 for the 10% ferric chloride solution. The sample, cut from plate into a rectangular shape of 0.75"x1.5"x0.065" was ground to 120 grit. The specimen was placed in a glass rack and immersed in the test solution at the desired temperature. Each alloy was exposed to the test solution for 30 days at room temperature and for 7 days at 135^{o}F and 170^{o}F although the test period was 24 hours and 9 hours for 316L stainless steel in 10% ferric chloride solution at 135^{o}F and 170^{o}F respectively. After a selected exposure time, the sample was removed from the solution, rinsed thoroughly to remove corrosion product, and weighted to 0.001g. The corrosion rates of these alloys, expressed in terms of mpy (mils per year), in the given environment are shown in Table 7. Corrosion rates can be expressed in a variety of ways. Weight loss in grams or miligrams and percent weight change of materials after exposure to the corrosion environment are poor ways of expressing corrosion resistance because these

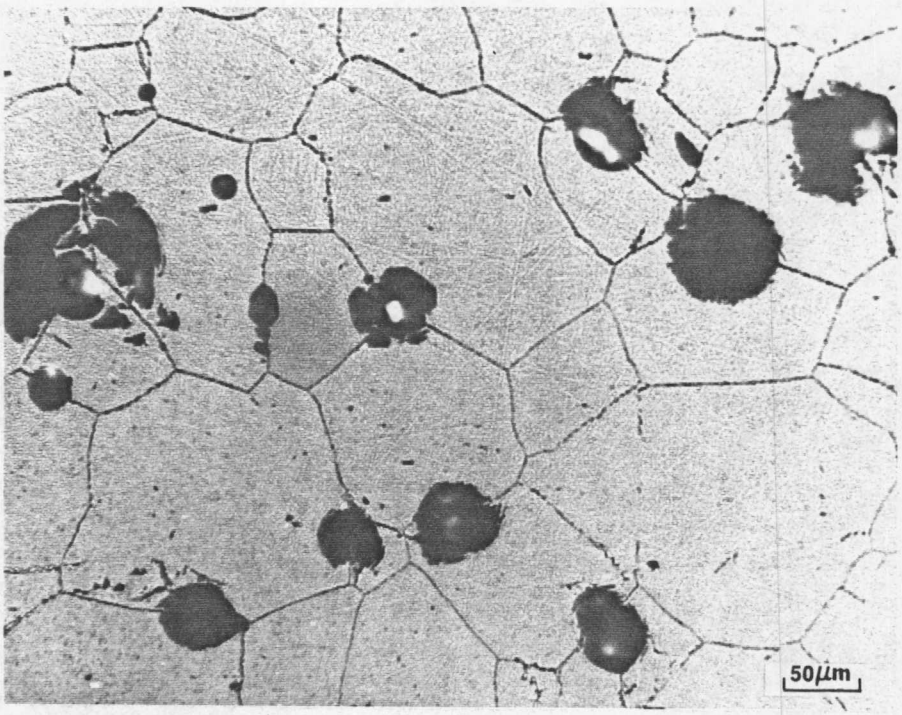

Figure 39. Pits formation along the sigma phase in AL6X heat treated at 1950°F for 1 hr and water quenched in 2.5% NaCl solution adjusted to pH=2 at 170°F.

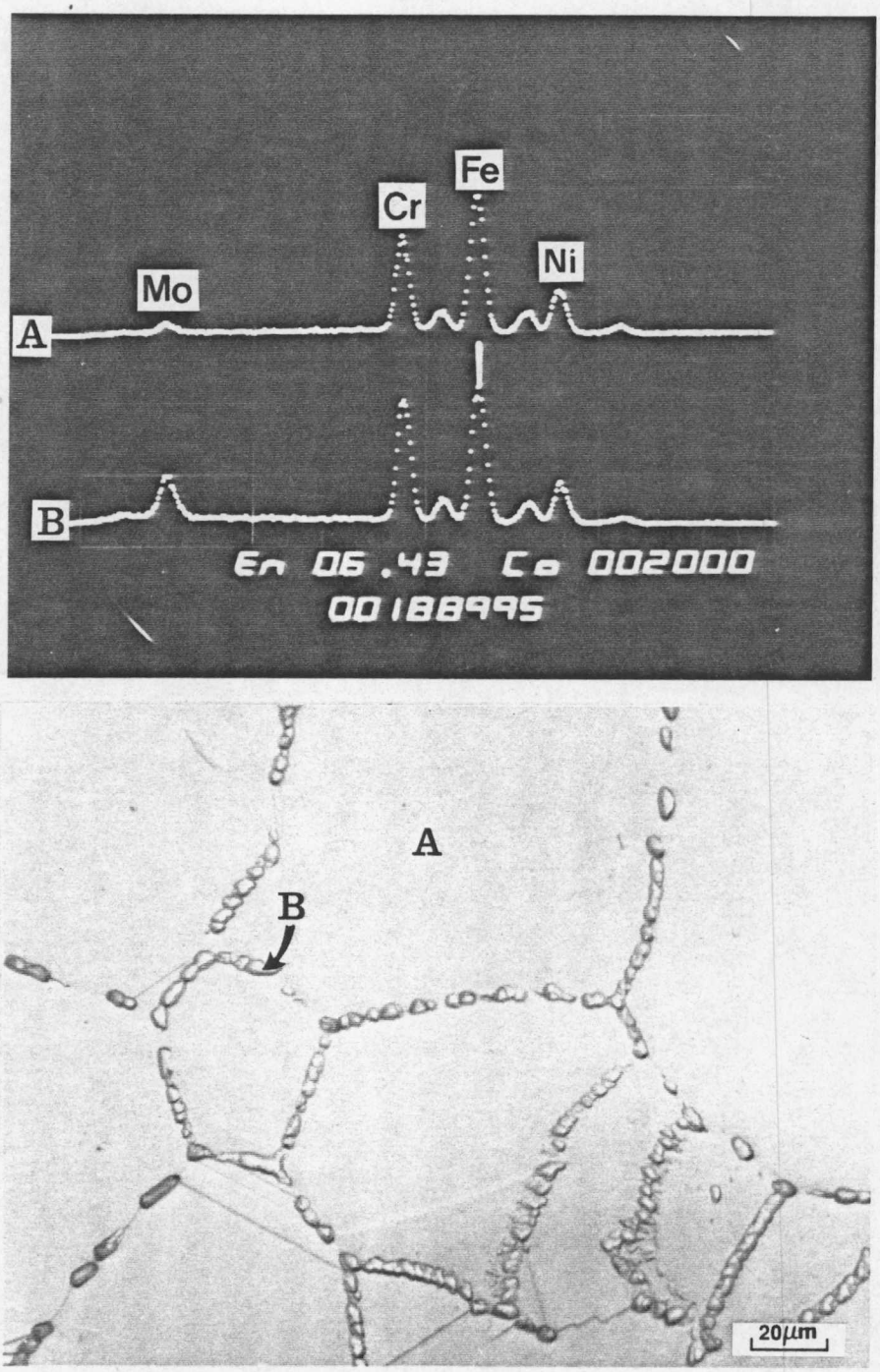

Figure 40. EDXA shows higher Cr and Mo at the sigma phase(B) with respect to matrix(A).

Table 7. Corrosion rate of 316L stainless steel and AL6X in ferric chloride solution.

	CORROSION RATE , MPY			
	316L S.S.		AL6X	
	1% $FeCl_3$	10% $FeCl_3$	1% $FeCl_3$	10% $FeCl_3$
R.T.	0.4	200.1	0.07	0.11
135°F	3.9	4673.1	0.15	0.31
170°F	17.4	11049.3	1.08	1121.2

expressions are influenced by the duration of the exposure and the shape of the exposed sample. Therefore, the expression of corrosion resistance must include the effect of the exposed area and the period of exposure. The corrosion rates were calculated from the weight loss using the following expression based on Faraday's law:

$$mpy = \frac{534W}{DAT}$$

where W = weight loss, mg

D = density of specimen, g/cm^3

A = area of specimen, sq.in

T = exposure time, hour.

Since these alloys respond to the test environment almost exclusively by crevice or pitting corrosion, use of the above expression which implies uniform corrosion is of limited value. Rather, visual examination combined with optical and scanning electron microscopy is required to evaluate the corrosion response. Although investigations have included statistical studies of the distribution and geometry of localized attack, this was not done in the present research since the objective was to identifiy the conditions under which localized corrosion did or did not occur and not necessarily the extent. The corrosion rate of these alloys increases with increasing temperature and increasing concentration of ferric chloride solution as shown in Table 7. Figures 41-43 show no pitting corrosion of either alloy at any of the temperatures in the 1% ferric chloride solution. The pitting corrosion, however, occurred in 316L stainless steel at all temperatures in 10% ferric chloride solution and at $170^{o}F$ the sample had lost almost 50% of its weight after only 9 hours exposure. As

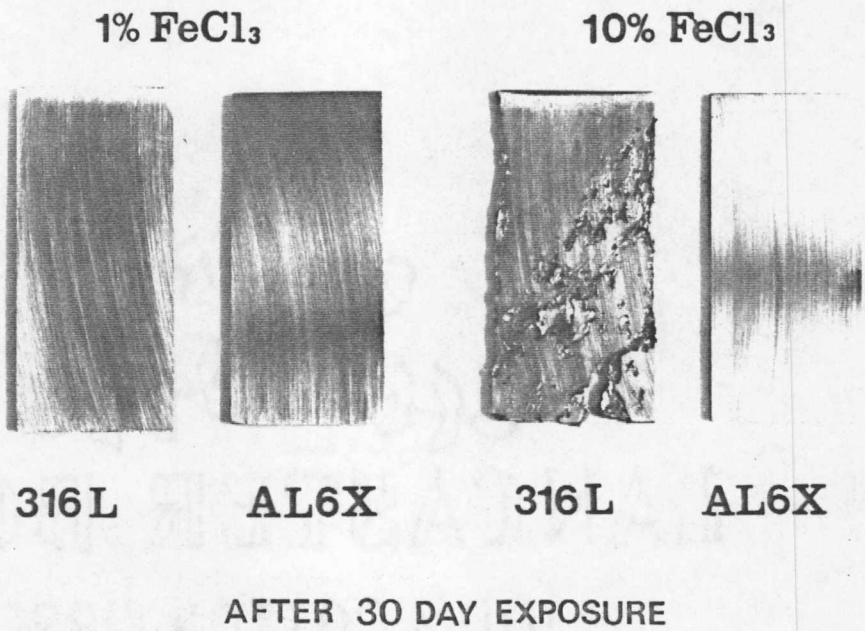

Figure 41. Photograph of 316L stainless steel and AL6X after immersion in ferric chloride solution at room temperature.

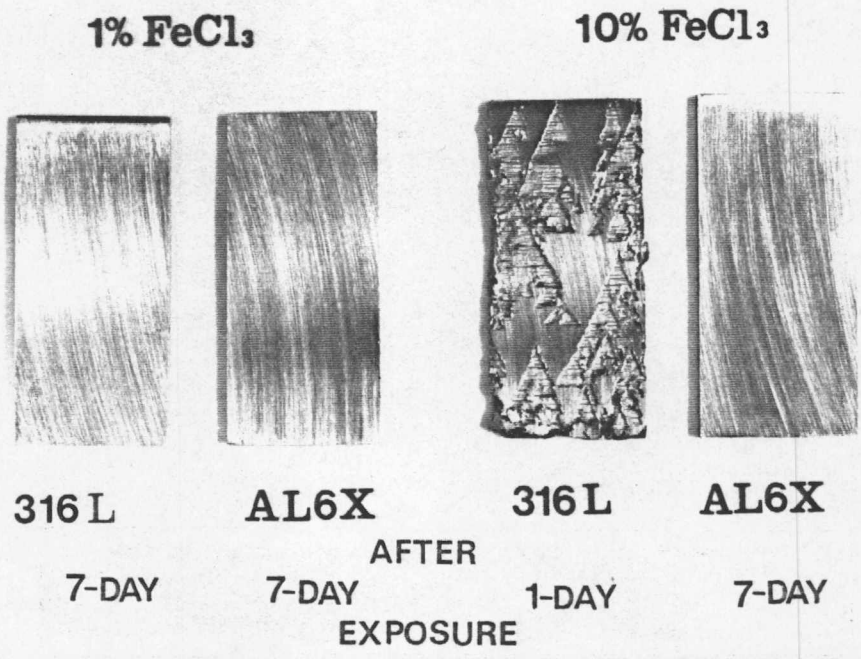

Figure 42. Photograph of 316L stainless steel and AL6X after immersion in ferric chloride solution at 135°F.

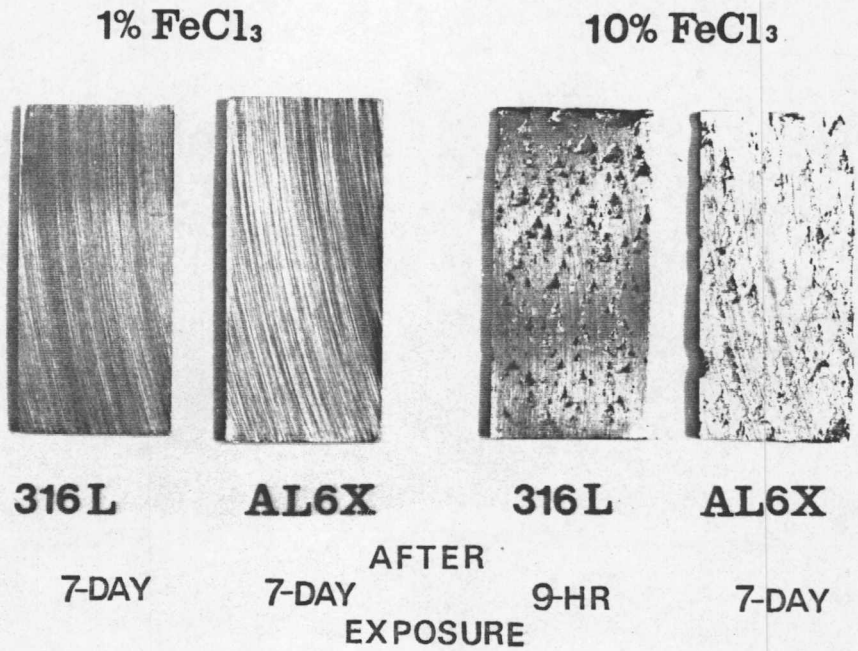

Figure 43. Photograph of 316L stainless steel and AL6X after immersion in ferric chloride solution at 170°F.

expected, the AL6X shows lower corrosion rates in all test solutions than the 316L stainless steel. The AL6X was essentially unattacked at the two lower temperatures but severely pitted at 170^{o}F in 10% ferric chloride solution. The weight loss was about 80% of its original weight after 7 days exposure of AL6X in 10% ferric chloride solution at 170^{o}F, the corrosion occurring mostly at the interior of the specimen under a partially retained passive surface as shown in Figure 43. As determined in the electrochemical measurement, AL6X shows a higher pitting potential than 316L stainless steel and the pitting potential of 316L stainless steel decreased with increasing chloride ion and increasing temperature. Therefore, one can expect the highest corrosion rate of 316L stainless steel in 10% ferric chloride solution at 170^{o}F and the test results show the highest corrosion rate in that environment.

Although a relationship between electrochemical and chemical tests for susceptibility to pitting corrosion is in controversy, it has been known that pitting corrosion will not occur when the corrosion potential is below a certain potential generally referred to as the critical pitting potential. It is observed that when pitting corrosion occurs there is a decrease in the corrosion potential. If pits form and repassivate, the potential decreases and then returns to values near the initial corrosion potential characteristic of the passive state. Progressive development of pits causes the potential to decrease and this lowered potential may not allow new pits to form on the passivated surfaces although previously formed pits may continue to grow. Thus in general, few severe pits may exist on an otherwise passivated surface. An interpretation of this occurrence can be given by reference to

Figure 44. Note that in this case the abacissa is in terms of total current rather than current density although the values are representative of 1 cm^2 of surface area. The curve ABCDHG represents the polarization curve when pitting occurs along DH due to the presence of chloride ion and the curve ABCDFG represents the polarization curve if the pitting corrosion did not occur and the passive film is maintained above the pitting potential. If the passive film did not form on the surface during polarization the current increases along the curve ABHG; however the segment BE will not be observed due to passivation along BCD. The curve XY represents the polarization of cathodic reactions such as the reduction of ferric ion or oxygen. In corroding systems, the potential of the surface will be at a corrosion potential at which the total current of all anodic reactions is equal to the total current of all cathodic reactions. When the sample is immersed in the solution, the corrosion potential, E_1, is determined by the intersection of the cathodic curve, XY, and the passive anodic curve, CDF. This occurs above the pitting potential, D, and therefore pits initiate on the surface after sometime (induction time for pit initiation).

The change in potential as pitting progresses is analyzed by shifting the curve ABHG for the unpassivated condition to lower currents determined by the unpassivated areas. These are shown as p_1q_1, p_2q_2 and p_3q_3 corresponding to 0.01%, 0.1% and 1% of the unpassivated surface due to pitting corrosion. The total anodic current at any potential is now the sum of the current over the passivated part of the surface plus that from the pitted regions or:

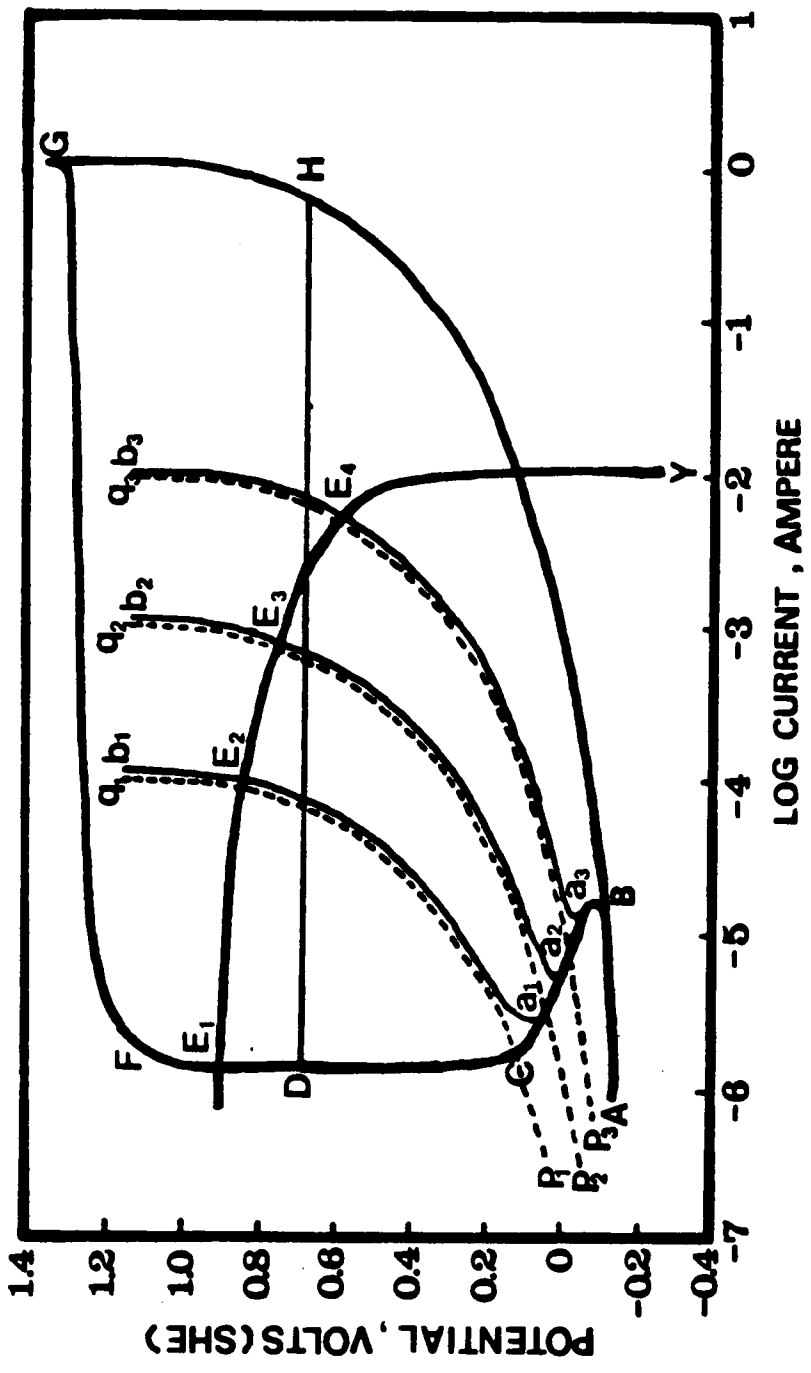

Figure 44. Decreasing in corrosion potential as a function of pit propagation.

$$I_{total} = i_{pass}A_{pass} + i_{pit}A_{pit}$$

where i_{pit} is much larger than i_{pass}, thus, the small increase in pit area allows large change in total current. Actually in this case, I_{total} is the averaged current density since an area of 1 cm^2 is being considered. The constructed polarization curve for 0.01% pitting corrosion is obtained by adding, at each potential, p_1q_1 to CDF to give the solid curve a_1b_1. Similarly at 0.1% pitting corrosion, the sum curve is a_2b_2 and at 1% pitting, the sum curve is a_3b_3.

The corrosion potentials are now given by the intersection of the summed anodic curves and the cathodic curve, XY. According to the example, E_2 is still above the pitting potential and both new pits should form and old pits grow. At 1% pitted surface the corroson potential will have fallen to E_4 which is below the pitting potential and new pits should not form. Old pits may continue to grow or may repassivate depending on the local conditions of potential and composition in the pit. Therefore, once a corrosion potential decreases to below a pitting potential the bulk surface is protected from pitting corrosion.

If crevices are present on the sample, pitting corrosion does not occur even though the environment is capable of producing a potential above the pitting potential. The reason is that for materials which undergo crevice corrosion before pitting corrosion, the total current increases due to the crevice propagation. The corrosion potential determined on the sample undergoing crevice corrosion is lowered by the same mechanism as explained above and never reaches the pitting potential. Thus, only crevice corrosion is observed. These results were

also observed by Wilde (59).

To study the pit propagation with time, the 316L stainless steel was immersed in 10% ferric chloride solution at 170^{o}F. The sample was removed every 1 hour, rinsed thoroughly under running water to remove corrosion product, weighted, and then re-immersed. Figure 45 shows the corrosion rate of the 316L stainless steel determined every hour by successive removal and re-immersion and Figure 46 shows the surface morphology. As shown in Figure 45 the corrosion rate increases on initial immersion and continues to a maximum value after three hours of exposure. It is evident in Figure 46 that pits are visible after one hour immersion and that pits both continue to be initiated and to propagate with time. After 3 hours exposure, however, additional pits did not form and only pit propagation occurred. Since the same sample was used in these successive exposures, the pit distribution and size can be followed by examination of the photographs taken at the progressive times shown in Figure 46. This behavior is consistent with the argument presented previously that the corrosion potential should decrease as pitting progresses. In this case, the corrosion potential was lowered below the pitting potential after 3 hours exposure. Although the sample was removed after each hour, rinsed, dried and weighed, the observation that the average of these rates shown in Figure 45 is consitent with the rate given in Table 7, page 93, for the specimen immersed directly for 9 hours indicate that conditions for the continued localization of the corrosion were quickly re-established.

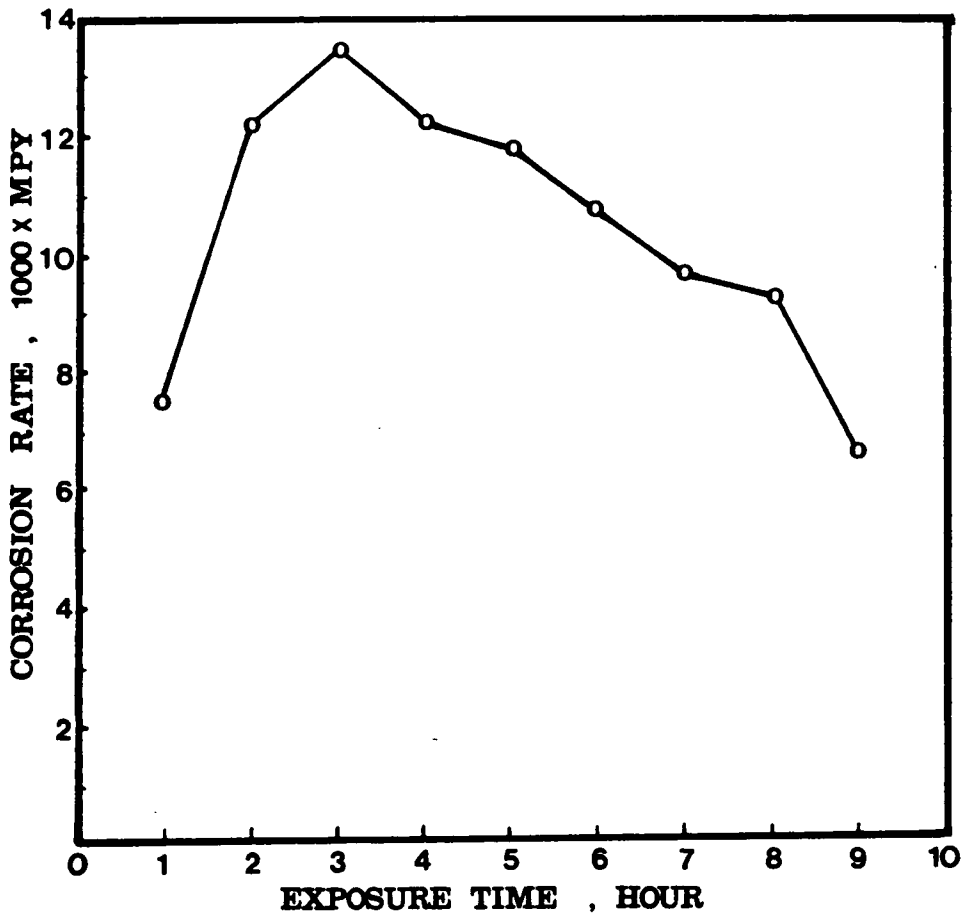

Figure 45. Corrosion rate of 316L stainless steel in 10% FeCl at 170°F.

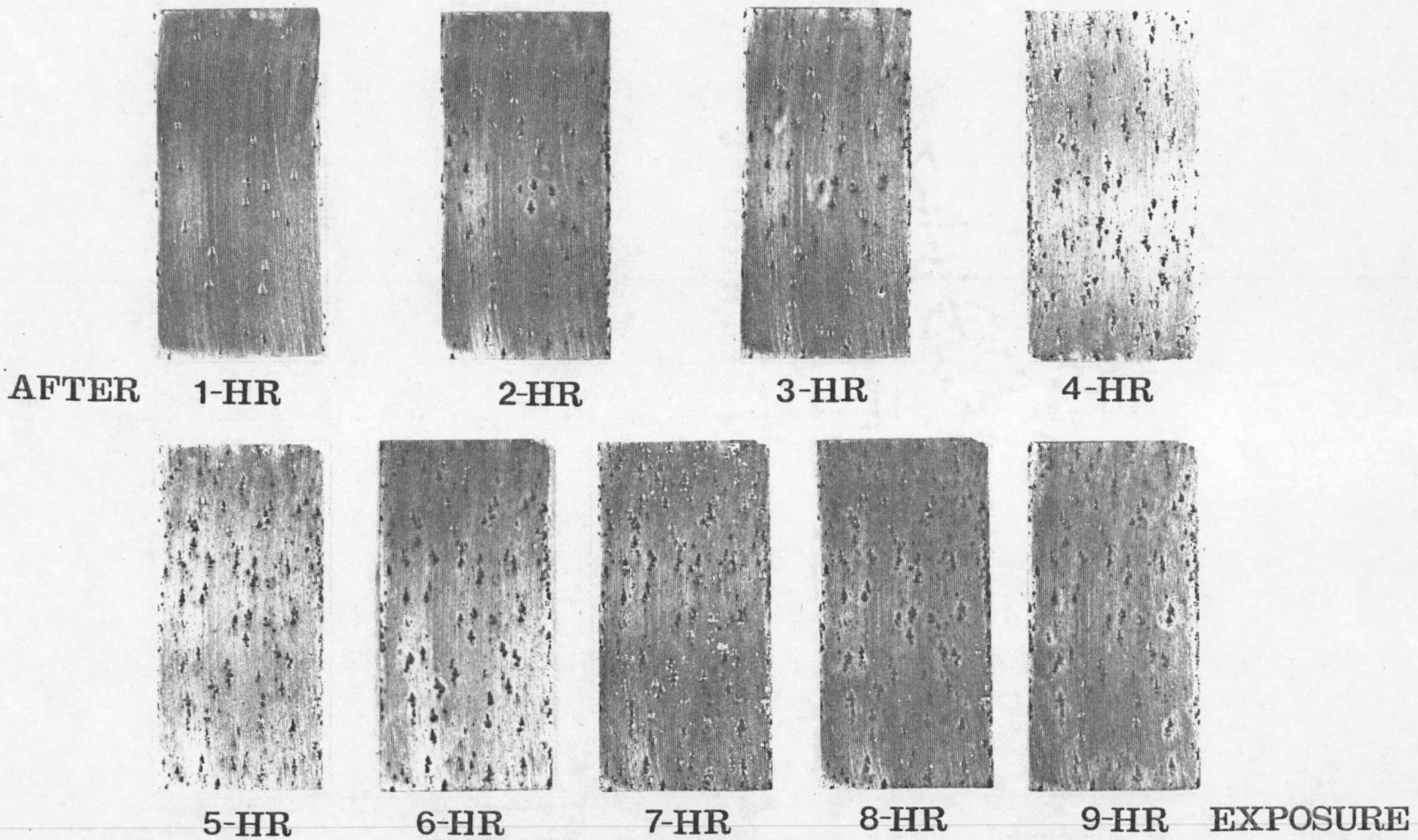

Figure 46. Photograph of 316L stainless steel taken at the progressive times after immersion in 10% ferric chloride solution at 170°F.

Comparison of Chemical and Electrochemical Tests

It has long been argued that the use of electrochemical accelerated tests for pitting corrosion studies leads to erroneous conclusions about the pitting susceptibility of alloys in long term corrosion behavior. France and Greene (5) reported a lack of correlation between electrochemical and chemical exposure tests on AISI Type 430 stainless steel in halide media. They argued that an electrostatic buildup of aggressive chloride ion at the metal interface occurred during electrochemical polarization, which did not necessarily occur at a freely corroding interface thereby leading to different behavior. Wilde and Williams (72) presented an excellent correlation between electrochemical and chemical techniques on 430 stainless steel in 1M sodium chloride, both in visually observed pitting susceptibility and metal weight loss data. Since the results of the current research just described provided additional insight into pitting phenomena as observed by eletrochemical and chemical methods, a series of experiments was conducted with the objective of a better understanding of the problems associated with correlating predictions of pitting corrosion by the two investigative methods. In these studies, 316L stainless steel was exposed in 5% sodium chloride solution adjusted to pH=2 at room temperature.

The potentiodynamic anodic polarization curve for 316L stainless steel in nitrogen purged 5% sodium chloride solution is shown in Figure 47. The curve was determined by increasing the potential, using a scan rate of 2.5 V/hr, after the open circuit potential was established. The current density increased at 0.78 V (SHE) indicating

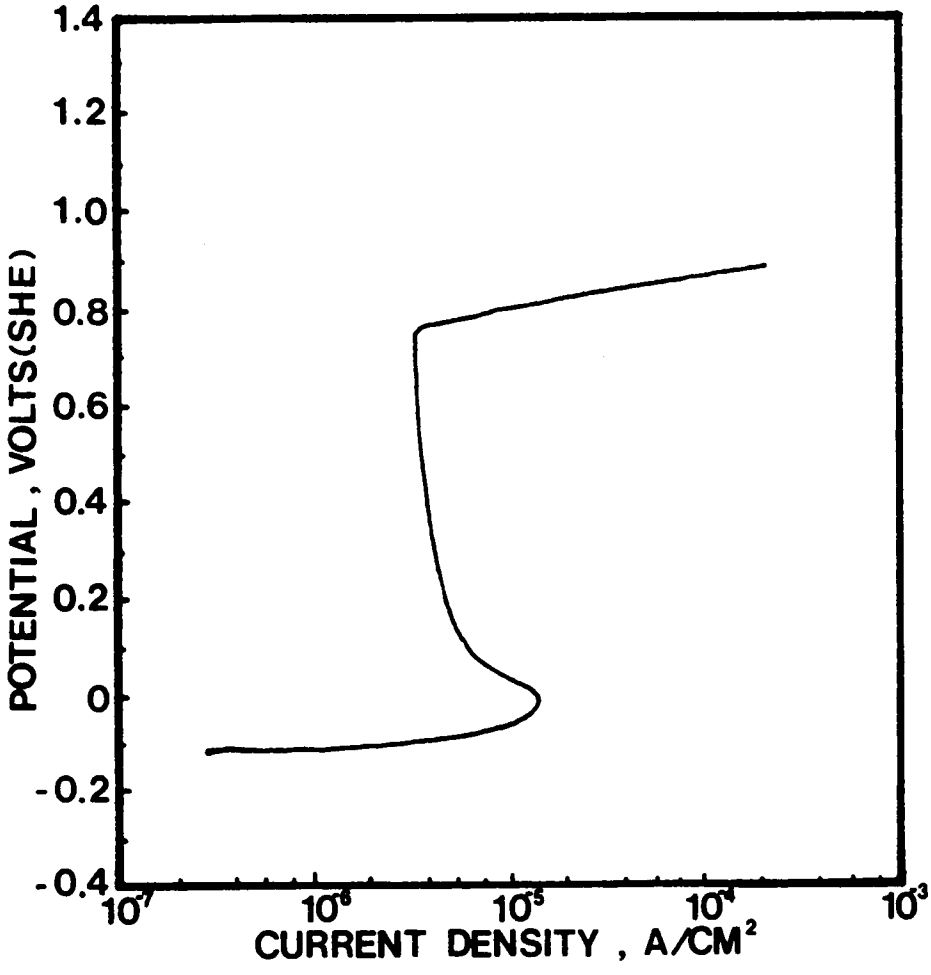

Figure 47. Anodic polarization curve of 316L stainless steel in 5% NaCl solution adjusted to pH=2 at room temperature.

the onset of pitting corrosion. Prolonged exposure to potentials above the pitting potential resulted in severe pitting corrosion as shown in Figure 48.

The fact that the pitting potential of 316L stainless steel is a function of scan rate was shown in Figure 14, page 51. Because of this scan rate dependence, a constant potential pitting test has been suggested as an alternative to give a well defined value of the pitting potential (68-69). This measurement excludes minor experimental procedure which was observed by manning (68) and phenomenon which might occur at other potential. In the present research, the pitting potential was determined by increasing the potential in 20 mV steps every 2 hours until the current increased with time. When the current increased during the process of increasing the potential, the pitting potential was said to be between the last interval of applied potential. Figure 49 shows the current density vs. time behavior at three applied potentials. The 316L stainless steel was polarized from the open circuit potential with a scan rate of 2.5 V/hr. The scanning was stopped when the potential reached 0.66 V (SHE) and the sample was held at that potential for 2 hours. As shown in Figure 49, the current density decreased to $10^{-6}A/cm^2$ with increasing time. The potential was increased in steps of 20 mV every two hours from 0.68 V (SHE) to 0.80 V (SHE) and no increase in current density was observed. At 0.80 V (SHE) the current density was $5 \times 10^{-7}A/cm^2$ and did not change with time for 2 hours as shown in Figure 49. The potential was again increased from 0.8 V (SHE) to 0.82 V (SHE) and the sample was held at that potential. After

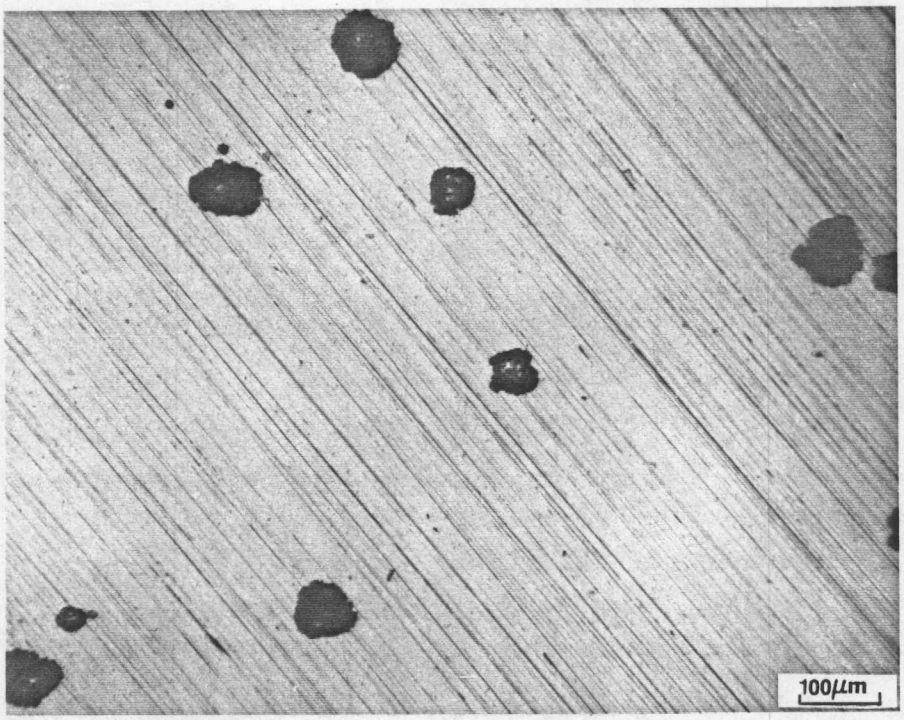

Figure 48. Electrolytically formed pits in the surface of 316L stainless steel in 5% NaCl solution adjusted to pH=2 at room temperature.

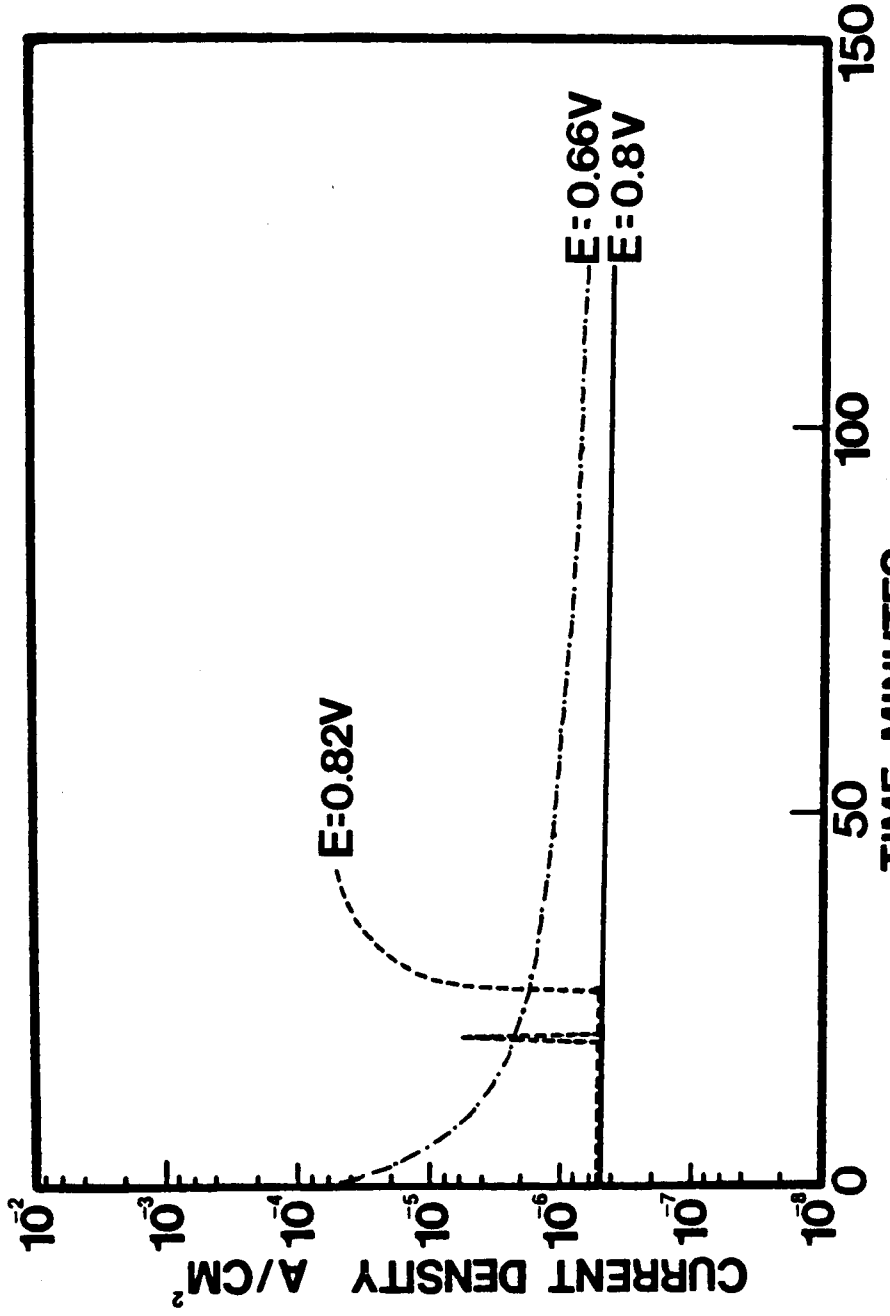

Figure 49. Current density vs. time behavior of 316L stainless steel at a fixed potential in 5% NaCl solution adjusted to pH=2 at room temperature.

20 minutes a short-duration current density spike indicated the brief formation of a pit and its repassivation. After 25 minutes, the current density increased rapidly with time to a value of 4×10^{-5} A/cm^2 at 40 minutes at which time the exposure was terminated. Therefore, the pitting potential determined by the constant potential measurement using 20 mV step for 2 hours is between 0.8 V (SHE) and 0.82 V (SHE) with an incubation time for pit initiation at 0.82 V (SHE) of about 25 minutes.

In contrast to the electrochemical method of determining pitting potentials by using a potentiostat as just described, the chemical method depends on controlling the potential by the selection and concentration of oxidizing agents. The species selected should as exclusively as possible influence only the corrosion potential with minimum interference with the pitting mechanism. In preliminary tests $Fe_2(SO_4)_3H_2O$ was used as an oxidizing agent. While the addition of $Fe_2(SO_4)_3H_2O$ increased the oxidizing power, the pitting potential of 316L stainless steel was also increased due to the inhibiting effect of the added sulfate ion on pit initiation. For example, pitting corrosion was not observed on the surface of 316L stainless steel in 5% NaCl + 100000ppm $Fe_2(SO_4)_3H_2O$ solution in which the oxidizing potential was 0.86 V (SHE). The inhibiting effect of the sulfate ion was confirmed by determining the anodic polarization curve for the 316L stainless steel in 5% NaCl with and without sulfate ion. The curves are shown in Figure 50 in which a pitting potential of 0.82 V (SHE) is observed in the absence of sulfate ion but the normal transpassive behavior with no pitting when the sulfate ion is present.

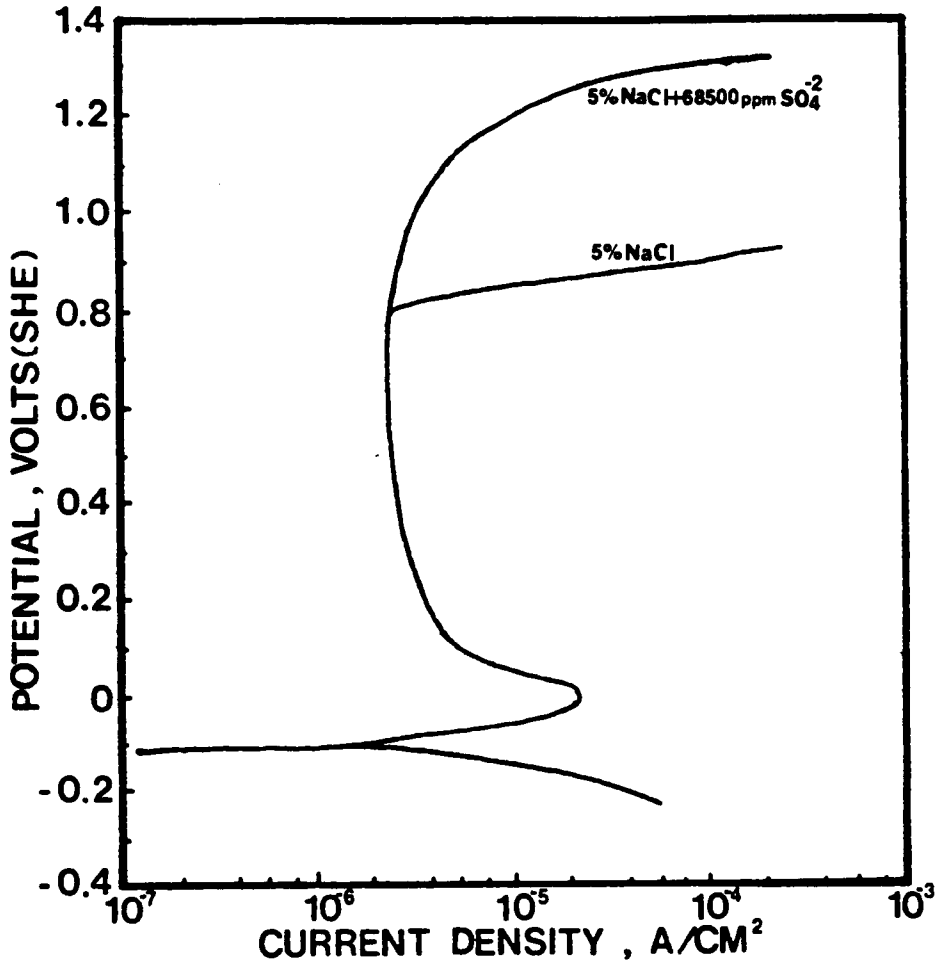

Figure 50. Polarization curves of 316L stainless steel in 5% NaCl solution adjusted to pH=2 at room temperature with or without SO_4^{2-}.

Thus, the pitting potential associated with chloride ion could not be determined using $Fe_2(SO_4)_3H_2O$ as an oxidizing agent. As a consequence, $FeCl_36H_2O$ was adopted to increase the oxidizing power. Special care was taken in preparing the solution in order to maintain the same chloride ion concentration in each to simulate the identical condition as the electrochemical test solutions. After adding the desired amount of $FeCl_36H_2O$, the chloride ion concentration was adjusted to have a same amount of chloride ion as a 5% sodium chloride solution by adding proper amounts of sodium chloride. The pH value was adjusted to two by sulfuric acid and nitrogen was sparged througout the test. The potential of 316L stainless steel was measured by an electrometer and recorded throughout the test. After the 316L stainless steel was immersed in the test solution, the corrosion potential increased due to the initial passivation process and remained constant if pitting or crevice corrosion did not occur. As shown in Table 8, additions of 0-75 g/l of $FeCl_36H_2O$ were made while adjusting the chloride ion concentration to 31940 ppm. Both the corrosion potential of the stainless steel and the potential of platinum were measured, the latter to determine the oxidizing potential of the environment. Pitting corrosion was not observed in any of the solutions listed in Table 8 even though the corrosion potential was increased to 0.76 V (SHE) by the dissolution of 75 g/l $FeCl_36H_2O$. Dissolution of $FeCl_36H_2O$ beyond 75 g/l increases the chloride ion concentration above 5% sodium chloride. It is possible to increase the corrosion potential above 0.76 V (SHE) by enriching the solution with $FeCl_36H_2O$, but the increase is marginal. For example, the corrosion potential was

Table 8. Corrosion potential of 316L stainless steel for each solution adjusted to pH=2 at room temperature.

CONCENTRATION		POTENTIAL, V(SHE)	
$FeCl_3 6H_2O$ (G/L)	Cl^- (PPM)	316L SS	Pt
0	31940	-0.1	0.26
0.25	31940	0.45	0.82
0.5	31940	0.5	0.82
1.0	31940	0.56	0.82
1.5	31940	0.59	0.82
2.5	31940	0.62	0.83
4.0	31940	0.65	0.84
5.5	31940	0.65	0.84
15	31940	0.67	0.85
75	31940	0.76	0.88

increased to 0.8 V (SHE) by dissolution of 130 g/l $FeCl_3H_2O$ in a preliminary test, an increase in corrosion potential of only 0.04 V even though $FeCl_36H_2O$ was increased from 75 g/l to 130 g/l, a net increase of 55 g/l. As a consequence the pitting potential of 0.82 V (SHE) could not be reached because of the problem of exceeding the chloride ion concentration. These observations, however, confirm the result obtained by the electrochemical method and are taken as a positive indication that pitting corrosion does not occur at 0.78 V (SHE) as shown by the chemical method. It is concluded that the pitting potential is definitely above 0.78 V (SHE).

Since the pitting potential could not be reached chemically by additions of $FeCl_36H_2O$ at room temperature and it is known that the pitting potential decreases with increase in temperature, additional tests to compare pitting potentials determined electrochemically and chemically were made by elevating the temperature. Potentiodynamic measurements established that the pitting potential of 316L stainless steel in 5% NaCl adjusted to pH=2 at 135^{o}F was 0.45 V (SHE). After the 316L stainless steel was immersed in 15g/l $FeCl_36H_2O$ solution adjusted to pH=2 at 135^{o}F, the corrosion potential which had been 0.67 V (SHE) at room temperature was observed to increase to 0.47 V (SHE) in about two minutes due to initial passivation after which it progressively decreased. The potential decreased with time indicating the onset of pitting corrosion as shown in Figure 51. Figure 52 shows the pit formed on the 316L stainless steel. Only one pit was detected on the total surface of 3 cm^2. As explained in the early section, the corrosion potential is lowered with pit propagation and once it goes

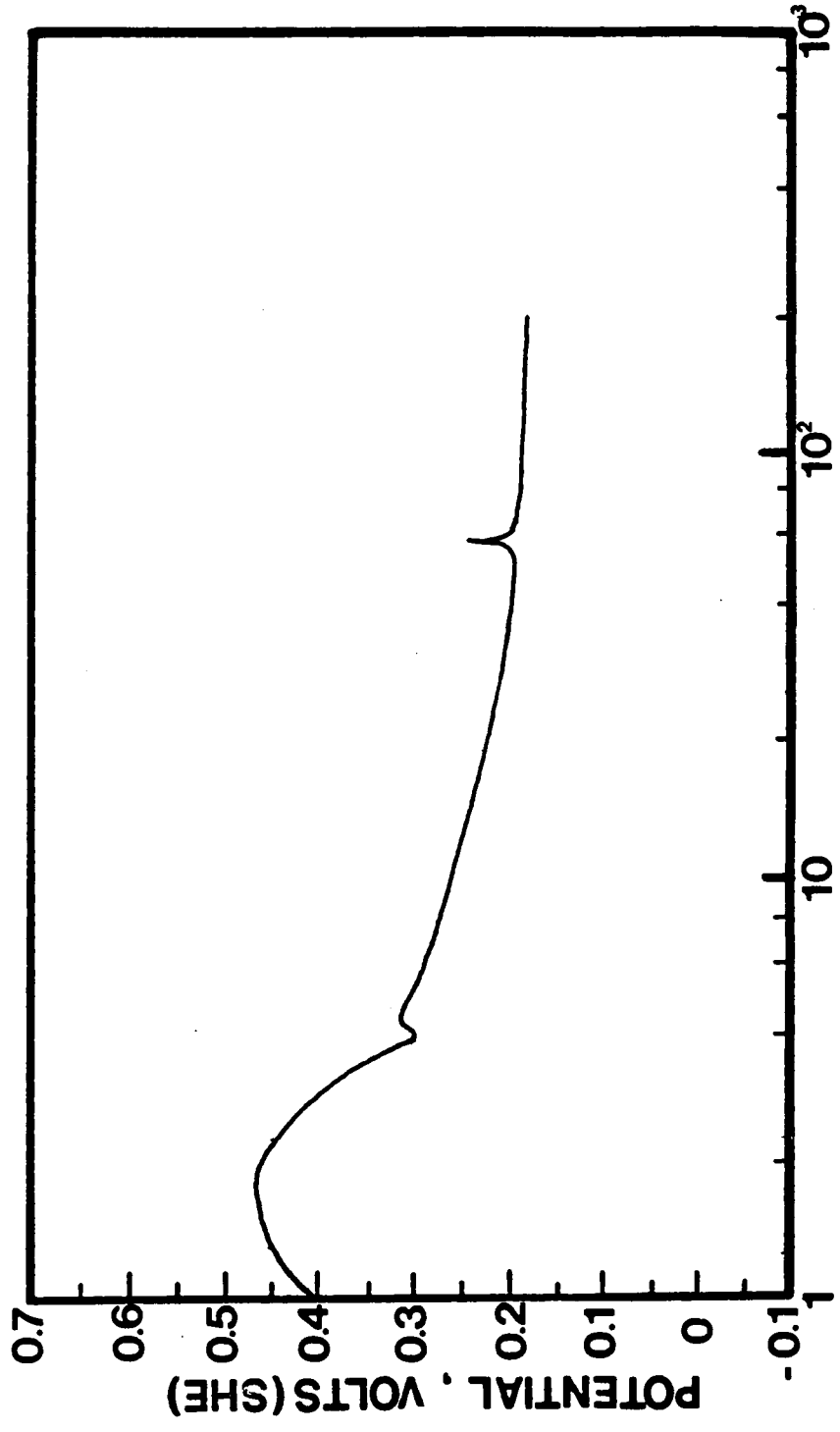

Figure 51. Corrosion potential vs. time behavior of 316L stainless steel in 15g/l $FeCl_3 6H_2O$ solution of pH=2 at 135°F and containing the same amount of Cl ion as 5% NaCl solution.

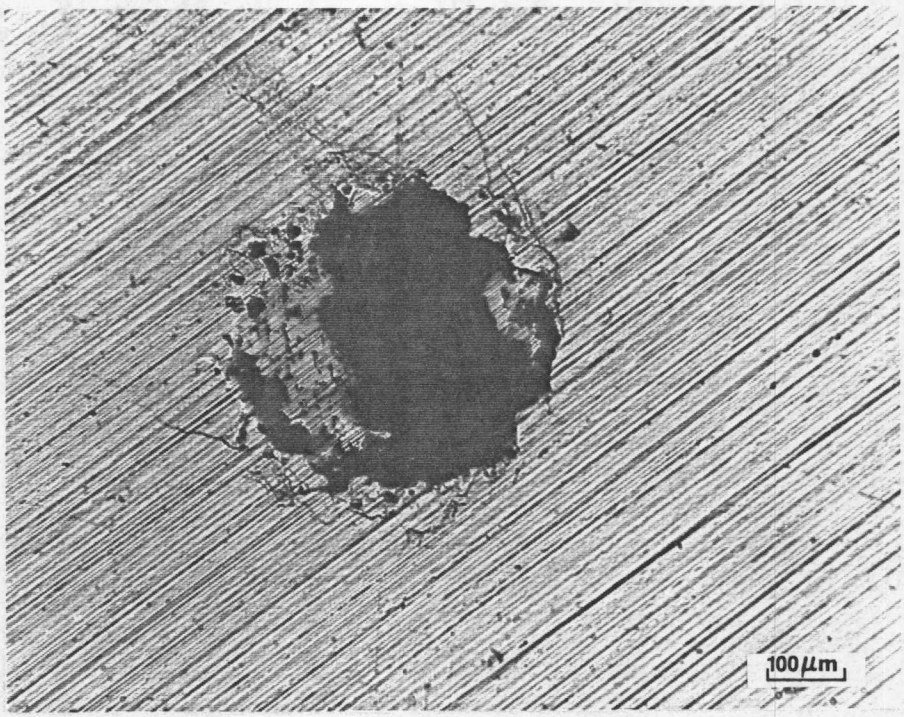

Figure 52. Pit formed in 316L stainless steel by immersion in 15g/l $FeCl_3 6H_2O$ solution of pH=2 at 135°F and containing the same amount of Cl ion as 5% NaCl solution.

below the pitting potential pits can not be initiated but the propagation of pits already formed continues. As shown in Figure 51, when the corrosion potential increases to 0.47 V (SHE) due to initial passivation process, a pit initiates and propagates since the corrosion potential, 0.47 V (SHE), is above the pitting potential. Once the propagation of a pit starts, the corrosion potential is lowered below the pitting potential and the rest of the surface is protected from pitting corrosion. Therefore, only one pit was formed on the whole surface of sample as shown in Figure 52. In electrochemical test, the applied potential is held above a pitting potential by the potentiostat and pits can initiate regardless of pit propagation. Therefore, many pits can be formed on the sample as was shown in Figure 48, page 108. Steigerwald (76) reported that pitting corrosion in the immersion tests took place at much lower potentials than the pitting potential. He measured the corrosion potential after 65 hours of exposure of Fe-Cr alloys to a 10 percent $FeCl_3 6H_2O$ solution. Because of the procedure he followed, he did not notice the change in corrosion potential as a function of time as shown in Figure 51. Therefore his conclusion is inconsistent based on an incorrect procedure.

In summary of the above discussion, a clear point was not made at room temperature because of the difficulty of increasing oxidizing power with $FeCl_3 6H_2O$ but pitting corrosion was observed at increased temperature. Thus, it can be concluded that a good correlation between the electrochemical and chemical methods exist if the proper measurements are made and the observations are properly interpreted.

CHAPTER 5

CONCLUSIONS

Based on the experiments determining the pitting behavior of 316L stainless steel and alloy AL6X in this research, the following conclusions have been reached.

1. In determining the pitting potential by electrochemical measurements, most samples fail by crevice corrosion at the metal/epoxy interface before pitting corrosion occurs because 316L stainless steel and alloy AL6X are more susceptible to crevice corrosion than pitting corrosion. Therefore, special care must be taken in preparing the sample to determine the pitting potential correctly without interference of crevice corrosion. Best result are obtained when the sample is prepassivated in 50% HNO_3 + 50% H_2O at 50^{o}C for 30 minutes before painting across the metal/epoxy interface and subsequently the passive film is removed from the exposed surface carefully by repolishing.
2. AL6X has much better resistance to pitting corrosion than 316L stainless steel due to higher chromium, nickel, and molybdenum contents.
3. The pitting potential of 316L stainless steel increases with a slower scan rate indicating that the passive film is thicker with a slower scan rate. The passive current density is decreased with a slower scan rate.
4. The pitting potential of 316L stainless steel is decreased

with increasing chloride ion concentration. However, the critical current density does not change significantly with chloride ion concentration.

5. A higher critical current density is observed when the potential is scanned from the cathodic region than from the open circuit poential due to hydrogen evolution during cathodic treatment.
6. Rapid decrease in the pitting potential of 316L stainless steel is observed by increase in temperature from room temperature to 135^{o}F but relatively small decrease occurs for a temperature change from 135^{o}F to 170^{o}F.
7. The pitting resistance of AL6X is not affected by solution annealing above 2050^{o}F but solution annealing at 1950^{o}F reduces the pitting resistance of AL6X.
8. Decrease in the pitting resistance of AL6X by solution annealing at 1950^{o} is due to the formation of sigma phase along the grain boundary.
9. Based on the results of immersion tests, pitting corrosion occurs in 316L stainless steel in 10% $FeCl_3$ at room temperature, 135^{o}F, and 170^{o}F but not in 1% $FeCl_3$. AL6X is only attacked by pitting corroison in 10% $FeCl_3$ at 170^{o}F.
10. In chemical measurements, the corrosion potential is observed to decrease with pit propagation. Once it falls below the pitting potential, the rest of the sample surface is protected from the pitting corrosion.

11. Based on the observation that the average corrosion rate determined every hour for 9 hours is consistent with the rate determined only once after 9 hours, conditons for the continued localization of the corrosion are quickly re-established.

12. The electrochemical test is a true and valid representation of the chemical test if the proper measurements are made and the test results are properly interpreted. For example, pitting corrosion occurs in 15 g/l $FeCl_3 6H_2O$ at $135^{o}F$ after the corrosion potential of 316L stainless steel reaches 0.47 V (SHE) which is close to the electrochemically determined pitting potential of 0.45 V (SHE).

LIST OF REFERENCES

LIST OF REFERENCES

1. F. L. LaQue, "The Problem of Localized Corrosion," **Localized Corrosion: NACE-3**, p. i47-i53,(1974).

2. H. C. Man and D. R. Gabe, "The Determination of Pitting Potentials," **Corr. Sci.**, Vol. 21, p. 323-326,(1980).

3. S. Szklarska-Smialowska and M. Czachor, "The Analysis of Electrochemical Methods for the Determination of Characteristic potentials of Pitting Corrosion," **Localized Corrosion: NACE-3**, p. 353-362,(1974).

4. R. F. Steigerwald, "Effect of Cr Content on Pitting Behavior of Fe-Cr Alloys," **Corrosion**, Vol. 22, p. 107-112,(1966).

5. W. D. France, Jr. and N. D. Greene, "Comparison of Chemically and Electrochemically Induced Pitting Corrosion," **Corrosion**, Vol. 26, p. 1-4,(1970).

6. R. J. Brigham, "Discussion: Chemically and Electrochemically Induced Pitting Corrosion," **Corrosion**, Vol. 26, p. 200,(1970).

7. A. J. Sedriks, **Corrosion of Stainless Steels**, New York, Wiley-Interscience, p. 9,(1979)

8. A. Piotrowski and R. Lebet, "The Electrochemical Parameters of Stainless Steel Passivation by Some Reversible Redox Systems," **Corr. Sci.**, Vol. 7, p. 231-237,(1967).

9. M. Nagayama and M. Cohen, "The Nature and Composition of the Passive Film," **J. Electrochem. Soc.**, Vol. 109, p.781-790, (1962).

10. G. Okamoto, "Passive Film of 18-8 Stainless Steel Structure and Its Function," **Corr. Sci.**, Vol. 13, p. 471-489,(1973).

11. J. Kruger, "Optical Studies of The Formation and Breakdown of Passive Films Formed on Iron Single Crystal Surfaces in Inorganic Inhibitor Solutions," **J. Electrochem. Soc.**, Vol. 110, p. 654-662,(1963).

12. C. L. McBee and J. Kruger, "Nature of Passive Films on Iron-Chromium Alloys," **Electrochimica Acta**, Vol. 17, p. 1337-1341,(1972).

13. G. C. Wood, "The Oxidation of Iron-Chromium Alloys and Stainless Steels at High Temperatures," **Corr. Sci.**, Vol. 2, p. 173-196, (1978).

14. G. Okamoto and T. Shibata, "Passivity and the Breakdown of Passivity of Stainless Steel," **Passivity of Metals**, The Electrochemical Society, p. 646-677,(1978).

15. W. Y. C. Chen and J. R. Stephens, "Anodic Polarization Behavior of Austenitic Stainless Steel Alloys with Lower Chromium Content," **Corrosion**, Vol. 35, p. 443-451,(1979).

16. M. Nagayama and G. Okamoto, :The Anodic Behavior of Passive Iron in Chromic Acid-Chromate Solutions," **Corr. Sci.**, Vol. 2, p. 203-210,(1962).

17. P. R. Openshaw and L. L. Shreir, "Oxidation of Uranium-Alumimium Intermetallic Compounds," **Corr. Sci.**, Vol. 3, p. 217-237, (1963).

18. N. D. Tomashov, G. P. Chernova and O. N. Marcova, "Effect of Supplementary Alloying Elements on Pitting Corrosion Susceptibility of 18Cr-14Ni Stainless Steel," **Corrosion**, Vol. 20, p. 166-173.(1964).

19. T. P. Hoar, D. C. Mears and G. P. Rothwell, "The relationships Between Anodic Passivity, Brightening and Pitting," **Corr. Sci.**, Vol. 5, p. 279-289,(1965).

20. T. P. Hoar, "The production and Breakdown of The Passivity of Metals," **Corr. Sci.**, Vol. 7, p. 341-355,(1967).

21. U. R. Evans, "Stress Corrosion: Its Relation to Other Types of Corrosion," **Corrosion**, Vol. 7, p. 238-244,(1951).

22. N. Zamin and M. B. Ives, "Effect of Chloride Ion Concentration on the Anodic Dissolution Behavior of Nickel," **Corrosion**, Vol. 29, p. 319-324,(1973).

23. Ja. M. Kolotyrkin, "Effects of Anions on the Dissolution Kinetics of Metals," **J. Electrochem. Soc.**, Vol. 108, p. 209-216,(1961).

24. Ja. M. Kolotyrkin, "Pitting Corrosion of Metals," **Corrosion**, Vol. 19, p. 261-268,(1963).

25. I. L. Rosenfeld and W. P. Maximtschuk, **Z. Physik. Chem.**, Vol 15, p. 25-47,(1960).

26. K. J. Vetter and H. H. Strehblow, "Pitting Corrosion in an Early Stage and Its Theoretical Implications," **Localized Corrosion: NACE-3**, p. 240-251,(1974).

27. N. D. Greene and N. G. Fontana, "An Electrochemical Study of Pitting Corrosion in Stainless Steels," **Corrosion**, Vol. 15, p.48-54,(1959).

28. J. R. Galvele, "Transport Process and the Mechanism of Pitting of Metals," **J. Electrochem. Soc.**, Vol. 123, p.464-474,(1976).

29. M. Pourbaix, **Atlas of Electrochemical Equilibria in Aqueous Solutions**, Houston, NACE,(1966)

30. J. Horvath and H. H. Uhlig, "Critical Potentials for Pitting Corrosion of Ni, Cr-Ni, Cr-Fe, and Related Stainless Steels," **J. Electrochem. Soc.**, Vol. 115, p. 791-795,(1968).

31. H. Okada, H. Ogawa, I. Itoh, and H. Omata, "Auger Electron Spectroscopic Analysis of the Passive Film of Stainless Steels," **Passivity and its Breakdown on Iron and Iron Base Alloys, NACE**, p. 82,(1976).

32. P. E. Morris, "Use of Rapid-Scan Potentiodynamic Techniques to Evaluate Pitting and Crevice Corrosion Resistance of Iron-Chromium-Nickel Alloys," **Galvanic and Pitting Corrosion-Field and Laboratory Studies, ASTM STP 576**, p. 261-275,(1976).

33. N. D. Grèene and G. Judo, "Relation Between Anodic Dissolution and Resistance to Pitting Corrosion," **Corrosion**, Vol. 21, p. 15-18,(1965).

34. M. Pourvaix et.al., "Potentiokinetic and Corrosimetric Investigations of the Corrosion Behavior of Alloy Steels," **Corr. Sci.**, Vol. 3, p. 239-259,(1963).

35. H. C. Man and D. R. Gabe, "A Study of Pitting Potentials for Some Austenitic Stainless Steels Using a Potentiodynamic Technique," **Corr. Sci.**, Vol. 21, p. 713-721,(1981).

36. J. B. Lumsden and R. W. Staehle, "The Effect of Surface Treatment on the Composition of Films on Austenitic Stainless Steels," **Passivity and Its Breakdown on Iron and Iron Base Alloys, NACE**, p. 75-76,(1976).

37. A. P. Bond and E. A. Lizlovs, "Anodic Polarization of Austenitic Stainless Steels in Chloride Media," **J. Electrochem. Soc.**, Vol. 115, p. 1130-1135,(1968).

38. E. A. Lizlovs and A. P. Bond, "Anodic Polarization of Some Ferritic Stainless Steels in Chloride Media," **J. Electrochem. Soc.**, Vol. 116, p. 574-579,(1969).

39. R. Bandy and D. V. Rooyen, "Pitting-Resistant Alloys in Highly Concentrated Chloride Media," **Corrosion**, Vol. 39, p. 227-236, (1983).

40. Z. Szklarska-Smialowsk, "Review of Literature on Pitting Corrosion Published Since 1960," **Corrosion**, Vol. 27, p. 223, (1971).

41. N. Bui, A. Irhzo, F. Dabosi, and Y. Limouzin-Maire, "On the Mechanism for Improved Passivation by Addition of Tungsten to Austenitic Stainless Steels," **Corrosion**, Vol. 39, p. 491-496, (1983).

42. N. D. Tomashov, G. P. Chernova and O. N. Marcova, "Investigation of Pitting Repassivation on 18Cr-14Ni Steels Additionally Alloyed with V, Si, Mo or Re," **Localized Corrosion: NACE-3**, p. 363-367,(1974).

43. Z. Szklarska-Smialowska and M. Janik-Czachor, "Pitting Corrosion of 13Cr-Fe Alloy in Na SO Solutions Containing Chloride Ions," **Corr. Sci.**, Vol. 7, p. 65-72,(1967).

44. Z. Szklarska-Smialowska, "Influence of Sulfide Inclusions on the Pitting Corrosion of Steels," **Corrosion**, Vol. 28, p. 388-396, (1972).

45. G. S. Eklund, "On the Initiation of Crevice Corrosion on Stainless Steel," **J. Electrochem. Soc.**, Vol. 123, p. 170-173, (1976).

46. P. E. Manning, D. J. Duquette, and W. F. Savage, "The Effect of Test Method and Surface Condition on Pitting Potential of Single and Duplex Phase 304L Stainless Steel," **Corrosion**, Vol. 35. p.151-157,(1979).

47. A. Szummer, Z. Szklarska-Smialowska and M. Janik-czachor, "Electron Microprobe Study of the Corrosion Pits Nucleation on Fe-16Cr Single Crystals," **Corr. Sci.**, Vol. 8, p. 827-831. (1968).

48. Z. Szklarska-Smialowska and M. Janik-Czachor, **Br. Corr. J.**, Vol. 4, p. 138,(1969).

49. M. Hasegawa and M. Osawa, "Corrosion Behavior of Ultrafine Grained Austenitic Stainless Steel," **Corrosion**, Vol. 40, p.371-374,(1984).

50. M. J. Johnson, "Relative Critical Potentials for Pitting Corrosion of Some Stainless Steels," **Localized Corrosion-Cause of Metal Failure, ASTM STP 516**, p. 262-272,(1972).

51. H. P. Leckie and H. H. Uhlig, "Environmental Factors Affecting the Critical Potential for Pitting in 18-8 Stainless Steel," **J. Electrochem. Soc.**, Vol. 113, p. 1262-1267,(1966).

52. H. H. Uhlig and J. R. Gilman, **Z. Physik. Chem.**, Vol. 226, p. 127-135,(1964).

53. J. M. Kolotyrkin, "Effects of Anions on the Dissolution Kinetics of Metals," **J. Electrochem. Soc.**, Vol. 108, p. 209-216,(1961).

54. H. P. Leckie, "A Contribution to the Applicability of Critical Pitting Potentials," **J. Electrochem. Soc.**, Vol. 117, p. 1152-1154,(1970).

55. T. Suzuki and Y. Kitamura, "Critical Potential for Growth of Localized Corrosion of Stainless Steel in Chloride Media," **Corrosion**, Vol. 28, p. 1-6,(1972).

56. R. J. Brigham and E. W. Tozer, "Temperature as a Pitting Criterion," **Corrosion**, Vol. 29, p. 33-36,(1973).

57. B. E. Wilde and E. Williams, "On the Breakdown of Passivity on Stainless Steels in Halide Media," **J. Electrochem. Soc.**, Vol. 116, p. 1539-1540,(1969).

58. M. Pourbaix, "Significance of Protection Potential in Pitting and Intergranular Corrosion," **Corrosion**, Vol. 26. p. 431-433, (1970).

59. B. E. Wilde, " On Pitting and Protection Potentials: Their Use and Possible Misuses for Predicting Localized Corrosion Resistance of Stainless Alloys in Halide Media," **Localized Corrosion: NACE-3**, p.342-350,(1974).

60. P. E. Manning, "Comparison of Several Accelerated Laboratory Tests for the Determination of Localized Corrosion Resistance of High Performance Alloys," **Corrosion**, Vol. 39, p. 98-102, (1983).

61. H. P. Hack, "Crevice Corrosion Behavior of Molybdenum-Containing Stainless Steels in Seawater," **Corrosion**, Vol. 39, p. 24-30, (1983).

62. M. A. Streicher, "Analysis of Crevice Corrosion Data From Two Sea Water Exposure Tests on Stainless Alloys," **Corrosion**, Vol. 39, p. 37-50,(1983)

63. M. G. Fontana and N. D. Greene, **Corrosion Engineering**, New York, McGraw-Hill, p. 297-346,(1978)

64. W. Schwenk, "Diskussion Der Eigenschaften Des Lochfrasspotentials Nichtrostender Stahle in Zusammenhang Mit Seinen Bestimmungmethoden," **Corr. Sci.**, Vol. 5, p. 245-254,(1965).

65. V. Hospadaruk and J. V. Petrocelli, "The Pitting Potential of Stainless Steels in Chloride Media," **J. Electrochem. Soc.**, Vol. 113, p. 878-883,(1966).

66. B. E. Wilde and E. Williams, "The Relevance of Accelerated Electrochemical Pitting Tests to the Long-Term Pitting and Crevice Corrosion Behavior of Stainless STeels in Marine Environments," **J. Electrochem. Soc.**, Vol. 118, p. 1057-1062, (1971).

67. A. Broli, H. Holtan, and K. Prestrud, "Use of Galvanokinetic Methods for the Determination of Characteristic for Pittng Corrosion on Aluminum," **Corrosion**, Vol. 30, p. 427-431,(1974).

68. P. E. Manning, "The Effect of Scan Rate on Pitting Potentials of High Performance Alloys in Acidic Chloride Solution," **Corrosion**, Vol. 36, p. 468-474,(1980).

69. Z. Szklarska-Smialowska and M. Janik-Czachor, "The Analysis of Electrochemical Methods for the Determination of Characteristic Potentials of Pitting Corrosion," **Corr. Sci.**, Vol. 11, p. 901-914,(1971).

70. N. Pessall and C. Liu, "Determination of Critical Pitting Potentials of Stainless Steels in Aqueous Chloride Environments," **Electrochimica Acta**, Vol. 16, p. 1987-2003, (1971).

71. ASTM G 48-76: Standard Test Methods for Pitting and Crevice Corrosion Resistance of Stainless Steels and Related Alloys by Use of Ferric Chloride Solution.

72. B. E. Wilde and E, Williams, "On the Correspondence between Electrochemical and Chemical Accelerated Pitting Corrosion Tests," **J. Electrochem. Soc.**, Vol. 117, p. 775-779,(1970).

VITA

In-Seop Lee was born in Kyung-Nam, Korea on April 3, 1959. He attended high school in Seoul, Korea and graduated from Dae Kwang High School in January 1977. The following March he entered the Yon Sei University in Seoul. After finishing his junior year, he joined military service. He rejoined university after completion of two and half years military service. He received a B.S. degree in Metallurgical Engineering in Feburary 1983. Study toward a M.S. in Materials Science and Engineering at The University of Tennessee began in the Fall of 1983. This degree was awarded in March 1986. He plans on continuing his education toward a ph.D. at The University of Tennessee. His ultimate goal is a career in teaching and applied research.

He resides at 1611 Laurel Ave. 707 with his wife, Eun-Ju, and daugher, Hyun-A, ages 6 weeks.

The author is a student member of the American Society for Metals, the Metallurgical Society of AIME and the National Association of Corrosion Engineers.